# Peculiar physical properties and the colossal magnetoresistance of manganites (Review)

V. M. Loktev*

*N. N. Bogolyubov Institute for Theoretical Physics, National Academy of Sciences of Ukraine, ul. Metrologicheskaya 14b, 03143 Kiev, Ukraine*

Yu. G. Pogorelov**

*Departamento de Fisica, CFP/IFIMUP, Universidade do Porto, Rua Campo Alegre 687, 4169-007 Porto, Portugal*

(Submitted August 10, 1999; revised October 13, 1999)
Fiz. Nizk. Temp. **26**, 231–261 (March 2000)

An attempt is made to analyze the most important physical properties of manganites of the La-Ca-Mn-O type, which exhibit the colossal magnetoresistance effect. The primary focus is on the peculiarities of these compounds which are reflected in their crystalline, electronic, and magnetic structures and which determine the possible mechanisms by which an external magnetic field can exert a substantial influence on the transport characteristics of the current carriers in manganites. The combined effect of these factors is to create the necessary conditions for a metal-insulator phase transition that is sensitive to an external magnetic field. Another major topic in this review is a discussion of the scientific problems confronting the physics of manganites. © *2000 American Institute of Physics.* [S1063-777X(00)00103-1]

## 1. INTRODUCTION

It is remarkable and symbolic that the last year of the 20th century is the anniversary of one of the most interesting, and, as it has turned out, nontrivial phenomena in solid-state physics: in 1950 the Dutch experimental physicists Jonker and Van Santen discovered an unexpected and interesting correlation between doping-induced electrical conductivity and ferromagnetism of the initially insulating manganese perovskites (manganites) $LaMnLO_3$, in which the rare-earth metal was replaced by an alkaline-earth substituent.[1,2] The initial three-component composites $LaMnO_3$ and $AMnO_3$, where $A=$ Ca, Sr, or Ba, are antiferromagnets (AFMs) with spins localized at the sites occupied by the manganese ions, while the compounds of the four-component stoichiometry $La_{1-x}A_xMnO_3$ with intermediate compositions ($0.2 \leqslant x \leqslant 0.5$) not only become strong ferromagnets but also manifest conductivity of the metallic type, which is observed only below the Curie temperature $T_C$. This unusual simultaneous radical change in their magnetic and electrical (including transport) properties is, all by itself, sufficient to generate interest in manganites, in particular, and in transition-metal oxides in general, from the standpoint of both experimental and theoretical research. Surprising as it may seem, this interest continues unabated to the present day.

The reasons for this interest are obvious—the interweaving, in one type of compound, of the diverse properties of metals and insulators, ionic and covalent crystals, systems with ferromagnetism, antiferromagnetism, and, as it turns out, orbital and charge ordering, systems with intermediate valence and disordered media and, finally, systems that can undergo phase separation. The aforementioned features and the phenomena associated with them have been studied in detail, and by the end of the 1980s and beginning of the 1990s they had been interpreted one way or another in terms of the concepts of a strong electron-electron correlation inherent to transition-metal oxides and the resulting crossover from localized to delocalized behavior of the electrons as their concentration changes. However, the sudden and unexpected discovery of high-temperature superconductivity (HTSC), which is peculiar to the oxides of only one transition metal—copper, was an indication that the overall level of the theory was inadequate for describing, in a manner consistent with the available experimental information, both copper oxides and oxides of other transition metals (including manganese), which, as multicomponent systems, must be classified as complex compounds. Moreover, the obvious similarity of certain of their properties, viz., the strong interaction of the carriers with lattice and spin excitations, the change of the transport properties under the influence of external factor (fields, temperature), and the ability to undergo a metal-insulator transition, and, possibly even more importantly, the differences, particularly the fact that the HTSC effect is observed in only one oxide, while a ferromagnetic metallic state is observed in the other transition-metal oxides, clearly show that our understanding (even qualitative) of the processes occurring in these systems cannot be considered satisfactory. In particular, the Fermi-liquid theory, which is valid for many metals (and an even more simplified version—the nearly free fermion theory) turns out to be inapplicable in practice for metallized transition-metal oxides, and it requires substantial refinement.

The situation became even more serious after the discovery of yet another ''supereffect''[3–8]—the exceptionally strong influence of an external magnetic field **H** on the electrical resistivity $R_H(T)$ of manganites in the neighborhood of the Curie point.[1)] This effect has come to be called the *colossal magnetoresistance* (CMR), and its value (see Fig. 1) in $La_{0.67}Ca_{0.33}MnO_3$ films reaches (in modulus) $\sim 10^5\%$ at

 

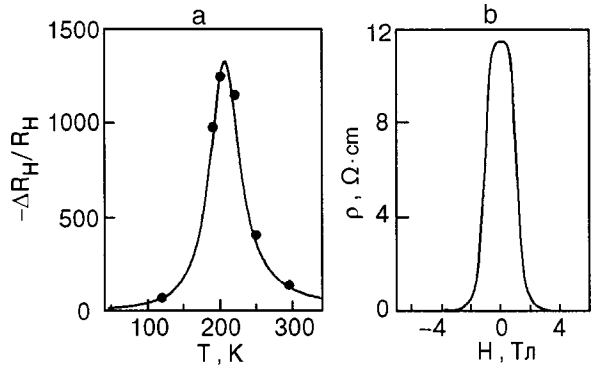


FIG. 1. Temperature dependence of the ratio $[R_H - R_0]/R_H$ (a) and the magnetic-field dependence of the resistivity $\rho$ (b) in $La_{0.67}Ca_{0.33}MnO_x$ films of thickness $\sim 10^3$ Å, annealed in an oxygen atmosphere.[7] At the maximum ($T \approx T_C$) the ratio $-\Delta R_H(T)/R_H(T) \approx 127000\%$, while $-\Delta R_H(T)/R_0(T) \approx 99.9\%$.

$T \sim 10^2$ K,[6,7] which is much larger than the values that had been obtained in other known systems.[2)] Of course, such an unusual sensitivity of the electrical resistance (which, generally speaking, is small) of manganese perovskites to the turning on of an external magnetic field has generated a booming interest, as in the case of HTSCs, and, as a result, an enormous number of publications in the scientific and especially the engineering journals, a large number of reports and conferences devoted to manganites on the whole or even to some particular properties of them.

The discoveries of high-temperature superconductivity and colossal magnetoresistance at nearly the same time have brought about a renaissance in the study of various transition-metal oxides, bringing into this field of study new methods, new approaches, and new ideas. It became rather obvious that none of the physical states peculiar to these compounds or the phenomena accompanying them could be considered in isolation, as unrelated to other properties, and that localized and delocalized carriers are not mutually exclusive but coexist in them. The features of the so-called exotic properties of the oxides are a direct reflection of the intimate relationship of the orbital, charge, spin, and lattice degrees of freedom in these compounds. However, their individual features (which are manifested, not least importantly, in the aforementioned differences among transition–metal oxides) cannot be ignored. Therefore the study of each specific oxide compound must proceed along the stated lines and take into account the specific physical parameters characterizing this compound (the composition, type of lattice, the main interactions, spectrum) and the existing external conditions (fields, temperature, etc.).

At the same time, one can hope that as such disparate (at first glance) phenomena as high-temperature superconductivity and the isotropic negative colossal mangetoresistance are studied further, it will be possible to establish the depth of the analogy between these systems belonging to the same physical class—transition-metal oxides—and the reasons for their differences. There is no doubt that the study of their fundamental properties is one of the most important fields of modern solid-state physics and its subfield—the physics of strongly correlated metals.

No less remarkable, in principle, are the potential uses (including commercial) of the colossal magnetoresistance, which make it extremely likely that highly sensitive sensors—a new generation of materials for magnetic recording, storage, and readout of information—can be created. This, in turn, requires new technologies for obtaining high-quality and reliable samples (single-crystal, ceramic, granular, etc.), which are also needed for purely scientific purposes.

In this review article, which is devoted to the physics of manganites, an attempt is made to describe the current status and understanding of the topic, and also to discuss the most important results of the recent period, concentrating on certain unsolved problems. Any presentation of limited length requires that a selection be made from the body of information available, and therefore cannot help but depend on the personal tastes and priorities of the authors, who (one would like to think) nevertheless attempt to be objective. Still, there are many papers (possibly quite important and interesting) that will not be mentioned, and therefore the list of references should not be considered exhaustive. In spite of this obvious incompleteness, we hope that this review will be useful for those who have the opportunity to become acquainted with it.

## 2. GENERAL INFORMATION ON THE CRYSTAL STRUCTURE AND MAGNETISM OF MANGANITES

Before turning to a systematic description of these extremely complex compounds, we must make a few opening remarks: the number of ternary perovskites of the type $RMO_3$ (R is a rare-earth metal, M is a transition metal) is in itself quite large. But when one takes into account the possibility of varying the rare-earth element, $R = $ La, Pr, Nd, etc. and considers in addition the practically unlimited set of solutions $R_{1-x}A_xMnO_3$, the number of compounds becomes extremely large indeed. Although they are all transition-metal oxides, or, in other words, members of a group of apparently physically related compounds, they turn out to be different, even in their initial (undoped) states. For example, while $LaMnO_3$ with M = Ti, V, Cr, Mn, Fe, and Co are antiferromagnetic insulators, those with M = Ni or Cu are paramagnetic metals (see Ref. 11). On the other hand, the completely doped systems $SrMnO_3$ are metals for all transition-metal elements except Ti and Mn. This ''unpredictability'' once again emphasizes beautifully that the ''input'' data—the chemical formula and especially the number of electrons in the partially filled $3d$ shell of the transition metal—are important characteristics determining the ''output'' properties of the respective oxides.

### 2.1. Basic lattice parameters

In accordance with the stipulated limitations, here we concentrate solely on the four-component manganites $La_{1-x}A_xMnO_3$, and among these, mainly on the best-studied system: La–Ca–Mn–O. This is the simplest representative (corresponding to $n = \infty$) of the Ruddlesden-Popper family—thermodynamically stable layered perovskites with the general formula $(R_{1-x}A_x)_{n+1}Mn_nO_{3n+1}$ ($n \geqslant 1$). As an example, Fig. 2 shows the structure of the undoped ternary oxide of this series with $n = 1$, i.e., $R_2MO_4$. Not surprisingly, it is identical to the lattice of the first HTSC $La_2CuO_4$. As

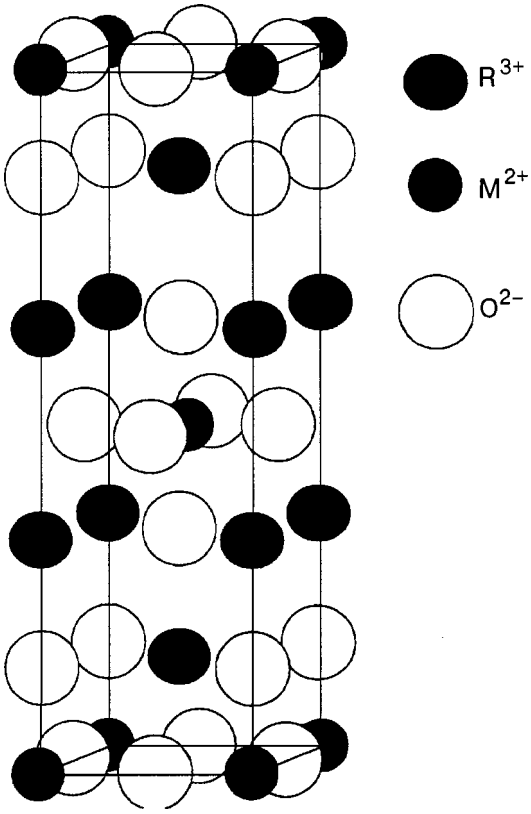


FIG. 2. Crystal cell of the first ($n=1$) term of the Ruddlesden-Popper series, the compound $R_2MO_4$, which has a pronounced layered structure. In this and subsequent figures the radii of the circles and the distances between them correspond to the relative scale of the ionic radii and inter-ion distances in the manganite lattices.

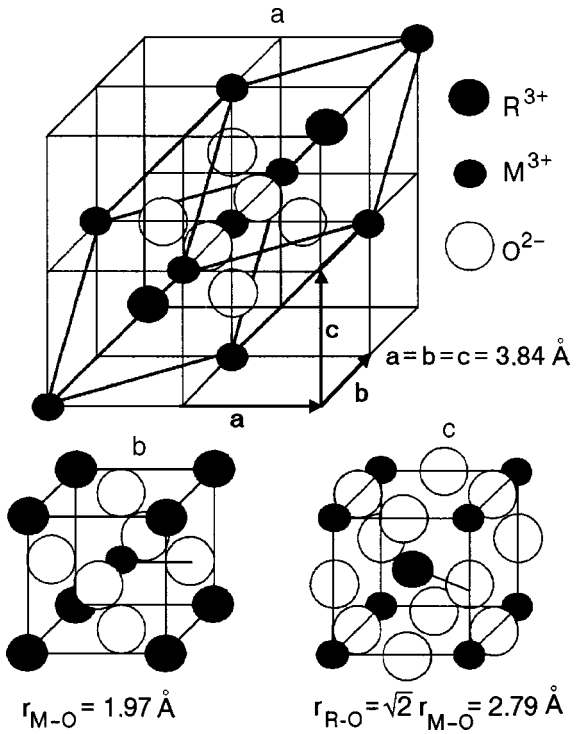


FIG. 3. Ideal cubic structure of the perovskite $RMO_3$ (a) and its basic elements: cubic cells with central transition-metal ions (b) and rare-earth ions (c).

follows from the general formula and can be seen from the figure, the oxides of this family consist of ''cuprate'' layers $MO_2$ separated by relatively large gaps that are increasingly filled with RO layers as $n$ increases. In copper oxides the coupling between layers is relatively weak, so that the electronic and magnetic properties of the system have a pronounced 2$D$ character, the role of which in high-temperature superconductivity is generally acknowledged and is often considered to be decisive.[12]

A successive increase in the number of RO layers, or, in other words, synthesis of the compounds $(R_{1-x}A_x)_{n+1}Mn_nO_{3n+1}$, leads to a systematic decrease in the spatial anisotropy of the lattice, and in the limit $n=\infty$ it becomes maximally isotropic—cubic.[3)]

The overall form and fragments of the ideal structure of $RMO_3$ are shown in Fig. 3. The main unit of this structure (like that for the lattices of HTSCs) is a rather rigid $MO_{6/2}$ octahedron (this last subscript is meant to emphasize that each ligand is divided between nearest-neighbor octahedra; because of these ''shared'' bonds it is impossible to have isolated or independent deformations or rotations of an octahedron taken individually). It is also seen in Fig. 3a how and to what extent one can lower the cubic crystal class by displacing the ions from their equilibrium positions in the cube by means of regular rotations and deformations of the octahedra, which have a transition-metal ion at the center. The actual lowering cannot be established in general form without specifying the particular transition-metal ion, since it is well known[13,14] that it is determined entirely by the ground electronic term (its degeneracy or nondegeneracy) of this ion in the cubic crystalline field. If this term is degenerate, then the degeneracy will quickly be lifted by distortion of the octahedra (the cooperative Jahn–Teller (JT) effect), the amount and symmetry of this distortion being dictated by the symmetry of the degenerate states and the strength of their coupling with the collective vibrational modes, and, ultimately, by the maximum reduction in energy.

It would not be worthwhile to examine all the possible distortions here, as there have been many papers on this topic (e.g., Refs. 15–22). We will only mention that the initial cubic system can undergo (depending on the form of the deformation and the axis of rotation of the octahedra) tetragonal, orthorhombic, or rhombohedral distortion, and all of these can be found among the various mixed transition-metal oxides.

However, in spite of the fact that the form of the lowering of the symmetry of the basic (i.e., undoped) lattice of the $RMO_3$ perovskites can, in principle, be established on the basis of group theory,[13,14,23] it is rather difficult to obtain a reliable value by means of a calculation. An even more uncertain situation exists for the solid solutions $R_{1-x}A_xMnO_3$, for which it is hard to obtain reliable information not only about the size of the distortions but even about their character. In such a case one uses a different approach and, on the phenomenological level, characterizes the deformation field that arises by the so-called tolerance factor $f_{\rm tol}$. This factor is defined variously: either in terms of the ionic radii[1,2]

$$f_{\rm tol}=\frac{r_{\rm A}^{+}+r_O}{\sqrt{2}(r_{\rm R}+r_O)}, \tag{2.1}$$

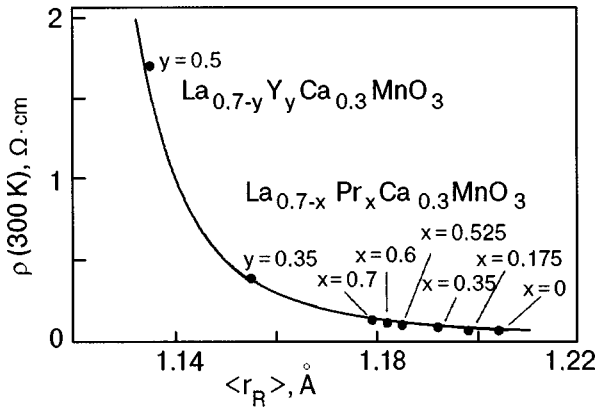


FIG. 4. Resistivity of manganites as a function of the volume-averaged ionic radius of the rare-earth element: $\langle r_R\rangle=(0.7-\{x \text{ or } y\})r_{\text{La}}+\{x \text{ or } y\}r_{\text{ProrY}}$ (Ref. 26).

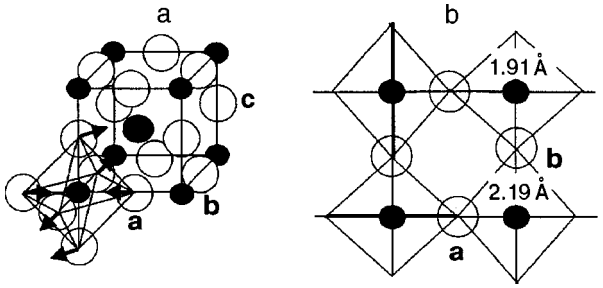


FIG. 5. Direction of the deformational JT displacements of the oxygen octahedra (a) and the doubled (for simplicity the slight orthorhombicity is not taken into account) structure of the basal plane (b) for the compound $LaMnO_3$. The indicated values are those of the long and short axes of the distorted octahedra. The heavy lines are the directions of the most strongly hybridized $p$ and $d$ orbitals of the oxygen and manganese ions (according to Ref. 25).

or in terms of the distance between atoms in the lattice[24,25]

$$f_{\text{tol}}=\frac{r_{\text{A-O}}}{\sqrt{2}r_{\text{M-O}}}. \tag{2.2}$$

In both cases $f_{\text{tol}}$ has a simple geometric meaning and qualitatively describes (for arbitrary $x$, the volume-averaged) degree of deviation of the lattice from the ideal cubic structure, for which $f_{\text{tol}}^{(\text{cub})}=1$, while the angle between M–O bonds in each M–O–M triple is 180°. Rotations and deformations of the octahedra, which cause a lowering of the space group, make $f_{\text{tol}}\neq f_{\text{tol}}^{(\text{cub})}$, and, although actually $|f_{\text{tol}}-f_{\text{tol}}^{(\text{cub})}|\ll 1$, knowledge of $f_{\text{tol}}$ in (2.1) in the case of mixtures or in (2.2) for pure but distorted structures enables one not only to assess the type of crystal-averaged deformation but also to estimate its value.

For doped structures, however, it is practically impossible to predict the latter, since for a heterovalent substitution ($R^{3+}\leftarrow A^{2+}$) the lattice distortions are caused by several factors. First, there is a different ion radius at some sites (chemical pressure), since $r_A\neq r_R$, which leads to local distortion. Second, even if these radii are chosen as close as possible, the difference in the charge states of the main and substituent ions gives rise to microscopic Coulomb fields that must be compensated, and this compensation is effected mainly by displacements, rotations, and deformations of the octahedra, which are the most labile structural units. Third, the dopant atoms are distributed (at least, for small $x$) quite randomly, and, hence, the distortions are of a statistical character. Finally, charge neutrality of the system as a whole requires changes in the valence of one of the constituent ions of the lattice, and this change is undergone by the transition-metal ion and is accompanied by a change in its electronic radius.

The effect of all these sources of deformation and internal stress is difficult to control, and $f_{\text{tol}}$ becomes a rather convenient (and sometimes the only) quantitative parameter characterizing the elastic state of the perturbed lattice. Many observable quantities can and, as experiment shows, do depend on $f_{\text{tol}}$. As an example, Fig. 4 shows the dependence (taken from Ref. 26) of the resistance on $f_{\text{tol}}$ in the form (2.1) for a number of manganites. The tolerance factor becomes even more indispensable in the study of layered manganites (members of the Ruddlesden–Popper series with $n\geqslant 1$), for which it is hard to find another such informative physical characteristic that can provide quantitative evidence of an integral change of their lattices under the influence of some dopant or another (see, e.g., Refs. 27–29).

Figure 5 shows the lowering of the symmetry of the cubic structure to orthorhombic, with a doubling of the unit cell, that is observed in $La_{1-x}Ca_xMnO_3$ for $x\leqslant 1$, including $x=0$. It is seen that the JT shift of the ligands brings about an especially strong deformation of the octahedra in the (001) plane, and, in addition, because of additional rotations of the octahedra in opposite directions, the $C_4$ axis is lost, so that the basis vectors are now $\mathbf{a}_{1,2}=\mathbf{a}\pm\mathbf{b}$, and the cubic manganite is transformed into the so-called orthomanganite, with two transition-metal ions in the unit cell. The orthorhombicity of the structure corresponding to the host compound $LaMnO_3$ is characterized by the ratio $c/a_1<\sqrt{2}$ (the so-called O′ structures),[25] which is preserved in $La_{1-x}Ca_xMnO_3$ up to $x\sim 0.1$. In the region $0.1\leqslant x\leqslant 0.4$ it is replaced by the O structure, in which $c/a_1>\sqrt{2}$ on account of the fact that the incorporation of Ca atoms tends to restore the cubic symmetry.

In the concentration region $0.5\leqslant x\leqslant 0.8$ these compounds on average have a rhombohedral structure with a small admixture of monoclinic distortions, which in the limit $x\to 1$ again goes over to an orthorhombic structure. The lattice symmetry observed in manganites is determined not only by their composition but also by the temperature; in particular, Refs. 30 and 31 report that increasing $T$ brings about a temperature-stimulated disproportionation (redistribution of the charge states) of the transition-metal ions, so that $2Mn^{3+}\to Mn^{4+}+Mn^{2+}$. This also alters the point symmetry of the lattice, affects the various bond lengths, and, as a result, changes the value of $f_{\text{tol}}$.[4)] We shall not dwell any longer on the structural features[5)] and the character of the local distortions of manganites; the interested reader is referred to a recent collection of papers on these topics.[33] We note only that it is extremely unlikely that the lattice deformations, which are described to a greater or lesser degree by a tolerance factor, are among the main causes underlying the CMR effect.

### 2.2. Manganese ion in the crystalline

The states of this variable-valence ion in crystalline fields of various symmetries have been the subject of many publications (see the monographs[13,14,34]). We shall therefore briefly mention only the information that will be needed below. First, it is readily verified that the charge balance in the compounds $RMnO_3$ requires that the manganese be found in the valence $Mn(III) \equiv Mn^{3+}$, while in the compounds $AMnO_3$ it must have the valence $Mn(IV) \equiv Mn^{4+}$, the $Mn^{3+}$ state being somewhat less stable chemically than $Mn^{2+}$ or $Mn^{4+}$. Since nonisovalent doping, or the substitution $A^{2+} \rightarrow La^{3+}$, causes charge exchange $Mn^{4+} \rightarrow Mn^{3+}$, positive charges appear in the subsystem of transition-metal ions. This indicates directly that the current carriers in the conducting phases of complex manganites with $x \leqslant 0.5$ should be holes. However, since the charge of the carrier depends on both the dopant and host elements, when $AMnO_3$ is doped by the substitution $La^{3+} \rightarrow A^{2+}$, for example, one must speak of electrons (the transition $Mn^{3+} \rightarrow Mn^{4+}$) and an electronic type of conductivity (provided, of course, that a conductivity appears). These simple and seemingly correct arguments nevertheless sometimes do not find confirmation in experiment. In particular, at high enough $T$ the Hall effect and the thermopower of thin films of manganites with $x < 0.5$ correspond to a negative sign of the carrier charge. A reasonable explanation for this is the aforementioned disproportionation and the onset of divalent manganese ions in addition to the tri- and tetravalent forms; these divalent ions correspond to $n$-type conductivity, or electrons. The latter have a high mobility and account for the observed[31] charge of the carriers.[6)]

Returning to the single-ion states, we recall that the neutral Mn atom has the electronic configuration $3d^5 4s^2$, and the free ion $Mn^{3+}$ therefore corresponds to the configuration $3d^4$ and the $Mn^{4+}$ ion to $3d^3$. The strongest influence on the states of the unfilled shells in an ionic crystal is the Coulomb field exerted by the charged ligands $O^{2-}$ nearest to the transition-metal ion, which form an octahedron around it, and the strongest component of this field is the cubic component. It splits the fivefold degenerate single-particle states of the $3d$ shell into two multiplets: a triplet $t_{2g} = xy$, $xz$, and $yz$, and a doublet $e_g = x^2 - y^2$, $3z^2 - r^2 \equiv z^2$, with a splitting of $\varepsilon_{e_g} - \varepsilon_{t_{2g}} \geqslant 1$ eV.[13,14] As a result, the electrons occupy first the $t_{2g}$ and then the $e_g$ multiplet.

In addition to the crystalline field, the single-ion states are shaped by the electron-electron correlation, the Coulomb part of which shifts the corresponding $n$-electron term $3d^n$ as a whole, and the exchange (at the same occupation) splits different terms according to the value of the total electronic spin $S$ of the ion. And if the electron-electron interaction in the ion does not exceed the strength of the crystalline field, then the sequence of states will obey Hund's empirical rule: the lowest term is the one with the highest possible spin, $S = n/2$. This means that the $Mn^{3+}$ has spin $S = 2$, while $Mn^{4+}$ has $S = 3/2$. The first corresponds to an electronic configuration $t_{2g}^3$, which, owing to the twofold degeneracy, causes a static JT deformation of the octahedra.[36,37] Here the instability is such (see Fig. 5) that the octahedra are stretched considerably ($r^a_{Mn-O} \approx 2.19$ Å) in the basal plane (001); the interplanar couplings are less strongly affected ($r^c_{Mn-O} \approx 1.96$ Å).[38] This collective deformation not only causes a doubling of the unit cell, but there is also an additional rotation of each octahedron, so that the Mn-O bond angle becomes slightly different from 180°.

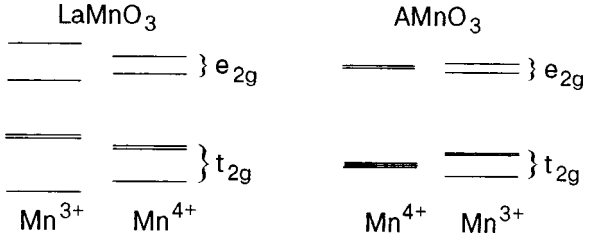


FIG. 6. Single-ion spectra of manganese in compounds containing one hole ($LaMnO_3$) and one electron ($AMnO_3$). It is seen that the spectrum of the $Mn^{4+}$ ion in $LaMnO_3$ is split (pseudodegenerate) and that the splitting of the $Mn^{3+}$ spectrum in $AMnO_3$ is smaller than in $LaMnO_3$, where it is due to the collective JT effect.

According to quantum-chemical calculations[34,39] and spectroscopic data,[40,41] the lowest energy belongs to the $z^2$ component of the doublet $e_g$ (the $z$ axis here is chosen locally—along the long axis of the octahedron). Interestingly, in HTSC cuprates in the same situation—with one hole in the $e_g$ doublet—the ground state is the $x^2 - y^2$ component of this doublet, and the octahedron is stretched along the $c$ axis. Here both an individual $Cu^{2+}$ ion in the cuprates and the corresponding $Mn^{3+}$ ion in the manganites, after the deformation has occurred, become pseudo-JT ions. This term is understood to mean that even the complete removal of an electron from the $Mn^{3+}$ ion in the $LaMnO_3$ crystal, which has a finite stiffness, does not lead to restoration of the cubic structure of the octahedron surrounding this ion. Thus the energies $\varepsilon_{x^2-y^2}$ and $\varepsilon_{z^2}$ remain nondegenerate, although the splitting between them is undoubtedly reduced to a pseudosplitting on account of the tendency of the octahedron containing the $Mn^{4+}$ ion to assume a higher degree of symmetry. Appreciable deformations are attained only in the collective JT effect.

The situation is different for the compound at the opposite end of the series, viz. $AMnO_3$, where the transition-metal ions have the electronic configuration $3d^3$, and the states of the doublet $e_g$, because they are not occupied, can remain degenerate, and the $MnO_{6/2}$ octahedra preserve their initial cubic symmetry.[7)] The introduction of a $La^{3+}$ ion converts one of the $Mn^{4+}$ ions to $Mn^{3+}$, which, under conditions of a rigid medium, is again unable to manifest fully its JT nature; in other words, the local deformation of the surroundings near such an isolated JT ion should be substantially smaller than in $LaMnO_3$, where the deformation is of a cooperative character. However, when the deformations can combine in such a way that the states $x^2 - y^2$ and $z^2$ in systems of the type $La_{1-x}A_xMnO_3$ with $x > 0.5$ are split, the situation changes so much that even the pseudo-JT effect can cause such interesting effects as orbital ordering (see Paragraph 4.1). The qualitative form of the single-ion spectra of $Mn^{3+}$ and $Mn^{4+}$ in the corresponding matrices $LaMnO_3$ and $AMnO_3$ is shown in Fig. 6.

### 2.3. Exchange interactions and magnetic structures

Knowing the electronic and spin states of the ion in some particular lattice structure, one can frame the question

of spin ordering and the spin excitations corresponding to it as the problem of finding the lowest-energy (along with the vibrational) branches of elementary excitations of the system. Of course, this problem is not a new one either in general or specifically for manganites, and a reliable theoretical foundation for it was laid in the pioneering papers by Anderson,[42] Anderson and Haswgawa,[43] Dzyaloshinski,[44] Moriya,[45] and many others (see the monograph[34]). In the simplest situation of two identical neighboring cation spins $\mathbf{S_n}$ and $\mathbf{S_{n+\rho}}$ ($\mathbf{n}$ and $\mathbf{n}+\boldsymbol{\rho}$ are nearest-neighbor sites), the Hamiltonian has the Heisenberg form:

$$H_{\rm ex}=\frac{1}{2}\sum_{\mathbf{n},\boldsymbol{\rho}} J_{\mathbf{n},\mathbf{n}+\boldsymbol{\rho}} S_{\mathbf{n}}\cdot S_{\mathbf{n}+\boldsymbol{\rho}}, \tag{2.3}$$

in which the exchange constant $J_{\mathbf{n},\mathbf{n}+\boldsymbol{\rho}}$ is determined by the superexchange interaction via the $p_\sigma$ and $p_\pi$ states of the anions (as a rule, these are the ions $O^{2-}$ or $F^-$, which have the same electronic configuration $1x^2 2s^2 2p^6$) and most often have an antiferromagnetic character (in the notion of Eq. (2.3) this means that $J_{\mathbf{n},\mathbf{n}+\boldsymbol{\rho}}>0$). Such a situation is realized in $AMnO_3$ compounds, where the ordering of spins $S=3/2$ in the undeformed cubic structure is related to the two-sublattice NaCl type: each spin moment of a given direction is surrounded by nearest-neighbor spins of only the opposite direction. On a fundamental level the theory also permits calculation of the anisotropy of the Dzyaloshinskii-Moriya exchange interaction in those cases when it is allowed by symmetry.[8)]

However, the deformation and rotations of the octahedra in the lattice lead to an appreciable change in the interatomic distances, especially in the basal plane, to the aforementioned bending of the line of ion-ion bonds in the triples of neighboring ions Mn–O–Mn, which affects the superexchange of the Mn–Mn pairs, and also to the splitting (see Ref. 12) of all the $p$ levels via which the virtual transfers of electrons take place. All this destroys the simple and unambiguous formation of exchange interactions of only the AFM type between transition-metal ions, and, as a result, the corresponding exchange constant for certain neighbors can acquire a FM character while still being of a superexchange origin, i.e., occurring via the states of the ligands.

Calculations of the exchange interactions between localized spins with the participation of the states of both the $e_g$ and $t_{2g}$ multiplets of the transition metal are extraordinarily laborious and do not always give values close to the observed.[47,48] Therefore, for finding the possible magnetic phase states it is simpler and more constructive to describe the exchange Hamiltonian (2.3) of the system by proceeding from physical arguments and representing the various measurable quantities by phenomenological parameters. Then, following Goodenough,[25,34] we will assume that $J^{2\,2}_{\mathbf{n},\mathbf{n}+\boldsymbol{\rho}}$ and $J^{3/2\,3/2}_{\mathbf{n},\mathbf{n}+\boldsymbol{\rho}}$ have AFM signs, while $J^{2\,3/2}_{\mathbf{n},\mathbf{n}+\boldsymbol{\rho}}$ has a FM sign (the superscripts indicate the spins $S=2$ and $3/2$ of the $Mn^{3+}$ and $Mn^{4+}$ ions, respectively). This, however, is insufficient, and, as we have said, the lattice distortions can alter the general rule.

In particular, in Refs. 46 and 47 where the LDA method was used to calculate the possible magnetic structures of $LaMnO_3$, it is shown that the most stable is the so-called $A$ structure (see Fig. 7), in which the spins in the basal planes

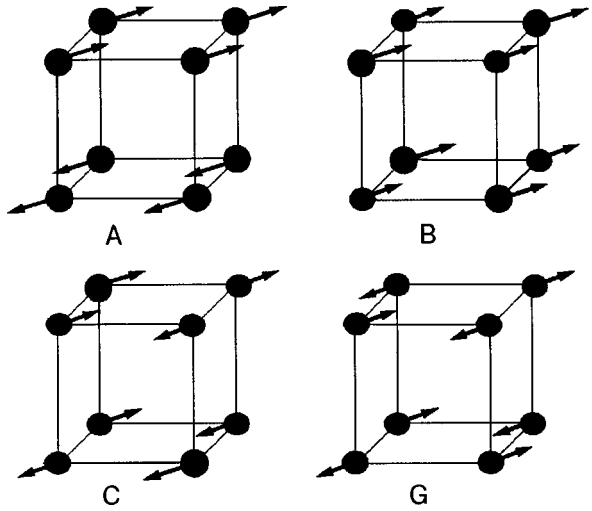


FIG. 7. Basic magnetic structures of the manganites $La_{1-x}A_xMnO_3$. The type-$C$ structure is shown for the composition $x=3/4$.

(with the doubled unit cell of the crystal) are collinear, i.e., have FM order. The global AFM structure of the crystal, however, survives on account of the relatively weak interplanar exchange, in which the contribution from the non-nearest neighbors turns out to be comparable to the nearest-neighbor contribution, which favors having oppositely directed magnetizations on neighboring planes.

Regardless of the predictions, the spin structures and the lattice parameters of the manganites $La_{1-x}A_xMnO_3$ of a large number of compositions $x$ were established experimentally back in 1955 by Wollan and Koehler[49] using neutron diffraction. Since that time the observed types of magnetic ordering, the main features of which have agreed with the calculations of Goodenough,[36] have become generally accepted. The main ones of these are illustrated in Fig. 7. We see that increasing the doping brings about a significant change of the magnetic order, of the type AFM↔FM↔AFM. Here the FM systems on the whole exist in a relatively narrow (around $x\approx 0.35$) interval of concentrations of the divalent metal. Interestingly, in that detailed paper, which was destined to become an extremely important work, it was emphasized that the FM order coexists with AFM regions, and that it is only in the vicinity of $x\approx 0.35$ that the AFM Bragg peaks have a vanishingly small intensity; this circumstance, which we think is of key importance, has been overlooked by many investigators. In that pioneering study they also measured the critical temperatures of the magnetic phase transitions. Although these temperatures depend on $x$ and have since been corrected slightly, let us give the values as reported in Ref. 49: $T_N^A\approx 140$ K, $T_C^B\approx 250$ K, $T_N^C\approx 140$ K, $T_N^G\approx 130$ K.

We conclude this Section with the general and nearly universally accepted form of the phase diagram of the magnetic states of the La–A–Mn–O manganites. According to the current ideas (see Refs. 25, 50, and 51), irrespective of the type of dopant [e.g., its electronic radius, which determines the value of the tolerance factor (2.1)] this diagram, as a rule, contains several main regions, which are shown in Fig. 8. These regions correspond more or less accurately to the following crystal structures: $0<x\leqslant 0.3$ to orthorhombic;

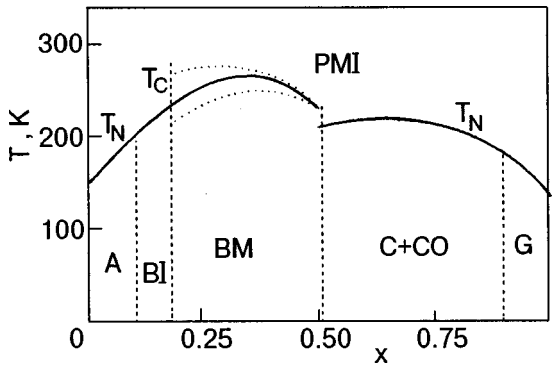


FIG. 8. Generalized phase diagram of the manganites: AFM insulator with a structure of the *A* type (region *A*); FM insulator with a structure of the *B* type (*BI*); FM metal (*BM*); AFM insulator with a structure of the *C* type and charge ordering ($C+CO$); AFM insulator with a structure of the *G* type (*G*). The vertical dashed lines qualitatively reflect the phase boundaries, while the dotted curves outline the region of the CMR effect.

$0.3 \leqslant x \leqslant 0.7$ to tetragonal, with $c<a,b$; $0.75 \leqslant x \leqslant 0.9$ to tetragonal, with $c>a,b$; and $0.9 \leqslant x \leqslant 1$ to cubic.[52]

## 3. FORMATION OF THE INSULATOR AND METALLIC PHASES OF MANGANITES

Up till now we have tacitly assumed that the hole (electron) created at one of the sites (of the $3d$ ions) remains in place. Of course, this is not completely true in reality; owing to the strong overlap of the $3d$ functions with the $p$ functions of the $z^2$ hole, if it is not expressly forbidden to do so, it will pass to one of the oxygen sites of the surrounding octahedron, from which it can move to another transition-metal ion. In other words, a carrier introduced into the system will tend to become ''smeared out'' over the crystalline medium, thereby decreasing its kinetic energy. However, its presumed free motion is limited by at least three circumstances: the AFM order existing in the crystal, the JT barrier to migration, and, finally, the Coulomb potential of the dopant that has produced the carrier. Before taking these up in order, let us discuss the question of the states via which an extra hole could move if the aforementioned impediments were not present.

### 3.1. Hamiltonian of a carrier in a crystal

The initial states for the actual electrons are again the $t_{2g}$ and $e_g$ states, hybridized with the $p_\sigma$ and $p_\pi$ orbitals; the latter are the $p_x$, $p_y$, and $p_z$ states of the $O^{2-}$ ion, the degeneracy of which is lifted by a crystalline field of lower than cubic symmetry. The simplest Hamiltonian, however, takes into account only the $z^2$ and $p_\sigma$ states (i.e., only those $2p$ functions of the ligands whose ''lobes'' are directed along the Mn–O bonds), and we will omit the other states, including all those of the rare-earth and alkaline-earth ions. Then the single-ion localized states are described by the second-quantized operator

$$H_{SI}=\sum_{\mathbf{n}} H_{\mathbf{n}}^{SI}; \tag{3.1}$$

$$H_{\mathbf{n}}^{SI}=\sum_{\lambda,\sigma}\Bigg[\varepsilon_\lambda a^+_{\mathbf{n},\lambda,\sigma}a_{\mathbf{n},\lambda,\sigma} + \frac{1}{2}\sum_{\lambda',\sigma'}\left(U_{\mathbf{n}}a^+_{\mathbf{n},\lambda,\sigma}a^+_{\mathbf{n},\lambda',\sigma'}a_{\mathbf{n},\lambda',\sigma'},a_{\mathbf{n},\lambda,\sigma}, + J_H a^+_{\mathbf{n},\lambda,\sigma}a^+_{\mathbf{n},\lambda',\sigma'}a_{\mathbf{n},\lambda',\sigma}a_{\mathbf{n},\lambda,\sigma'}\right)\Bigg],$$

where $\varepsilon_\lambda$ is the energy of the one-electron $3d$ and $2p$ levels; $U_{\mathbf{n}}(\equiv U_d, U_p)$ is the Coulomb (for $\lambda=\lambda'$ the Hubbard) repulsion at the site; $J_H$ is the Hund exchange, which is important only for the transition-metal ions; the operator $a^+_{\mathbf{n},\lambda,\sigma}$ creates an electron in the state $\lambda$ with spin $\sigma$ at the site $\mathbf{n}$ (since the role of the lattice doubling is not taken into account here, there is no index for the crystal sublattice; see Fig. 5).

The main inter-ionic process, cation-anion $pd$ hybridization, can be represented by an operator of the form

$$H_{\text{hyb}}=\sum_{\mathbf{n},\boldsymbol{\rho}}\sum_{\lambda,\lambda',\sigma} t^{\lambda,\lambda'}_{\mathbf{n},\mathbf{n}+\boldsymbol{\rho}}a^+_{\mathbf{n},\lambda,\sigma}a_{\mathbf{n}+\boldsymbol{\rho},\lambda'\sigma}, \tag{3.2}$$

in which $t^{\lambda,\lambda'}_{\mathbf{n},\mathbf{n}+\boldsymbol{\rho}}$ is the amplitude of the intersite $pd$ transition from the state $\lambda$ to the state $\lambda'$. The Coulomb and direct exchange interactions of the electrons on different ions are neglected for the sake of simplicity.

The Hamiltonian consisting of operators (3.1) and (3.2) is none other than the Hamiltonian of the many-band theory of metals in the tight-binding representation, whose applicability to manganites, in particular, derives from the pronounced localized character of the $3d$ functions (as compared to $s$ functions, for example). The total operator $H=H_{\text{hyb}}+H_{SI}$ is assuredly of the Hubbard type, since it consists of two competing terms, the second of which, characterized by the intra-atomic parameters $U_{\mathbf{n}}$ and $J_H$, is larger than the first.

As we know,[53] for $U_d>|t|\equiv|t^{\lambda,\lambda}_{\mathbf{n},\mathbf{n}+\boldsymbol{\rho}}|$ the system has a tendency to become insulating. This inequality holds in transition-metal oxides, and therefore in the undoped state they are AFM (Mott-Hubbard) insulators with a localized character of the charges, and the neighboring spins of the latter (we have in mind the unfilled ionic shells of the transition metal) are coupled (see Eq. 2.3) by a superexchange interaction $j_{\mathbf{n},\mathbf{n}+\boldsymbol{\rho}}\sim t^4/U_d^3$ (Refs. 54 and 55). In the insulating phase all of the states are mixed states, and its ground state, owing to the presence of inter-ion covalent bonding, is at minimum a linear combination of the $Mn^{3+}O^{2-}$ and $Mn^{2+}O^-$ configurations nearest in energy.

The contribution of each of these depends not only on $U_d$ but also and to an equal degree on one other extremely important quantity: $\Delta_{CT}=\varepsilon_d-\varepsilon_p$, which is the energy difference of the bare levels, or the charge transfer gap. Analysis of the many variants arising here (see, e.g., Refs. 56–58) implies that in the process of creation and transfer of the carrier, the states of the cation and anion compete with one another, and if $\Delta_{CT}>U_d$, then the creation of an oxygen hole is preferable. This is the situation that exists in the cuprates. If the opposite inequality holds, then the carrier will have a predominantly $d$ character.

At the present time there is no firm opinion as to the type of the carrier in manganites, and one can find experimental evidence in favor of both the first[59] and second[41] scenarios of metallization. There are other configurations mixed in:

$$Mn^{4+}O^{2-} \leftrightarrow Mn^{3+}O^{-} \tag{3.3}$$

in $LaMnO_3$ with an extra hole, or

$$Mn^{3+}O^{2-} \leftrightarrow Mn^{2+}O^{-} \tag{3.4}$$

in $AMnO_3$ with an extra electron (we note that the mixing shown in Eq. (3.3) corresponds to the ground state here). In other words, it is seen that in both cases the carrier has contributions from both the *d* and *p* states. Nevertheless, the majority of investigators are inclined toward the view that the carrier in the metallic phases of manganites of the La–A–Mn–O type are closer to the *d* type and move mainly via $e_g$ states.

Of course, to separate the *d* and *p* subsystems on the basis of (3.3) and (3.4) in the case of their strong hybridization is impossible, and to assign the carrier to only one of these is only partially correct—it simply reflects the larger contribution of the corresponding state to the wave function of the delocalized carrier. Judging from Fig. 5, we would say that the JT deformation of the octahedra leads to a rather noticeable inequivalence of the ligands with respect to the transition-metal ion, and this cannot help but affect their quantum states. Therefore, it is not ruled out that the wave function of the carrier is a hybridized orbital consisting of states of the most strongly coupled triple O–Mn–O (according to Ref. 25, these are the ions lying along the long axis of the octahedron). However, to use such functions in a concrete calculation is complicated by their nonorthogonality in the crystal. Figure 9 shows a simplified and almost universally used energy diagram for the manganites, corresponding to *d* holes in $LaMnO_3$ and to *d* electrons in $AMnO_3$. The change in the type of carrier in $LaMnO_3$ on doping in this scheme would only mean that the *p* band comes to lie closer to the Fermi level $\varepsilon_F$ than does the $z^2$ band.

More precisely, the question of the type of carrier in oxides containing Mn most likely does not have a unique answer. Unlike the cuprates, for example, where, according to numerical calculations that have been confirmed by experiments, one can with a high degree of certainty regard a hole as being an oxygen hole, since $U_d > \Delta_{CT}$ (there is no contribution from the valence state $Cu^{3+}$), the manganites belong to an intermediate type. The wave function of the carrier in the manganites, owing to the relatively close values observed for $U_d$ and $\Delta_{CT}$ (e.g., according to Ref. 63, $U_d \approx 3.5-5$ eV, $\Delta_{CT} \approx 3-4.5$ eV) should contain comparable contributions from the states of the cations and anions. This mainly pertains to the $e_g$ states, which are hybridized with the *p* states of the $\sigma$ type. The states of the $t_{2g}$ electrons, on the contrary, are hybridized more weakly with the latter and thereby maintain their relatively localized nature. Therefore, the delocalization in $La_{1-x}A_xMnO_3$ with increasing *x* occurs via the bands of the $e_g$ orbitals. But whatever the type of carrier in manganates, it remains indisputable that their magnetic and conducting properties are the result of a competition between the localized and free behavior of the hybridized $e_g$ electrons.

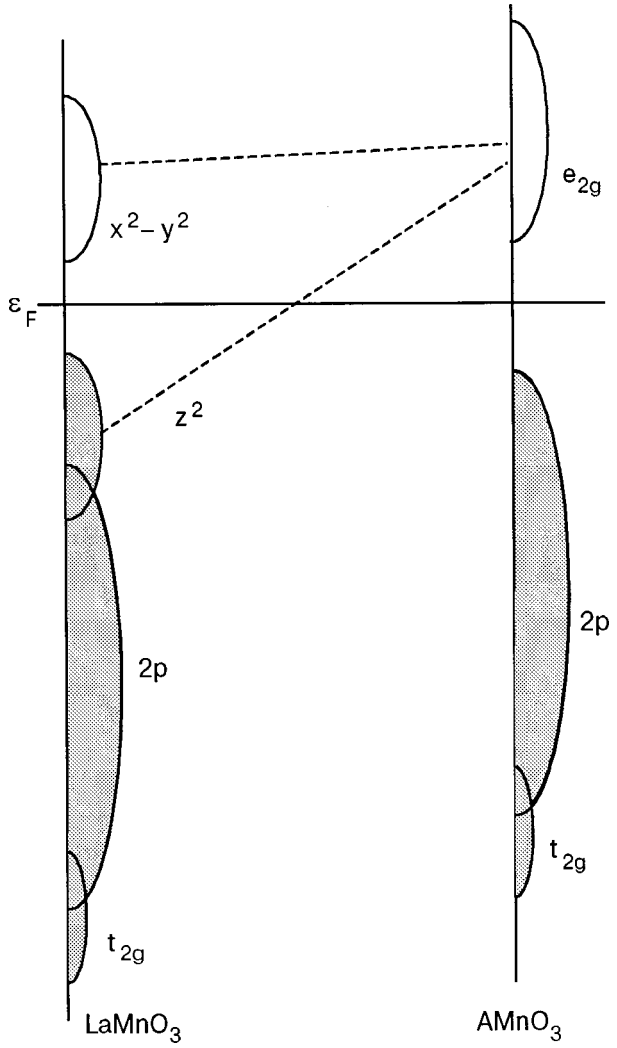


FIG. 9. Schematic diagram of the electronic density of states of undoped manganites. The shaded regions correspond to electron-filled bands. It is seen that the admixture of a divalent dopant to $LaMnO_3$ leads to the emptying of the $z^2$ band and its gradual merging with the $x^2-y^2$ band in $AMnO_3$, where these bands are degenerate.

### 3.2. Double exchange

Knowing or assigning the carrier type, it would seem to be extremely simple to transform in the standard way from the wave functions in the coordinate representation to the wave functions characterized by the wave vector **k**, which describe the motion of a free particle (carrier) in a translationally invariant medium. As we have said, however, the theory of the metal-insulator transition in manganites is not yet fully developed, although many details of their metallization have been explained (see Refs. 11, 53, 63, and 64). The difference between these compounds (and transition-metal oxides in general) and ordinary metals is primarily that many of the actual interaction parameters in them (see Paragraph 3.1), including the widths of the bands, belong to the same energy scale. At the same time, in metals and doped semiconductors the width $W \equiv 2tz$, where *z* is the number of nearest neighbors, is much greater than all the other interactions (electron-electron, between carriers and other excitations, etc.).

There is one more difference—the proximity of the electronic state of manganites and cuprates to the metal-insulator

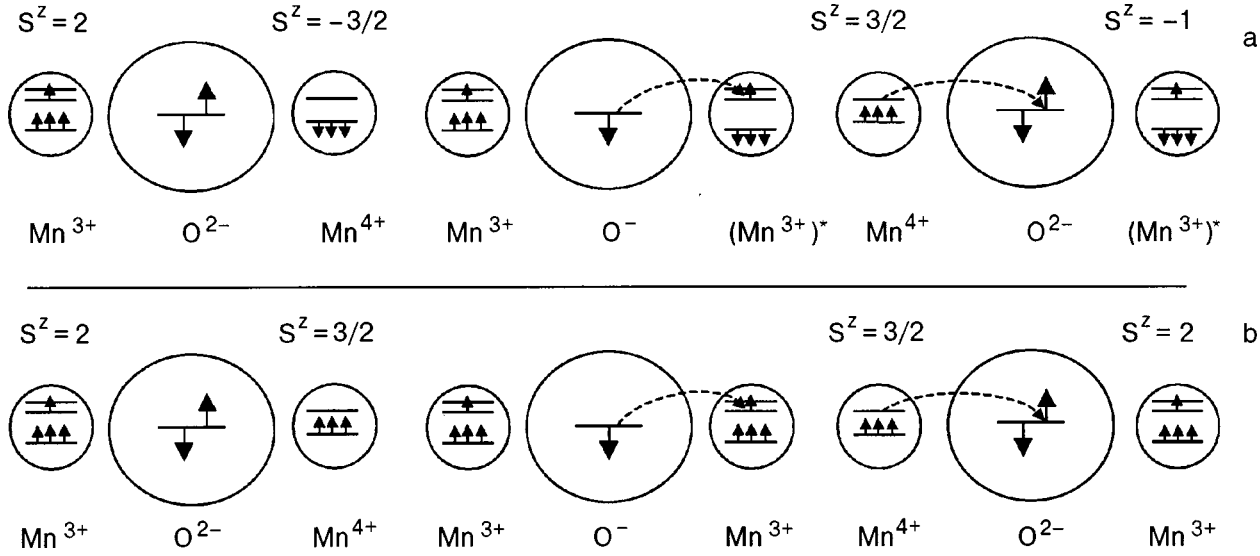


FIG. 10. Scheme of the two-step transfer on an electronic configuration (carrier) between transition-metal ions having opposite (a) or the same (b) spin directions. In both cases the inter-ion transition of an electron is allowed and is not limited by the conservation of spin, although in the first case one of the ions in the final state is in an excited $(Mn^{3+})^*$ state (nonresonant transfer) or else the transition is accompanied by the creation of a spin excitation in the crystal.

transition, which is the reason for the relatively low density of mobile carriers created exclusively by doping (besides the introduction of divalent ions for trivalent ions, sometimes superstoichiometric oxygen is used).[65]

Even taking into account these rather general and well-known circumstances, one must provide an answer to the following question: how can a carrier go from one transition-metal ion to another if it is located in an AFM medium? The transition of a carrier, whether an $Mn^{4+}$ hole in $LaMnO_3$ or an $Mn^{3+}$ electron in $AMnO_3$, always involves the charge exchange $Mn^{4+} \leftrightarrow Mn^{3+}$ (see Fig. 10). And if this transition occurs in an AFM ordered crystal between nearest neighbors with opposite orientations of the spins (Fig. 10a), then it inevitably leads to a final state of the other multiplet type, which, in accordance with Hund's rule and the large value of $J_H$, is highly excited. Thus in a collinear AFM the hole or electron is ''trapped'' [unless one assumes: i) motion over its own magnetic sublattice, or the participation of non-nearest neighbors, ii) the contribution of spin excitations, leading to incoherent transfer, iii) the influence of the spin-orbit interaction, which lifts the spin forbiddenness], since the transition to any neighboring transition-metal ion involved a large energy cost and therefore is substantially suppressed.

However, as was clearly established way back in Refs. 1 and 2, the conductivity and ferromagnetic moment of the system $La_{1-x}A_xMnO_3$ appear practically simultaneously on increasing $x$. More precisely, there is still a lack of complete clarity and reliable quantitative data as to whether one of these effects is attendant on the other or whether this is actually a simultaneous transition in terms of concentration and temperature. For this reason the temperature lines of the metallic and magnetic transitions are not distinguished in Fig. 8.

The question of the possible mechanism of the metallization of manganites was first raised by Zener[66] in an attempt to provide an interpretation for the results of Jonker and Van Santen. Zener considered the two characteristic situations for a moving carrier—for parallel and antiparallel spins of the $Mn^{4+}$ and $Mn^{3+}$ ions. Only the first corresponds to a resonant (without energy cost) transition, which occurs in two stages with the participation of the ligand (see Fig. 10b). Zener called this real inter-ion tunneling of a carrier *double exchange* in order to distinguish it from the superexchange interaction, where all the transitions of a carrier between ions are virtual. Superexchange can coexist with double exchange, at least on account of the $t_{2g}$ electrons, but the $e_g$ electrons can also contribute to it.

Ultimately, on a qualitative level the metallization of manganites has been interpreted as a self-consistent and carrier-induced rearrangement of the spins from the collinear AFM state to a saturated FM phase; this rearrangement lowers the energy of the system on account of the appearance of states corresponding to delocalized (free) carriers, or, what is the same, conduction bands of finite width. This interpretation presupposes the condition $J_H \gg W$, which leads to a strictly parallel arrangement of the spins of all the $t_{2g}$ and $e_g$ electrons within each ion.[9)]

Zener's arguments as to the stabilization of the metallic state through the establishment of FM order was based on one-electron transfer between a pair of ions; the problem for a crystal was first considered by de Gennes.[70] Using the results of Ref. 43 on the dependence of the double exchange on the angle $\theta_{\mathbf{n}} - \theta_{\mathbf{n}+\boldsymbol{\rho}}$ between the spin directions of the ions involved in the tunneling, $t_{\mathbf{n},\mathbf{n}+\boldsymbol{\rho}} = t\cos[(\theta_{\mathbf{n}} - \theta_{\mathbf{n}+\boldsymbol{\rho}})/2]$, he wrote an expression in the quasiclassical approximation for the energy $\varepsilon$ (per unit cell) of the homogeneous state $(\theta_{\mathbf{n}} - \theta_{\mathbf{n}+\boldsymbol{\rho}} = \theta)$ of a two-sublattice AFM with $x$ carriers:

$$\varepsilon = -\varepsilon(0)x\cos\frac{\theta}{2} + I_{AFM}zS^2\cos\theta, \tag{3.5}$$

where $\varepsilon(0)$ is the energy of the bottom of the conduction band, with a dispersion relation $\varepsilon(\mathbf{k}) = tz\gamma(\mathbf{k})$; $\gamma(\mathbf{k}) = z^{-1}\Sigma_\rho \exp(i\mathbf{k}\cdot\boldsymbol{\rho})$ is the structure factor; $z$ is the number of nearest neighbors from the other magnetic sublattice; $I_{AFM}$

$\equiv I_{\mathbf{n},\mathbf{n}+\boldsymbol{\rho}}$ is the interaction constant of the AFM superexchange interaction between the spins of $Mn^{3+}$ ions separated by a vector $\rho$. We see from (3.5) that the first term decreases and the second increases the energy, and the minimum energy corresponds to the value

$$\cos\frac{\theta}{2}=\frac{tx}{4I_{AFM}S^2}, \tag{3.6}$$

which leads to a FM moment $\mathbf{M}=2\mathbf{S}\cos\theta/2\sim x$, where $\mathbf{S}$ corresponds to the direction of the sublattice magnetizations.[10)] A simple estimate shows that the susceptibility remains the same as in the AFM state, and this agrees with the data of Ref. 49. In addition, the observed behavior of the canting angle as a function of $x$ is satisfactorily described by relation (3.6) in the interval $0.1\leqslant x\leqslant 0.2$. As a physically obvious result, expression (3.6) does not contain the FM exchange, although the latter sometimes determines the type of AFM structure that is realized (see Fig. 7). Here the slope of the curve of $\cos\theta/2(x)$ depends on $t$ and $I_{AFM}$, but not on $I_{FM}$, and it therefore cannot be estimated from the values of $W$ and $T_N$, since the latter contains contributions from both exchanges. It is probably unnecessary to repeat that a carrier introduced in the lattice by doping can move freely via sites having the same spin direction as the carrier. This indicates that in the existence region of the $A$ structure, $La_{1-x}A_xMnO_3$ should be a metal with a rather anisotropic (close to 2D) conductivity: the motion along the FM layers is free, while transverse motion is impossible.

It should be noted that in the AFM sublattices the canting angle (3.6) which is due to quasiparticles (i.e., to current or charge excitations), does not depend on the structure of the crystal, and the AFM exchange is the only factor resisting the complete collapse of the spin subsystem. In this sense relation (3.6) is reminiscent of the canting of the AFM sublattices in an external magnetic field, where the role of the latter is played by the product $tx$, while the critical (and, generally speaking, $T$-dependent) concentration for the ''spin-flip'' transition, $x_{\text{flip}}$, is determined by the point at which $\theta=0$.

There is an important difference, however: while the double exchange depends only on the first power of $\cos\theta/2$, the AFM exchange $I_{AFM}\sim\cos^2\theta/2$. If it were not for this difference, the energy (3.5) would not contain the competing terms that lead to the presence of a minimum. Moreover, since the external field, in inducing the FM moment, does not alter the conductivity of the initial (undoped) AFM system, the FM state (saturated or not) in the framework of the double exchange model can only be metallic. This is one of the factors that make the metal-insulator transition in manganites unique.[11)]

As a result of the onset of an angle not equal to $\pi$ between the sublattices, the system is no longer a completely ordinary metal: it is distinguished from the familiar FM metals (Fe, Co, Ni, etc.) by the presence of a conduction band with carriers of only one spin polarization, since the opposite one corresponds, as we have said, to the high-lying $d$ state of the transition-metal ion and, hence, to another band of this metal. Such conducting systems have been given the name *half metals*,[12)] which are already the subject of a wide literature (e.g., Refs. 47 and 72–74). These are members of the ''bad'' metals group (see Paragraph 3.4), for the description of which the standard theory has limited possibilities. Because of this non-Fermi-liquid behavior, the reasons for which remain essentially unclear, they are often considered strange objects. As an example, we note the following: it would seem that, under conditions of complete spin polarization, the carriers in a half metal at low temperatures should be described well by the Landau theory of a Fermi liquid. However, the optical conductivity of $La_{1-x}A_xMnO_3$ systems contains a large incoherent contribution, which depends on the frequency[75–77] and is evidence of the existence of a rather strong spin scattering of the carriers, which, as is stated in the review by Imada *et al.*,[64] contradicts the double exchange model.[13)]

Calculations of the canting angles in the framework of this model have been carried out for many specific situations. Essentially, however, these studies have not advanced beyond the de Gennes results on the gradual, smooth, and uniform variation of this angle. Reports that the double exchange can initiate the formation of a helical magnetic structure[78,79] have not been confirmed.[80]

More interesting is the recent paper by Van der Brink and Khomskii,[81] which raises the question of the ''charge'' asymmetry of the behavior of manganites with respect to their doping by holes and electrons. Using the de Gennes approach, those authors made use of the degeneracy of the $e_g$ orbitals of the manganites $AMnO_3$ (see Paragraph 2.2) in explicit form and generalized the double exchange model, representing its Hamiltonian by the expression [see (3.2)]

$$H_{DE}=H_{\text{ex}}-J_H\sum_{\mathbf{n},\lambda,\sigma}S_{\mathbf{n}}a^{+}_{\mathbf{n},\lambda,\sigma}\hat{\sigma}a_{\mathbf{n},\lambda,\sigma}$$

$$-\sum_{\mathbf{n},\boldsymbol{\rho}}\sum_{\lambda,\lambda',\sigma}t^{\lambda,\lambda'}_{\mathbf{n},\mathbf{n}+\boldsymbol{\rho}}a^{+}_{\mathbf{n},\lambda,\sigma}a_{\mathbf{n}+\boldsymbol{\rho},\lambda',\sigma}, \tag{3.7}$$

which hybridizes all the $e_g$ states ($H_{ex}$ is defined in (2.2) $\hat{\boldsymbol{\sigma}}$ is the Pauli matrix, and $\mathbf{S_n}$ refers to the low-spin state of the manganese ion $\mathbf{n}$). We note that, for the operator $H_{DE}$ in the form (3.7) the states of the ligands are assumed to be excluded, and this Hamiltonian must therefore be regarded as phenomenological, in which an inter-ion (between transition-metal ions) hop of electrons corresponds to their tunneling, while the spin-carrier interaction [the second term in (3.7)] corresponds to the operator of the Kondo lattice model.

Taking into account the symmetry relations between these effective transfer integrals $t^{\lambda,\lambda'}_{\mathbf{n},\mathbf{n}+\boldsymbol{\rho}}$ for $\{\lambda,\lambda'\}=\{x^2-y^2,z^2\}$ (Ref. 82), the authors of Ref. 81 were able to express the latter in terms of a single parameter $t$ and then, for the case $T=0$, to find the eigenenergies of the system and the equilibrium angles for AFM structures of types $A$ and $C$ (Fig. 7), which are observed in $Nd_{1-x}Sr_xMnO_3$ and $Pr_{1-x}Sr_xMnO_3$, respectively, near $1-x\leqslant 1$. The main theoretical result of Ref. 81 was the phase diagram of the electron-doped manganites in the variables $t-x$, although the fact that the JT character of the $Mn^{3+}$ ion was not taken into account in that study makes it to some extent open to criticism.

We conclude this Section with two remarks. The first concerns the assumption, made in the overwhelming majority of papers, that the free carrier moves via the transition-

metal subsystem. If this assumption is abandoned and an ''oxygen'' (in general, anion) concept is adopted, then the AFM order will no longer be an obstacle to the carrier motion,[12] and the causes of the ferromagnetism will again be an open question. It must be kept in mind, however, that the strong *pd* hybridization must necessarily ''switch on'' the states of the transition metal, and the double exchange model actually retains its conceptual basis in application to manganites.

The second remark pertains to the polarizing effect of the carriers on the AFM spins, which has been re-examined on more than one occasion after Zener (see Ref. 64) and, e.g., in the theory of the one-band Hubbard model is the subject of the Nagaoka theorem:[83] for $U_d=\infty$ and $T=0$ even a single carrier completely polarizes the spin subsystem along which it moves. A rigorous proof of this theorem for the more realistic case of a finite but small concentration of mobile charges has apparently never been given. Moreover, one can find analytical and numerical (as well as experimental) results which suggest that the FM state of a strongly correlated metal is not the lowest state, and that the AFM state cannot be spatially uniform here (see Sec. 4 below).

On the whole, one can state that the investigation of the phase diagrams of manganites continues, but there is no longer any real hope that the double exchange model in its simplest form (in particular, the role of the JT doubling of the $LaMnO_3$ lattice (see Fig. 5) in the metallization process has not been sufficiently studied) can serve as a basis for even a qualitative, much less a quantitative, description of the observed features of the metallic states of these compounds.

### 3.3. The role of lattice deformations and the Jahn–Teller effect

Thus the initial AFM order is one of the factors that do not allow a carrier to move freely along the lattice in lightly doped manganites. Another, no less important factor, is the JT character of the $Mn^{3+}$ ion in a cubic crystalline field. Although this property of the $Mn^{3+}$ ion is well known,[36,84] for quite a long time it was not considered to have any relevance to the CMR effect. The first to invoke the JT effect in the description of the electric and magnetic properties of manganites were Millis, Littlewood, and Shraiman[85] (see also Ref. 51), which showed that the use of the double exchange model alone leads to appreciable quantitative disagreement between the calculated and measured quantities (particularly of the resistance in the vicinity of $T_C$).

The treatment in Ref. 85 was based on the simplest one-band Hamiltonian of the double exchange model (essentially corresponding to the Kondo lattice Hamiltonian [see (3.7)] for $\lambda=\lambda'=z^2$). After calculating the effective FM exchange, those authors estimated the Curie temperature of $La_{1-x}Ca_xMnO_3$; in particular, for $x\approx 0.2$ and $t\approx 0.2$ eV the Curie temperature has the value $T_C=tzx\approx 0.25$ eV,[14] which is practically an order of magnitude greater than the values known from experiments, $\sim 10^2$ K (see Fig. 8). In addition to the estimates of $T_C$, that paper also gave a calculation of the contribution of spin fluctuations (for $S=3/2$ they were considered in the framework of a classical approach) to the electrical resistance of the system in the double exchange model, and it was concluded that they are incapable of causing the observed drop in the electrical resistance $R_H(T)$ near $T_C$ in an external magnetic field **H**. Moreover, in such an approach the value of $R_0(T)$, even for $T$ somewhat less than $T_C$, continues to grow before starting to fall. And although the function $R_H(T)$ on the whole reflects the experimental picture in a qualitative way, neither the value of $R_0(T_C)$ (the difference is several orders of magnitude) nor the field dependence of $R_H(T_C)$ is reproduced. As a result, it was concluded in Ref. 85 that it is necessary to look for fundamentally new mechanisms for the CMR, and a deformation mechanism based on the JT effect was proposed as a possible candidate.

That paper launched a new stage in the study of the CMR of manganites by making use of the concepts of static and dynamic JT instabilities, JT polarons and bipolarons, virtual phonon exchange between carriers, band insulators (the band insulator model can in principle be used to describe the ground state of the undoped compound $LaMnO_3$ with allowance for the JT doubling of its lattice).[15–22,75–77,86–99] The influence of the vibrational degrees of freedom on the transport and magnetic properties of manganites became even more obvious after the discovery of the *colossal isotope effect*, or the shift $T_C(^{16}O)-T_C(^{18}O)\approx 20$ K, in various La–A–Mn–O compounds upon the total substitution $^{16}O\leftarrow{}^{18}O$ (Refs. 100 and 101).

The necessity of taking into account the local restructuring of the lattice is already evident in relations (3.3) and (3.4). In fact, despite the aforementioned large percent covalent character of the bond in the ion-ion interaction in manganites, each hop of a carrier between sites occupied by transition-metal ions causes a local change in the valence (charge fluctuation), which is ''sensitive'' to the completely symmetric (breathing) mode $A_g$ (which is ordinarily ignored on account of its high frequency), and also an entangling of the $e_g$ states due to the twofold degenerate quadrupole (shear) mode $E_g$ (Refs. 13, 14, and 23). In both cases the characteristic modes of the octahedra are meant.

The corresponding phenomenological interaction operator of such a carrier, belonging to the subsystem of transition-metal ions, with local deformation-related displacements of the ligands can be written in the form[86–88]

$$H_{JT}=g_{JT}\sum_{\mathbf{n},j=1,2}\left[\sum_{\lambda,\lambda',\sigma}a^{+}_{\mathbf{n},\lambda,\sigma}Q^{\lambda,\lambda'}_{\mathbf{n}}(j)a_{\mathbf{n},\lambda',\sigma}+\frac{\kappa_{JT}}{2}Q^2_{\mathbf{n}}(j)+\frac{M_{JT}}{2}\dot{Q}^2_{\mathbf{n}}(j)\right], \tag{3.8}$$

where $g_{JT}$ is the elastic *JT* interaction constant, $Q_{\mathbf{n}}(j)$ is the operator of the $j$th normal mode of the *JT* vibrations of the octahedra (in the first term the notation indicates that $Q_{\mathbf{n}}(j)$ is a matrix in the space of the doublet $e_g$) at site **n**, and $\kappa_{JT}$ and $M_{JT}$ are their elastic constant and reduced mass.

The Lang–Firsov shift transformation (see Ref. 102) can eliminate from the operator $H_{\text{eff}}=H_{JT}+H_{DE}$ the trilinear interaction [the first term in Eq. (3.8)], which in the mean-field approximation for the lattice renormalizes the double-exchange integral: $t\to t\exp[-\lambda^2_{JT}(1+2n_{JT})]\equiv t_{JT}\ll t$ ($\lambda_{JT}=g_{JT}/\Omega_{JT}$ is the dimensionless *JT* coupling constant, and $n_{JT}$ is the average number of *JT* phonons with frequency

$\Omega_{JT}=\sqrt{\kappa_{JT}/M_{JT}}$). We see that the width of the band, $W_{JT}=2t_{JT}z$, depends on $T$ as a result of the polaron narrowing (even without allowance for the spin degrees of freedom); here an inhomogeneous distribution of angles of rotation of the spins near the carrier is also possible.[103] Thus, in a crystal a carrier becomes a charged *magnetoelastic polaron*, or a phonon- and magnon-dressed carrier, and these dressings directly influence the effective mass; the double exchange model is thereby generalized to include both the static displacements of the ions and the rotations of their spins.

The self-consistent calculation of the average magnetizations of the localized and delocalized subsystems (or one of these and the angle $\theta$) demonstrates[86,87] that the experimental and theoretical data can agree only in the case of a sufficiently large constant $\lambda_{JT}(\geqslant 1)$, and the dependence of the latter on the mass $M_{JT}$ also permits a consistent interpretation of the colossal isotope effect. Analysis of the various regimes in those papers showed that for low $T$ and $x\geqslant 0.2$ the system is always a FM metal. However, its behavior in the region of high $T(\sim T_C)$ now depends on $\lambda_{JT}$, and only for $\lambda_{JT}>1$ is the transition through $T_C$ accompanied by a maximum on the $R_0(T)$ curve and its rather rapid drop if $\mathbf{H}\neq 0$.

These and other studies (including experimental ones) give convincing evidence that an integral part of the CMR effect in manganites is some manifestation of the coupling of the carriers with the lattice. However, the value $g_{JT}$ of this coupling, its dependence on $x$ (which can be very substantial), and even the sign of the charge remain among the unanswered questions. Moreover, as we have said, the appearance of carriers in the lattice leads to pseudo-*JT* ions $Mn^{3+}$, and therefore the expectation of a too-large constant $\lambda_{JT}$ and large *JT* deformations is problematical. True, one can't help but notice that in aggregations (or clusters) of *JT* ions the corresponding lattice deformations should be collectivized. In other words, if it is assumed that valence-inhomogeneous states can form, then the elastic energy advantage in them can already be significant.

There is one more difficulty—the thermal stability of polarons, which is a nearly universal assumption in the theoretical works (see Refs. 86–88, and 99), can scarcely be ensured even in the region near $T_C$, where the energy $g_{JT}^2/\Omega_{JT}$ of the *JT* coupling is apparently slightly above $10^2$ K. Moreover, there is experimental evidence that as $x$ increases, the *JT* distortions rapidly vanish[92] and that the FM ordering also suppresses them strongly.[90]

The specifics of manganites are such that not only the JT deformations affect the width of the conduction band; additional narrowing occurs on account of the increasing average amplitude of the thermal rotations of the octahedra ($t\sim\cos\varphi$,[25,43] where the difference $\pi-\varphi$ corresponds to the angle between the directions of the nearest Mn–O bonds containing a common ligand), and also expansion of the lattice (recall that the Grüneisen coefficient in manganites is anomalously large).[18,19] All of this also promote localization of the carriers with the formation of polarons, the lifetime of which should decrease on account of their thermal decay (the thermally activated transition to the free band state).

To summarize, one has to acknowledge that the uniting of the *JT* deformation and the double exchange has advanced considerably our understanding of transport phenomena in manganites (see, e.g., Refs. 51 and 95). At the same time, it can hardly be regarded as conclusively proven that these deformations are critical for the CMR effect. Such a peak of $R_0(T)$ accompanies the magnetic phase transition in many FM semiconductors[104] that do not contain any kind of JT ions. Therefore, we believe that the kinetics of the carriers in a deformable and magnetically fluctuating medium requires further study.

### 3.4. Impurity states in manganites

Formally neither the AFM nor the JT effect can impede the free propagation of a carrier through an ideal crystal, provided that one is not interested in the width of the corresponding conduction band (or the effective mass of the carrier). And if one remains within the conceptual framework of the double exchange model (with or without allowance for vibrations), it is impossible to understand why a hole located in the magnetic *A* structure of $LaMnO_3$ will not be free, at least within the FM planes at $T\to 0$. The answer is actually simple: it is localized in the attractive Coulomb field of the dopant, as was mentioned by de Gennes back in Ref. 70 (see also Ref. 95). As $x$ increases from zero it is impossible to pass through a phase of localized electronic states. No less important, however, is the fact that each carrier in doped oxides has ''its own'' dopant, and this, in turn, indicates that oxides (manganites, HTSCs) are bad metals, for in them $k_F\overline{r}_{\rm dop}\sim 1$ (where $\overline{r}_{\rm dop}\sim x^{-1/3}$ is the average distance between dopants, and $k_F$ is the Fermi momentum), whereas even in ''dirty'' ordinary metals this quantity is much greater than unity.

Let us consider an isolated dopant $A^{2+}$ substituting for $R^{3+}$ in the $RMnO_2$ lattice (see Fig. 11). In the simplest approximation one can assume that the Coulomb potential of the $A^{2+}$ ion will influence only its nearest neighbors, the levels of which will be shifted by an amount $-\Delta\varepsilon_{\rm Coul}$ relative to the levels of the other ions of the matrix. The hole can move without impediment over each FM square in the first coordination sphere of the *A* structure, even when the local JT distortion at each of the sites is taken into account;[15] here this distortion is ''symmetrized,'' taking on a collective character. We note that if $t_{JT}\gg\Omega_{JT}$ then the lattice will respond to the motion of the hole only adiabatically, remaining in a practically static deformed state.

The motion of a carrier over the four sites splits its level into three: two nondegenerate, with energies $-\Delta\varepsilon_{\rm Coul}\pm 2_{JT}$, and a twofold degenerate level with energy $-\Delta\varepsilon_{\rm Coul}$. If it is taken into account that $t_{JT}\geqslant 0.1$ eV,[39,62] then only the lowest level, with energy $-\Delta\varepsilon_{\rm imp}\equiv\Delta\varepsilon_{\rm Coul}-2t_{JT}$, will actually be occupied. Its twofold (with respect to the number of squares) degeneracy is lifted by the double exchange, with the result that a local FM moment $m_{\rm imp}=2\langle S^Z\rangle\cos\theta_{\rm imp}/2$, arises, for which the condition $\cos\theta_{\rm imp}/2=t_{JT}/I_{\rm AFM}$ will hold, where $I_{\rm AFM}$ is the only exchange having AFM sign that exists between the FM ordered planes in the *A* structure,[16)] and the $z$ axis is chosen along the initial AFM vector. It is quite likely that by virtue of the strong inequality $t_{JT}\gg T_N$ a saturated (or nearly saturated) FM state ($\theta_{\rm imp}\approx 0$) of the center arises, and the observed canted phase (see Ref. 25) is only a consequence of the anisotropic ex-

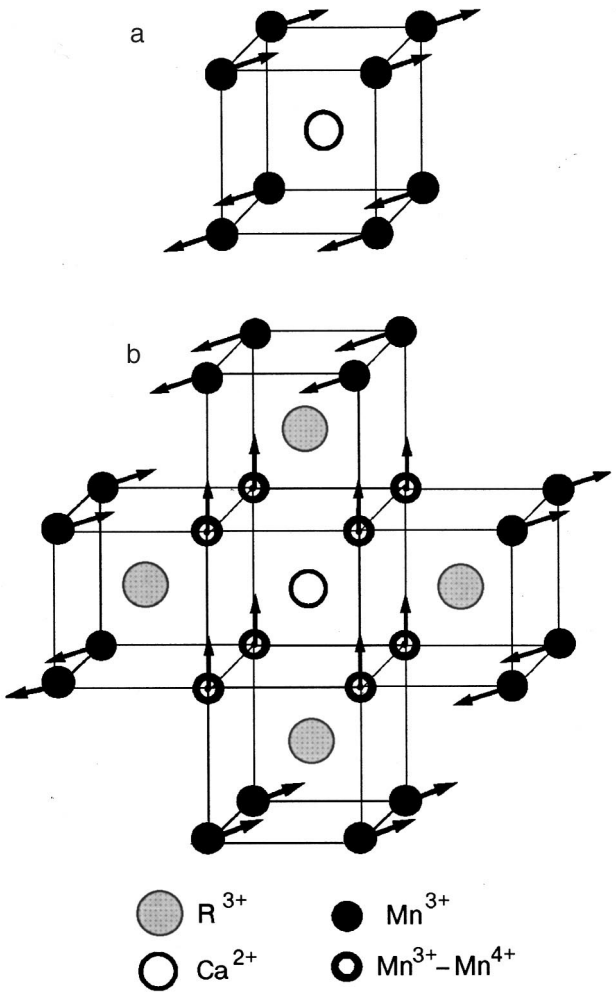


FIG. 11. Directions of the perturbed manganese spins nearest to the $A^{2+}$ ion in $R_{1-x}A_xMnO_3 (x \ll 1)$ without (a) and with (b) allowance for the double exchange (for completeness of the picture, in the second case the spins of the nearest-neighbor environment are also indicated). The orientation of the impurity magnetic moment formed (microferron spin) is isotropic in the plane perpendicular to the AFM vector of the matrix.

change interaction inherent to the orthorhombic structure of $LaMnO_3$.

It is easy to see that each such center (in Nagaev's terminology, ferron,[105] and in the given case, *microferron*) is found in a zero mean exchange field produced by the unperturbed spins surrounding it. The subsystem of these randomly distributed centers in a regular lattice, owing to the indirect (for $x \ll 1$) alternating-sign interaction through the spin excitations of the matrix must necessarily form (against the background of the long-range AFM order) a spin-glass phase[106] (see also the review[107]), the existence of which in manganites with $x \leqslant 0.1$ at sufficiently low temperatures has been reported more than once.[27,108,109]

If we once again restrict consideration to small values of $x$ and to the $A$ structure corresponding to them, the conduction band will be two-dimensional. In this case any ionic level shifted by a finite amount (this also pertains to the deformation shift) creates in the crystal a local (one-impurity) electronic state with energy

$$\varepsilon_{\rm imp} = -W_{JT}^{2D} \exp(-W_{JT}^{2D}/\Delta\varepsilon_{\rm imp}), \tag{3.9}$$

where $W_{\rm JT}^{\rm 2D}$ is the width of the this band with allowance for the $JT$ renormalization. Thus an electronic state localized near a charged dopant has a radius

$$r_{\rm el} = a\sqrt{W_{jT}^{2D}/\varepsilon_{\rm imp}} \tag{3.10}$$

($a$ is the lattice constant). In the case of manganites, however, there is another impurity radius—the magnetic radius—which specifies the inhomogeneous distribution $\theta(r) = 1/2(\pi - \theta_{\rm imp})\exp(-r/r_{\rm mag})$ and is related only to the exchange interactions.[107] The relationship between $r_{\rm el}$ and $r_{\rm mag}$ determines which transition, the metal-insulator or FM-AFM, will occur first as the doping is increased. Clearly, for $r_{\rm el} > r_{\rm mag}$ this will be the first of these transitions, while in the opposite case it will be the second. And, since many experiments (e.g., Ref. 26; see also Refs. 25 and 35) indicate the existence of a narrow region of concentrations $x$ for which a FM insulator exists (see Fig. 8), the scale of $r_{\rm mag}$ is apparently somewhat larger than that of $r_{\rm el}$. In practice, however, it is ordinarily assumed that the two transitions, the magnetic and electronic, occur simultaneously, especially when one is talking about a finite temperature at a constant composition; that corresponds to the assumption that these scales are similar, making the transitions close together.

Following Refs. 106, 107, and 110, it is easy to write the critical concentration of the transition from the insulating to the metallic state. This transition and the corresponding abrupt change in the electronic resistance of the system occur when $x$ reaches a value $x_{\rm MI} = (a/r_{\rm el})^2$, where the radius $r_{\rm el}$ is given in (3.10). From the observed value of the concentration $x_{\rm MI} \approx 0.16$ (Refs. 50, 90, 95, and 111), we find $r_{\rm el} \approx 2.5a$, or, in other words, the electronic impurity states of the manganites must be classified as rather *deep states* on the energy scale, and on the spatial scale, as states of *small radius*, which begin to overlap only at relatively high dopant concentrations.[17)] Of course, it is rather easy to satisfy the inequality $r_{\rm mag} > r_{\rm el}$ here, and indeed the magnetic transition to the FM insulator phase can slightly precede the metal-insulator transition in concentration. This, in turn, means that the magnetic impurity states already overlap in the FM system, but each hole moves within the confines of its own cluster.

For $x = x_{MI}$ the overlap of the wave functions of the electronic impurity states reaches a value such that a metal-insulator transition occurs, free carriers arise, and a Fermi level is formed in the metallic phase.[110] However, even then a portion of the carriers occupying the deep levels near and below the bottom of the conduction band continue to remain in localized states (localized at fluctuational aggregations of dopants[104,110]). Most likely this is the reason why an appreciable number (up to 20%)[98] of localized (i.e., not participating in transport) carriers are observed in the metallic phase, along with local deformations that are peculiar to the insulating phase.[92,113,114]

Knowing the values of $x_{MI}$ and $r_{\rm el}$ and using the known value of the band width $W \sim 1$ eV,[39,62] we obtain the value $|\varepsilon_{\rm imp}| \approx 0.1$ eV, which turns out in fair agreement with the values obtained for the activation gaps from measurements of the thermopower;[3,94] this is generally consistent with the assumption of the existence of localized states contributing to the thermally stimulated transfer of energy and charge.

The metal-insulator transition in manganites is also rather peculiar in that the system as a whole goes from a 2D AFM insulator to a 3D ferromagnet metal. Its inherent FM properties (magnetic susceptibility, the spectra of spin excitations, their relaxation, magnetization processes, etc.) are important areas of study in the physics of manganites. For example, the spin-wave band is well established, $\Omega_{sp}^{FM}(q) = \Omega_{gap} + Dq^2$, with $\Omega_{gap} = 0.35-0.75$ meV,[89] 2 meV,[115–117] and $D = 130-188$ meV,[89] the width of which in the calculations for the case $T=0$ is determined by a single parameter $t$ (or $t_{JT}$). It determines the intensity of the interaction of spin excitations with the carriers and is thus a characteristic of one of the sources of electrical resistance in the metallic phase of these compounds.

In regard to the problems of the transition of manganites from the FM to the paramagnetic (PM) phase, it should be noted that because of the presumably strong coupling of the electronic and vibrational degrees of freedom in them this transition may easily be first-order (as was reported in Refs. 91 and 118), and for that, rather trivial, reason.

Actually the same picture of the formation of the impurity state should be preserved if one is considering a low concentration of La in $AMnO_3$, or for $x \to 1$ in the compounds $La_{1-x}A_xMnO_3$. The difference lies in the structure of such a center, which no longer has a layered structure, since the surrounding ions of the matrix form a simple AFM structure of the $G$ type (Fig. 7). In this case a FM moment is apparently not formed, because, as we have said, it would be necessary for a single carrier to keep a relatively large AFM cluster in the FM state (we recall that the inter-ion hopping matrix element $t$ is also subjected to a $JT$ reduction to $t_{JT}$), and it may be that the metal-insulator transition in the region of electron-doped manganites cannot be brought about. Actually, it is confirmed by the experiment that the system $La_{1-x}A_xMnO_3$ in the composition interval $0.5 \leqslant x \leqslant 1$ remains in the nonconducting phase.

Returning to the half metal ($0.16 \leqslant x \leqslant 0.5$), we note that the quasiparticle excitations at the Fermi level in it are always damped on account of the scattering of carriers on the strongly fluctuating regions of short-range order (including microferrons) near $T_C$. However, the detailed dependence of this residual (for $T \to 0$) damping or (which is the same) resistance in manganites on the dopant concentrations, magnetization, and external magnetic field has not been investigated, as far as we know.

A somewhat different approach to the problem of the CMR, but which is also based on the presence of defects in the crystal, was developed by Nagaev,[104,119] who finds a close analogy between manganites and degenerate FM semiconductors in which a portion of the collectivized electrons, interacting with static fluctuations of the density of ionized donors, can be trapped by localized states. The remaining carriers undergo only scattering. If the system on the whole is magnetic, then, on the assumption that the free carriers and localized spins of the magnetic ions form different subsystems, it is asserted that the decay of the magnetic order in the neighborhood of impurities that scatter carriers will be slowed.[18)] Moreover, increasing the temperature up to a certain point even increases the scattering intensity, and consequently $R_0(T)$ increases. Increasing $T$ further, however, eventually leads to the complete destruction of the FM regions, with the result that the resistance begins to fall off, and a maximum appears on the $R_0(T)$ curve in the critical region. Ultimately, it is concluded that the CMR effect itself is due entirely to the presence of static disorder caused by the various impurities (not only dopants). Finally, Gor'kov (see Ref. 95) analyzed a percolation mechanism for the metallization and CMR of manganites as inhomogeneous solid solutions and showed that approach also to be consistent with the available experimental data.[19)]

This result will be confirmed or refuted by further study; however, one cannot help but notice that the experiments in which record values of the CMR have been observed in manganite films have used extremely imperfect films with high defect densities. Nevertheless, the almost total neglect of the many peculiar features of manganites in these approaches makes their implication somewhat difficult to check.

### 3.5. Pseudospin (Hubbard) operators in the description of manganites

Starting with the paper by de Gennes[70] and the later paper by Kubo and Ohata,[69] the electric and magnetic properties of manganites have been described using the *sd* exchange model of Vonsovkii, Shubin, and Kasuya (see Ref. 120). However, unlike the limiting case $t \gg J_H$ studied in those papers, which leads to the Kondo effect, manganites represent an example of real objects for which the opposite inequality holds. That inequality corresponds to the complete fine tuning of the spin of the ''free'' carrier to the spin of the core, $S_{core}$, since they always maintain complete mutual ferromagnetic collinearity ($J_H < 0$). In the case of manganites the free carrier is assumed to be that which moves via the $e_g$ states (degenerate or otherwise), while the spin $S_{core}$ is formed from the spins of the electrons of the half-filled $t_{2g}$ multiplet or is just the spin $S = 3/2$ of the $Mn^{4+}$ ion. Here the temperature behavior of the spins of the free carriers and that of the carriers united into the core are often treated independently (see, e.g., Refs. 69, 85 and 121–124), even though the strong Hund exchange in the framework of the Kondo model makes the assumption of their independence somewhat artificial, since the state $Mn^{3+}$ can be considered to be one of the basis states in the sequence $Mn^{2+}, Mn^{3+}, Mn^{4+}$. Therefore, the so-called free electron should not even adiabatically follow the spins of the core, and it would seem that the states of the ions should determine (in the case of narrow-band metals such as manganites) the form of the Hamiltonian corresponding to the motion through the crystal not of the true carriers, like *s* electrons, but of ionic states.

Such a Hamiltonian is not difficult to write on the phenomenological level in the tight-binding approximation, by introducing pseudospin operators, which have been used successfully in the theory of excitons in magnetic insulators.[125] These pseudospin operators can be constructed for any spin and number of states, but to avoid being burdened by the details (generalization is awkward but does not present any fundamental complications), let us consider an idealized version.

Let the ion have two nondegenerate levels 1 and 2, which in the AFM insulator phase are occupied by two electrons in such a way that the total spin of the ion is $S = 1$

(projections $M_S=\pm 1,0$). The appearance of a hole means that the higher-lying (by assumption) state 2 is emptied, and therefore $S_{\rm core}=1/2$ (its projections $\sigma=\pm 1/2$). We introduce pseudospin operators according to the definitions

$$X_{\mathbf{n}}^{1,1/2}=|1\rangle_{\mathbf{n}}\langle 1/2|,\quad X_{\mathbf{n}}^{0,\overline{1/2}}=|0\rangle_{\mathbf{n}}\langle -1/2|, \tag{3.11}$$

which formally couple all of the existing configurations with different numbers of electrons and thereby change the multiplet type of the ions. Among the pseudospin operators are those which lead to the creation of a singlet two-electron state, the inclusion of which would expand the basis (3.11), meaning only that a ''non-Hund'' state, i.e., the finiteness of $J_H$ in comparison with $t$, is taken into account. The commutation relations for the pseudospin operators belonging to the same site follow directly from their written form [see (3.11)], while the commutation relations for those belonging to different sites, as one would guess, are of the Fermi type. In this sense the pseudospin operators are similar to the Hubbard operators, which are also used in a similar model. Their commutation relations with the spin operators are easily written from the action of operators in the bracket representation: $S_{\mathbf{n}}^{+}=\sqrt{2}(|1\rangle_{\mathbf{n}}\langle 0|+|0\rangle_{\mathbf{n}}\langle -1|)$, etc.

Actually, the simplest effective Hamiltonian of the double exchange model for electrons realizing transitions between ions of different AFM sublattices and, hence, with different characteristic quantization axes, can be represented by the expression [see Eq. (3.2)]

$$H_{DE}=-t\sum_{\mathbf{n},\rho}\sum_{\sigma}\left(\cos\frac{\theta_{\mathbf{n}}-\theta_{\mathbf{n}+\rho}}{2}a_{\mathbf{n},2,\sigma}^{+}a_{\mathbf{n}+\rho,2,\sigma}+\sin\frac{\theta_{\mathbf{n}}-\theta_{\mathbf{n}+\rho}}{2}a_{\mathbf{n},2,\sigma}^{+}a_{\mathbf{n}+\rho,2,\overline{\sigma}}\right), \tag{3.12}$$

where $\overline{\sigma}=-\sigma$. Now writing the eigenfunctions (with $H_{DE}$ not taken into account) $\psi_{\mathbf{n}}^{S,M_g}$ in the form $\psi_{\mathbf{n}}^{1,1}=a_{\mathbf{n}1\uparrow}^{+}a_{\mathbf{n}2\uparrow}^{+}|0\rangle$, etc., and $\psi_{\mathbf{n}}^{S_{\rm core},\sigma}$ in the form $\psi_{\mathbf{n}}^{1/2,1/2}=a_{\mathbf{n}1\uparrow}^{+}|0\rangle$, etc. (noninteracting ions), we easily transform the operator (3.12) to

$$H_{DE}=-t\sum_{\mathbf{n},\boldsymbol{\rho}}\left[\cos\frac{\theta_{\mathbf{n}}-\theta_{\mathbf{n}+\rho}}{2}(X_{\mathbf{n}}^{+}X_{\mathbf{n}+\boldsymbol{\rho}}+Y_{\mathbf{n}}^{+}Y_{\mathbf{n}+\boldsymbol{\rho}})+\sin\frac{\theta_{\mathbf{n}}-\theta_{\mathbf{n}+\boldsymbol{\rho}}}{2}(X_{\mathbf{n}}^{+}Y_{\mathbf{n}+\boldsymbol{\rho}}+Y_{\mathbf{n}}^{+}X_{\mathbf{n}+\boldsymbol{\rho}})\right], \tag{3.13}$$

$$X_{\mathbf{n}}^{+}=X_{\mathbf{n}}^{1/2,1}+X_{\mathbf{n}}^{\overline{1/2},0}/\sqrt{2},$$

$$Y_{\mathbf{n}}^{+}=X_{\mathbf{n}}^{\overline{1/2},\overline{1}}+X_{\mathbf{n}}^{1/2,0}/\sqrt{2},$$

which, according to (3.12), describes transitions of a carrier between all possible spin sublevels of two ions found in different Hund valence states.

The Hamiltonian $H_{DE}$ of the inter-ion hops must be supplemented by the single-ion energy operator [see (3.1)], which in the present case has the form

$$H_{SI}=(\varepsilon_2-\varepsilon_1)\sum_{\mathbf{n},\sigma}P_{\mathbf{n}}(\sigma), \tag{3.14}$$

and the exchange interaction operator (2.3) which, however, must take into account the two spin states of the ion:

$$H_{\rm ex}=\frac{1}{2}\sum_{\mathbf{n},\boldsymbol{\rho}}(J_{\mathbf{n},\mathbf{n}+\boldsymbol{\rho}}^{1,1}\mathbf{S}_{\mathbf{n}}\cdot\mathbf{S}_{\mathbf{n}+\boldsymbol{\rho}}+J_{\mathbf{n},\mathbf{n}+\boldsymbol{\rho}}^{1/2,1/2}\sigma_{\mathbf{n}}\cdot\sigma_{n+\boldsymbol{\rho}}). \tag{3.15}$$

The operator $H_{SI}$ in (3.14) does not contain the Hund exchange, which in a number of papers has been considered as the source of the interaction of the mobile carrier with the spin of the core, while the operator in (3.15) does not contain the static exchange interaction of mobile holes with the surrounding spins, which is provided by the double exchange.[20] On the other hand, the energy difference $\varepsilon_2-\varepsilon_1$ between the eigenstates of the ion must necessarily include both its Hund constant (which was mentioned in Ref. 95) and its Coulomb (Hubbard) constant, and thus in the pseudospin representation the single-ion Hamiltonian $H_{SI}$ has the diagonal form that is usual even for the multiband Hubbard model.

Indeed, the operator $P_{\mathbf{n}}(\sigma)$ in (3.14) is the projection operator onto the doublet state with spin projection $\sigma$. The operators $P_{\mathbf{n}}(M_S)$ for the spin triplet can be specified in an analogous way. Together they satisfy the natural ''conservation law'':

$$\sum_{M_S}P_{\mathbf{n}}(M_S)+\sum_{\sigma}P_{\mathbf{n}}(\sigma)=1, \tag{3.16}$$

since (by definition) the ion does not have any other eigenstates. Besides condition (3.16), it would seem very well justified to assume that there are also ''partial'' restrictions making it possible to relate the average of the projection operators with the carrier density $x$ in the system, specifically: if, as occurs in the manganites $R_{1-x}A_xMnO_3$, the carrier (hole) creates an ionic state with a lowered value of the spin, then it is clear that the following inequalities must be satisfied [see (3.16)]:

$$\left\langle\sum_{\sigma}P_{\mathbf{n}}(\sigma)\right\rangle=x,\left\langle\sum_{M_S}P_{\mathbf{n}}(M_S)\right\rangle=1-x, \tag{3.17}$$

where $\langle ...\rangle$ denotes configurational and thermodynamic averaging.

The same relations (3.17) are actually valid for the operator of the longitudinal (in the local coordinate systems) spin projections: $\langle\sigma_{\mathbf{n}}^{Z}\rangle=x\langle\sigma^{Z}\rangle_T$ and $\langle S_{\mathbf{n}}^{Z}\rangle=(1-x)\langle S^{Z}\rangle_T$, from which we obtain the spin projection averaged over the crystal: $S_{\rm av}^{Z}=x\langle\sigma^{Z}\rangle_T+(1-x)\langle S^{Z}\rangle_T$, which is identical to the value obtained by another method in Refs. 69 and 85. It determines the magnetization of the crystal, the dispersion relation of the two (according to the number of spins; see also Ref. 127) branches of spin excitations, and also the shift ($\sim S_{\rm av}^{Z}$) of the bottom of the conduction band.

What is important for the carriers, however, is not so much the shift of the edge of the conduction band but the behavior of its width $W$ (or $W_{\rm JT}$), which also changes at the Curie point, and this change can be of a critical character. Indeed, according to the commutation relations of the pseudospin operators (3.11), the projection operators and their averages become factors on which the value of $W$ depends (see Ref. 125). This means that the latter is a function not only of $\langle S^{Z}\rangle_T$ as a spin-wave band, but also of $\langle(S^{Z})^2\rangle_T$, $\langle(S^{Z})^3\rangle_T$, etc. Here the averages of even powers, which are nonzero even in the PM phase, allow the carrier to move in the region of the spin-disordered state, although the value of $W$ in it will be substantially smaller. At the point $T_C$ and in

its close proximity the averages of the odd powers of the spin operators, including the first power (the magnetization), begin to arise in a critical manner. Here the width of the conduction band increases rather sharply, and it is not ruled out that a tendency of the carriers toward localization at impurities or polaron levels specifically in the fluctuation region gives way to a tendency toward their free motion, i.e., in places where the influence of the external magnetic field is particularly strong. This is important, since in the interpretation of the experimental transport data the temperature behavior of the band width is ordinarily ignored, and it is assumed (see review[128]) that $W$ can depend only on the composition of the system and the tolerance factor.

The above-described dynamics of the carrier motion in a magnetic medium has not yet been investigated, and therefore the foregoing discussions are basically qualitative. However, the applicability of the pseudospin operators in the theory of magnetic narrow-band metals, including various kinds of statistical models,[129] is not in doubt.[21)] Transitions between different spin sublevels of the ionic basis in a half metal are brought about through the participation of spin excitations (magnons), by introducing into the theory an interaction of the latter with the carriers. In this case it is not small, being determined by the same matrix element [see (3.13)] as the band width itself. In addition, one can in principle include JT deformations and local (impurity) Coulomb fields in the Hamiltonian of the system, although the problem then becomes extraordinarily difficult, and a completely consistent treatment on the whole scale is scarcely feasible at the present time.

## 4. NONMAGNETIC TYPES OF ORDERING IN MANGANITES

In the paper by Wollan and Koehler,[49] which we have cited in several places previously, in addition to the types of spin ordering in the manganite lattices, it was noted that the diffraction patterns of some $La_{1-x}Ca_xMnO_3$ samples with relatively large $x \geqslant 0.5$ exhibited superstructural peaks unrelated to the magnetism. Then Goodenough proposed a qualitative explanation based on the mutual ordering of the $Mn^{3+}$ and $Mn^{4+}$ ions.[36] Moreover, it was pointed out that charge order of this kind is inextricably linked to another type of order—orbital, one example of which is clearly seen in Fig. 5b, where the ordering of the $z^2$ orbitals lying in the *ab* basal plane of $LaMnO_3$ leads to its doubling. Recently a number of experimental facts have appeared which not only tend to support Goodenough's hypothesis but also contain new and somewhat unexpected information about the behavior of doped manganites and oxides in general.

### 4.1. Charge and orbital orderings

One of the first sufficiently reliable observations of this effect was apparently made in Ref. 130, in which the system $La_{0.5}Ca_{0.5}MnO_3$ was studied. The composition corresponding to it (see Fig. 8) borders between the metallic and insulator regions, and the conductivity has semiconductor temperature behavior. The spin order observed here belongs to the *C* type AFM structure (Fig. 7). Substitution of the $La^{3+}$ ion for the $Ca^{2+}$ ion in the cubic lattice of $CaMnO_3$ creates in this crystal a JT ion $Mn^{3+}$, which tends to deform the ideal octahedron on account of the splitting of the now occupied $e_g$ level

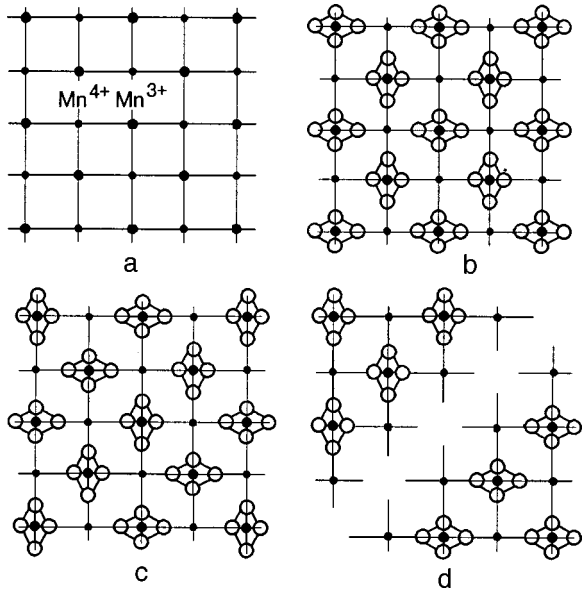


FIG. 12. Form of the charge ordering (a) and the possible types of orbital ordering corresponding to it ($b-d$) in the system $R_{1-x}A_xMnO_3$ in the case of half doping ($x=0.5$).

(see Fig. 6). In the region of low $La^{3+}$ concentrations, i.e., $1-x \ll 1$, the JT ions occupy random positions, and the local deformation, which, as we have said, is of the pseudo-JT type, is relatively small. A decrease in $x$, or an increase in the number of rare-earth ions, will lead to the interaction of close-lying $Mn^{3+}$ ions, the density of which is progressively increasing, and their effects (including on one another) are compelled to be coordinated in such a way that the stresses arising in the lattice are reduced, and the global deformation due to the JT distortions is optimized. As long as the concentration $x \geqslant 0.5$ the compound $La_{1-x}Ca_xMnO_3$ remains an insulator for the reasons discussed above; this means that there are no mobile charges in it, and, hence, the deformations created by the different dopants are not averaged out (by the carriers, at least) but largely remain localized and static.

The interaction between $Mn^{3+}$ ions has two components—a Coulomb component (in an ionic insulator it is weakened slightly on account of the dielectric permittivity) and a deformation component. The first is isotropic and most likely should govern the charge ordering. The second, which is also long-ranged, is anisotropic, and it is the overlapping elastic fields from various sources (the JT ions $Mn^{3+}$) that determine the form of the mutual ordering of the $z^2$ orbitals in the basal plane. Essentially, we are talking about the appearance of one more microscopic scale having dimensions of length, which specifies the period of the ordering of charged elastic quadrupoles in the cubic medium (or of the analogous quadrupoles on a square lattice), the direction of the axes of these multipole moments being ''tied'' to the axes of the lattice.

The charge ordering of the PM ions of different valences which is observed in experiment at an equal number of each is shown in Fig. 12a; it has a simple AFM form. The spins $S=2(Mn^{3+})$ and $S=3/2(Mn^{4+})$ of this subsystem also form an AFM lattice, although the magnetic correlation length in each of the sublattices is different.[130] In addition, FM chains

of spins are observed along the *c* axis. More interesting physically, however, is the orbital ordering, which is ordinarily understood to mean the arrangement of the long axes of the octahedra containing $Mn^{3+}$ ions (or, equivalently, of the doped holes surrounded by local JT distortions of the quadrupole type) with respect to one another in the *ab* plane (this is sometimes called ordering of JT polarons; see, e.g., Ref. 131).

Figures 12b, 12c, and 12d show three of the possible configurations of this type, which are difficult to choose among solely on the basis of general arguments. For example, Fig. 12b corresponds to a doubling of the lattice owing to the appearance of inequivalent $Mn^{4+}$ ions (more or less close spacing of the ligands). Figure 12c also shows a doubled structure, but the $Mn^{4+}$ ions are in noncentrosymmetric positions and are slightly displaced from their initial positions at the sites of the square lattice. Finally, Fig. 12d shows a structure without doubling, in which the deformation created by the different $Mn^{3+}$ ions add together and the lattice becomes orthorhombic, but the crystal as a whole should become twinned, separating into domains with deformation axes perpendicular to each other. The neutron-scattering data indicate that the structure shown in the Fig. 12c is realized; this might be further checked by examining the optical spectra of the $Mn^{4+}$ ion, which should contain lines that are dipole-forbidden in centrosymmetric lattices.

Even more unusual are the results obtained recently for compounds with $x>0.5$, viz., $La_{0.33}Ca_{0.67}MnO_3$ ($x=2/3$) and $La_{0.25}Ca_{0.75}MnO_3$ ($x=3/4$), in which *stripe structures* (or simply stripes) were observed.[132] These stripes, which were first discovered in lightly doped perovskite compounds (nickelates), which are close in their crystal and electronic structure to HTSCs,[133] and then later in HTSC cuprates with less than optimal doping (the so-called underdoped regime), are now attracting a great deal of attention. Although the experimental information on the stripes is not yet sufficient for developing a complete and consistent theory, there are indications that the stripes correspond to a separate region on the phase diagram of copper oxides, and it is not infrequently conjectured and even blithely stated that these stripes are not only connected with the initial AFM order in cuprates but also with the phenomenon of HTSC itself (see the reviews[134,135]). However, whereas in cuprates the stripes (according to the present ideas) are peculiar to their anomalous (striped) metallic state, in manganites the stripes form, exist, and are observed in the insulating phase, in which the distribution of the transition-metal ions of different valences along one of the crystal axes becomes nonuniform. As in $La_{0.5}Ca_{0.5}MnO_3$, the corresponding charge ordering along the $\langle 110 \rangle$ direction (the diagonals of the square lattice in Fig. 12a) in $La_{1-x}Ca_xMnO_3$ compounds with so-called commensurate concentrations remains chainlike. The orbital ordering also retains its form, but the chains formed by quadrupoles with different orientations of the principal axes go in an irregular manner (see Fig. 13).

The point is that the cell of the doubled structure with $x=2/3$ should contain two $Mn^{3+}$ and four $Mn^{4+}$ ions. In that case the following sequences of ions are possible in the basal plane in the direction perpendicular to the chains: *i*) $Mn^{3+}-Mn^{3+}-Mn^{4+}-Mn^{4+}-Mn^{4+}-Mn^{4+}$, *ii*) $Mn^{3+}-Mn^{4+}-Mn^{3+}-Mn^{4+}-Mn^{4+}-Mn^{4+}$, and *iii*) $Mn^{3+}-Mn^{4+}-Mn^{4+}-Mn^{3+}-Mn^{4+}-Mn^{4+}$, and at first glance it seems that the most regular of these, the third, should be observed. However, experiment shows that the second type of sequence is realized. Here the main structural element—the stripe ''sandwich'' $Mn^{3+}-Mn^{4+}-Mn^{3+}$—retains its special stability in other commensurate structures as well. This indicates that between two JT deformed chains of $Mn^{3+}$ there are forces, undoubtedly of an elastic origin, which link them into a single stable stripe, a necessary unit of which is another, intermediate chain of isotropic $Mn^{4+}$ ions. Apparently, these already formed stripes of three chains predominantly repel one another, and this prevents their further ''condensation'' and tends to make the distance between them the maximum possible for each given composition. It would seem that the latter is reminiscent of the ''Wigner crystallization'' of triple chains, which was conjectured in Ref. 130. However, one can scarcely agree with this completely, since the maximum distance of the $Mn^{3+}-Mn^{4+}-Mn^{3+}$ stripes from one another is observed only in commensurate compositions or in compositions that can be represented as periodically alternating stripes (transverse-stripe structure).

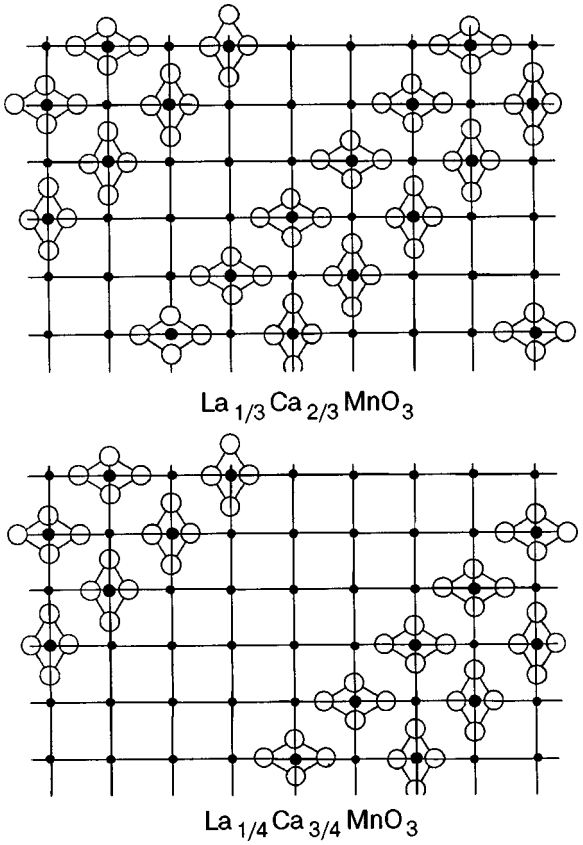


FIG. 13. Orientation and periods of repetition of the $Mn^{3+}$-$Mn^{4+}$-$Mn^{3+}$ stripes and also the orbital ordering corresponding to the latter in the basal plane of different manganites (the undistorted octahedra are not shown); —$Mn^{4+}$; ●—$Mn^{3+}$.

Experiment, however, shows[132] that in samples of incommensurate compositions (e.g., for $x=5/8$) there occurs a decomposition into domains having the closest stable commensurate compositions (in this case $x=2/3$ and $x=1/2$, which occupy 75% and 25% of the volume, respectively,

since for $0.75\times 2/3+0.25\times 1/2=5/8$). In this case no grouping into stripes containing more than two chains of JT ions was observed. The lengths of the observed stripes ranged from 200 to 500 Å. In addition, measurements with a tunneling electron microscope have shown that the period ($\approx$4.5 Å) in the $Mn^{3+}-Mn^{4+}-Mn^{3+}$ chains is considerably smaller than the average ($\approx$5.5 Å), while in the stripes of $Mn^{4+}$ ions it is greater (up to $\approx$6.5 Å). A crude estimate of the Coulomb energy cost $e^2(4.5^{-1}-5.5^{-1})$ gives around $0.6\,\mathrm{eV/Mn^{3+}}$ ion, which is comparable to the gain in the JT energy. Then the correlation length of the stripes in the direction perpendicular to the chains is $\sim(2-3)\times 10^2$ Å (in the planes in which they lie) and up to $\sim 10^3$ Å (along the planes formed by the triple chains).[22)] From what we have said, we conclude that the fluctuations of the stoichiometry of the dopants can and should also influence the formation of a periodic chain (stripe) ordering in transition-metal oxides.

This ''pairing'' of JT chains with the formation of periodically distributed extended stripes is also observed in other manganites; as is stated in Ref. 132, this pairing is in need of a re-examination or at least a refinement of the spin ordering proposed by Wollan and Koehler in $R_{1-x}A_xMnO_3$ with $0.5<x\leqslant 1$. The observed collapse of the stripes (including for $x=1/3$)[92] in a magnetic field[136] or under external pressure[137] is possibly due to the onset of conductivity (to an increase in the probability of the charge exchange $Mn^{3+}-Mn^{4+}\leftrightarrow Mn^{4+}-Mn^{3+}$ on account of the fine rotations of the spins) or, what would have the same effect, to a decrease in the JT deformations and the resulting lowering of the energy.

For these reasons the $Mn^{3+}-Mn^{4+}-Mn^{3+}$ stripes in manganites cannot be 1D metals, for any charge transfer within a stripe is reflected in the elastic part of its binding energy and should lead to the decomposition of the structure itself. In other words, the appearance or disappearance of the stripes depends on the outcome of the competition between the JT deformations, which are created by charge-localized polarons, and the double exchange, which comes into play when the carriers are free.

The existence of the stripe phases described above or of stripe structures of a different sort having periods of a microscopic scale (in both manganites and cuprates) was not predicted by any of the existing theories. Therefore, the causes of the formation of conducting and nonconducting stripes, their properties, and the physical effects resulting from these properties are still waiting for a theoretical interpretation. This problem is of lively interest and topicality for the development of the theory. It should also be taken into consideration that the stripes in manganites are insulators and that practically any external influence (whether it be a static magnetic field or an alternating electromagnetic field, pressure, temperature, etc.) can relatively easily bring about in them a metal-insulator transition,[138] the properties of which for such elastically and electronically anisotropic objects are practically unknown (the study of the magnetism and metallization of ''spin ladders'' in HTSCs has not included any specifics as to deformations, including JT ones).[139,140]

Experimental studies must also answer a number of questions. Is the formation of stripe phases an inherent property of lightly doped oxides, or are they a side effect of some external factors? What ordering, if any, arises in the *R-A* subsystem? (For example, in the form of the same or nearly the same stripe structure, but chiefly, a nonuniform ordering corresponding to the charge distribution of the dopants over the manganite samples, since in the insulating phase (see Paragraph 3.4) the introduced charge, or the transition-metal ion of a new valence, and the dopant providing the charge attract each other.) How precisely is the oxygen stoichiometry maintained in oxides, and, finally, one of the most important questions: how are the stripes related to such phenomena as CMR and HTSC? This last problem, of course, is not just for experimentalists.

#### 4.2. Phase separation

In the previous Subsection we spoke of a special—stripe—type of inhomogeneous ordering in the insulating phase of doped manganites. Before that, in discussing the problem of their metallization, we described the possibility that it is a metal-insulator transition in a disordered medium, where the impurity states, which are beginning to overlap, cause a delocalization of the carriers, the motion of which through the AFM medium is brought about by the turning on of the double exchange. But this again raises the question: does this transition occur in the entire volume of the sample or do the metallic regions in manganites coexist with insulating regions (something like the case of cuprates)?

The first scenario of metallization was implicitly assumed above. However, the structure consisting of insulating (AFM) and metallic stripes (domains), which are present in HTSCs, raises the question of when and in what cases is the separation into domains preferable to a homogeneous state? A conclusive answer to this question has not yet been found (see Ref. 135).

As to the manganites, it was long assumed that the observed nonuniformities of the metallic state are largely due to the structural disorder in the samples themselves or to the developed fluctuations of the magnetic order, which are manifested in pronounced FM correlations near and above $T_C$, where the CMR effect in itself is manifested in the highest measure. Nevertheless, we recall that a superposition of AFM and FM neutron scattering peaks in certain samples was noted many years ago.[49]

Therefore, it is not accidental that a rather large resonance was created by the results of Ref. 141, which convincingly demonstrated that the FM and AFM regions in doped $La_{1-x-y}Pr_yCa_xMnO_3$ with $x=3/8$ and $0\leqslant y\leqslant 0.25$ are indeed spatially separate and form metallic and insulating domains, respectively (see Fig. 14). In the metallic, unlike the insulating domains, no charge ordering of any kind was present, for the reasons discussed above (the holes are delocalized). Both kinds of domain were irregular in shape with a rather large average size ($\approx 5\times 10^3$Å), and the magnetization vectors of the different FM regions were disordered. In an external magnetic field there was a percolation transition (in the terminology of the authors) to a metallic phase, accompanied by the CMR effect. Here the AFM domains are not ''consumed'' by the FM domains, and the separation into domains has a stable character.

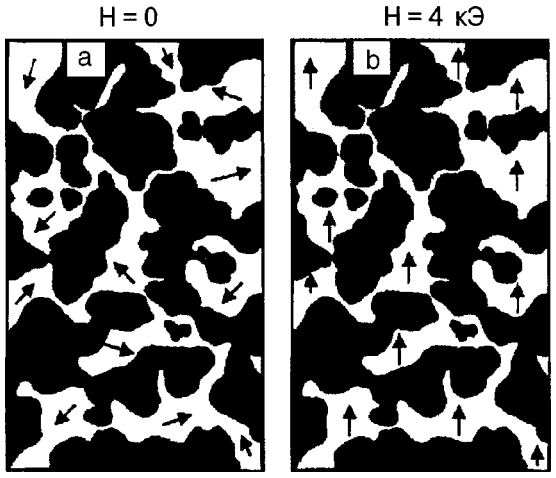


FIG. 14. Submicron domain structure of the doped manganite $La_{1-x-y}Pr_yCa_xMnO_3$ ($x=3/8$).[141] The dark regions correspond to the AFM insulator domains, the light regions to the FM metallic domains. The arrows indicate the random directions of the magnetization of FM domains in the absence of an external magnetic field ($H=0$) and their alignment in a field $H=4$ kOe.

In the analysis of these experiments in Ref. 142, the authors called attention to the relative ease with which the charge ordering is suppressed by external influences (see Paragraph 4.1), and it was concluded that the free energies of the insulating AFM and metallic FM domains are close to each other. In this regard, their stable existence over a wide range of manganite compositions (in Ref. 141 the substituent used was Pr instead of La, in order to create an internal pressure, which, through the tolerance factor, influenced the transport characteristics but did not eliminate the macroscopic domain structure) was called unprecedented in Ref. 142. As an additional reason for this conclusion they named the large mismatch between the elastic stresses arising at the metal-insulator boundary. The richness of the self-organizing structures in lightly doped oxides (classical and quantum) is too great and unexpected to permit such a rapid recognition, explanation, and description.

At the same time, in continuing the comparison of manganites and cuprates, it should be noted that the phase separation in the metallic state of the latter has already been studied for several years, and it has been shown that charge separation is in principle possible (see the review[143] and the references cited therein). Moreover, charge separation is invoked to explain the process of domain formation in doped layered HTSC oxides, on the basis of a comparison of the energies of different charge distributions. In manganites it is due to the double exchange, which in the presence of a strong intra-ion (Hund) exchange interaction and an inter-ion exchange interaction can make a nonuniform distribution of carrier density preferable to a uniform distribution. Here the elastic contribution from the JT deformations is thought to be nonneligible. In Ref. 143 (see also Ref. 25) a list of around twenty different experimental results is presented which would directly or indirectly support the assumption that the charges are spatially separated.

However, here it must be kept in mind that if charge separation really is present, it will inevitably lead to regions with a high density of charges of one sign, and hence to a large repulsive Coulomb potential, and this has been called into question in the paper by Ivanov and one of the present authors.[144] There, in addition to a discussion of some models of domain formation in doped oxides, it was shown[144] that the separation into metallic and insulating (including stripe) domains (even though their shape and magnetic state were not considered) is a common property of metals with a low density of delocalized carriers. It is important that the domains in the stable inhomogeneous state of the system be neutral. Neutrality can, in particular, be provided by dopants (as we have said, practically nothing is known of their behavior), which are also, generally speaking, capable of being redistributed over the sample under the influence of Coulomb forces during its growth, or by nonstoichiometric oxygen, the mobility of which in oxide lattices is generally high, or by $R^{3+}$ vacancies, which inevitably arise[128] in the preparation of samples.[23)] The authors of Ref. 141 gave special emphasis to the circumstance that no volume segregation of electric charges was observed in their samples and that on average the domains were charge neutralized. It can be supposed that the condition of electrical neutrality is critical for the formation of domains in both the insulator and metallic phases of transition-metal oxides. The shape and size of the domains are the result of the kinetics and thermodynamics of the formation of the structure of the solid solutions. On the other hand, as was shown by Gor'kov and Sokol,[95] if the lattice (JT) component is not neglected in the overall energy balance, then the electrical neutrality of the domains can in principle be dynamically violated. Here, however, the domains can exist only in the form of ''droplets,'' i.e., they must be very small, governed by the Coulomb energy.

On the whole, the problem of domain formation in transition-metal oxides still requires clarification, and one can agree that the novelty and unexpectedness of the results on the stripe structures of manganites, in particular, and also the rate at which information is being revised, make it impossible to reach reliable conclusions about the results of some particular experiment. It can only be said with certainty that the intensive efforts of investigators should produce fruit, possibly soon.

## 5. CONCLUDING REMARKS

It may seem strange that in a review article on the subject of the colossal magnetoresistance (CMR) we have not devoted a special Section to the CMR itself. This was deliberate. First, there are already the review articles, still current and valuable, by Ramirez,[35] Gor'kov,[95] and Nagaev,[119] the first of which deals mainly with the available experimental results and methods of studying the CMR, and the second and third of which set forth the authors' ideas about the possible causes of this effect. Second, practically all the theoretical approaches and proposed models of the CMR that we know of in one way or another rest on the concept of double exchange, and there is now a firm consensus that this mechanism is inadequate for describing the CMR. Any new ideas are apparently not yet fully ripe. Moreover, in light of the experimental facts that have appeared (and continue to emerge), there is a justified suspicion that even the foundations of the theory may need to be revised to take into account the various defects and inhomogeneities (including

fluctuations). The plausible, but still in need of verification, hypothesis that the CMR is a consequence of a metal-insulator (semiconductor) transition under suitable circumstances (the presence of an external magnetic field and the proximity of the critical temperature of the specific—AFM↔FM—magnetic transformation). Therefore, we have considered it useful to: *i*) attempt to generalize the accumulated information about the main physical properties and phase diagram of the manganites, which as far as we know, has still not been set forth in a unified form; *ii*) present the most recent experimental results which demonstrate the nonstandard properties of the manganites, in which the lattice, magnetic, and electrical properties are intimately and nontrivially interwoven; *iii*) present arguments as to the interactions and mechanisms that can (or cannot) have relevance to the CMR effect. While the experimental data remains inconsistent in the details (quantitatively and sometimes even qualitatively), they basically confirm the presence of the aforementioned connection, and chiefly, the unconditional existence of a very large and jumplike increase in the conductivity of the samples in the neighborhood of $T_C$ under the influence of an external magnetic field.

We wanted to draw certain analogies between manganites and cuprates, but we have to report that in the absence of a deep understanding of their properties it is extremely difficult to do this. It must be mentioned, however, that even the concept of a pseudogap, an attribute so specific to the electronic (and spin) structure of HTSCs, is now being invoked[147] for the description of the photoemission spectra of a number of manganese oxides,[24)] and that nanostructures of successively alternating layers of HTSC cuprates and manganites are being prepared and investigated. Both of these types of oxide compounds, which are members of the same class of solids and have ''super'' properties, are perovskite systems with a strong electronic correlation, and in both systems the insulator phase has AFM ordering and the physically most important ions $Cu^{2+}$ and $Mn^{3+}$ have a JT nature. In these systems nonisovalent doping brings about a transition to a metallic state, the structure of which, as a rule, has an inhomogeneous—domain—character, and the magnetism of the conducting regions is different (albeit in different ways) from the initial. In both cases the dopants introduce structural and magnetic disorder to the system, and the ligand is oxygen. However, the consequences of these physically similar processes in transition-metal oxides are the CMR effect (in manganites) and HTSC (in cuprates), and these effects do not have an obvious commonality.

The question of what models will be retained as the theory is developed further—double exchange, Jahn–Teller, Kondo, band or Mott–Hubbard insulator, polaron, bipolaron, statistical, impurity, etc.—is not so important. Each of them, by illuminating some aspect of some oxide or other, makes it possible to penetrate more deeply into the properties of these systems. Thanks to the aforementioned ''overlap'' of the HTSC and CMR regions, certain questions of solid-state physics are seen in a new light. For example, there is the fact that bad (including half) metals in certain situations may not obey the Landau theory of the Fermi liquid, and no other approach as general and effective has been developed. It is almost beyond doubt (see, e.g., Ref. 150) that the theory must include such new factors as: *i*) the coexistence of structures with several (including nanometer) spatial scales; *ii*) the competion of the AFM and FM ordering in the presence of a strong electron-phonon (JT) interaction; *iii*) the influence of well-developed fluctuations and the tendency of the system to form domains with different characters of the conductivity; *iv*) certain chemical and, possibly, technological aspects which are essential for the formation of samples (in other words, the history of the samples), etc.

It would not be an overstatement that the CMR, like HTSC, has issued a challenge to the theorists, and they have not yet been able to answer it. Finding a way out of this situation (and not waiting around for the next big anniversary to do this) would not only make it possible to put this remarkable effect to use in a more expeditious and predictable way but would also stand as an achievement for all of physical science.

One of us (VML.) thanks Prof. J. Bessa Sousa for kind attention and hospitality during his stay at the University of Porto, M. A. Ivanov for a discussion and helpful comments, and E. V. Gomonay and S. F. Mingaleev for assistance in the preparation of the manuscript. This review could not have been written were it not for the program PRAXIS XXI 2/2.1/FIS/302/94 and support from the grants NATO Fellowship in Portugal CP (UN) 13/C/99/PO and PRAXIS XXI BPD/14226/97.

*E-mail: vloktev@bitp.kiev.ua
**E-mail: ypogorel@fc.up.pt

1)This phenomenon was first observed by Searl and Wang,[9] but their reports remained practically unnoticed, and, unfortunately, are seldom mentioned as being among the pioneering papers.

2)Recall that, for example, in metallic films consisting of layers of magnetic and nonmagnetic metals, the analogous change, which is called the giant magnetoresistance (GMR), ordinarily does not exceed $10^2$% at $T\sim 4.2$ K (see Refs. 7 and 10).

3)Although at the present time not much can be said about why this should be, it is hard to ignore the fact that the perovskites possessing truly unique properties—HTSC and CMR—lie at points of the Ruddlesden–Popper series which are infinitely far apart with respect to $n$. True, a smaller CMR effect is also observed in layered manganites with $n=2$, and these compounds have been intensively investigated in the last 2–3 years.

4)Indeed, $r_{Mn^{2+}}\approx 0.85$ Å, $r_{Mn^{3+}}\approx 0.7$ Å, and $r_{Mn^{4+}}\approx 0.5$ Å; for comparison, some other radii are $r_{La^{3+}}\approx 1.2$ Å, $r_{Ca^{2+}}\approx 1.05$ Å, and $r_{O^{2-}}\approx 1.4$ Å. One can see how strong the doping-induced local distortion can be.

5)We will mention one thing: the measured values of the Grüneisen coefficient in $La_{0.65}Ca_{0.35}MnO_3$ vary from $85(40\text{ K}\leqslant T\leqslant 260\text{ K})$ to $25(T\approx 600\text{ K})$,[18,19] whereas in most solids (one of the rare exceptions being fullerite)[32] it has a value of 2–5.

6)Here is an appropriate place to mention that in Ruddlesden-Popper compounds with $n>1$ the ionic composition of the transition metal is not so simple. In particular, it is easy to see that for $n=2$, for example, or in the layered system $R_3Mn_3O_7$, the manganese ion, even in the insulating phase, should exist in states of different valence ($Mn^{2+}$ and $Mn^{3+}$) with equal concentrations. The substitution of divalent alkaline-earth ions for the rare-earth metal in this compound should give rise to mobile holes in the transition-metal subsystem, but it remains unclear which of the charge exchange processes, $Mn^{2+}\rightarrow Mn^{3+}$ or $Mn^{3+}\rightarrow Mn^{4+}$, is responsible for them.

7)Actually the octahedra suffer small rotations, which mix the states of the multiplets $e_g$ and $t_{2g}$; these are usually neglected, and the lattices of these systems are assumed completely isotropic.

8)It should be noted that for many compounds, including pure $LaMnO_3$ and $AMnO_3$ and also $La_2CuO_4$, the anisotropic exchange, owing to the rotations of the octahedra, is actually allowed and gives rise to a weak ferromagnetic moment.[46] However, as in the case of the magnetic anisotropy, it is hard to imagine that its existence is reflected in the basic physical prop-

erties of transition-metal oxides, in particular, CMR or HTSC.

[9)] Recent optical data indicate that $J_H \approx 1.5$ eV, while the transfer integral $t \approx 0.1$ eV,[43] although nowadays it is assumed to be somewhat higher.[64,69] Meanwhile, abandoning the condition $J_H \to \infty$ (more precisely, taking into account the finiteness of $J_H$) leads to the formation in the AFM crystal of a narrow ($W \sim t^2/J_H$) band, which is ordinarily neglected, for under real conditions it cannot provide coherent transport of fermions through the crystal.

[10)] A quantum calculation[69] of this angle gives the formula $\cos\theta/2 = (S_{\rm tot} + 1/2)/(2S_{\rm low} + 1)$, where $S_{\rm tot}$ is the total spin of the pair and $S_{\rm low}$ is the spin of the manganese ion in the low-spin state (in this case it is the spin of $Mn^{4+}$).

[11)] Interestingly, the influence of the currentless excitations—excitons—on the magnetic state of the system would be somewhat different. In fact, the width of the magnetic exciton band in antiferromagnetic insulators (like the exchange interaction between localized spins) is proportional to $\cos^2\theta/2$ (Ref. 71). Consequently, increasing the concentration $x_{\rm ex}$ of such excitations can only change the sign of the coefficient (or $I_{AFM}Sz - Wx_{\rm ex}$) multiplying the cosine and thereby cause a first-order transition from the collinear AFM to the FM structure.

[12)] These should not be confused with semimetals, which are systems of a completely different physical nature. In them the conduction band is characterized by an anomalously small Fermi surface, irrespective of magnetism (which is generally not present). Another important difference is that the conduction band of a semimetal has $2N$ places for electrons, while a half metal has $N$; this has a general resemblance to the case of Hubbard subbands in strongly correlated metals.

[13)] It is hard to agree with this, for the large Hund exchange constant $J_H$ in manganites does not allow one to treat the carrier as isolated from the ion on which it is found, although this is almost always assumed (see Paragraph 3.5).

[14)] The value given can be assumed to be somewhat overestimated. First, calculations[39] show that $t$ is at least a factor of two lower, and second, the value $z = 6$ corresponds to a cube, which possibly has not yet formed at $x \approx 0.2$. Nevertheless, the main assertion as to the inadequacy of the double exchange model for explaining the CMR effect remains valid.

[15)] We are not talking about the local distortions caused by the $A^{2+}$ ion itself, which are quickly reflected in the tolerance factor, the change of which we are neglecting.

[16)] Its relatively small value may explain why the FM phase in $La_{1-x}A_xMnO_3$ is shifted into the region $x < 0.5$. On the $AMnO_3$ side the carriers (electrons) must contend with the AFM exchange from all the neighbors in the cubic lattice at once.

[17)] The same physical conclusion was reached by the authors of Ref. 112 by proceeding from an experimental study of the transport properties of a large number (including fluorine-substituted) orthomanganites. Another finding of that study, that there is no direct link between the resistance, magnetoresistance, and ferromagnetism in conducting and nonconducting manganites, cannot be regarded as conclusive and requires verification.

[18)] We note that the spin–spin FM correlations are also suppressed more weakly in the microferrons described above than in the matrix.

[19)] It is appropriate to note in this regard that the increase in the number of microferrons with increasing $x$ and their joining into a single infinite metallic cluster are also consistent with a percolation approach.

[20)] In some papers (e.g., Refs. 119 and 126) it is assumed that a hole occupying a $p$ orbital enters into such a strong exchange interaction with the spins of neighboring $Mn^{3+}$ ions that it forms a bound complex with them—a small-radius magnetic polaron, for which the double exchange model no longer applies. However in such a case it is more logical to use it not for oxygen holes but for the motion of such polarons over the AFM lattice.

[21)] The phenomenological approach proposed in the paper of Lyuksyutov and Pokrovsky[129] for describing the CMR admits correct incorporation of the thermodynamic relations between the number of delocalized (owing to the formation of polarons) carriers and localized polarons while conserving the total number of each. In that approach (see also Ref. 128) the transition of the PM insulator to a FM metal occurs specifically by the thermal redistribution of carriers between their free and bound (localized) states, and this, in turn, can depend on $H$.

[22] It should be kept in mind that the stripe structure pertains only to the *ab* planes. Being correlated, the stripes of different *ab* planes themselves form *ac* or *bc* planes with ordering of the corresponding character.

[23)] It is pertinent to point out that the CMR depends appreciably on the technology used to obtain the real (including granular and/or defect-containing) samples. For example, in Refs. 145 and 146 it was shown for the particular case of $La_{1-x}Sr_xMnO_{3-\delta}$ ($0.15 \leqslant x \leqslant 0.3$) that the drop in the CMR at the transition point depends on technological parameters such as the sintering temperature. These measurements again attest to the fact that the macrostructure of manganites, if it is not the direct physical cause of the CMR effect, undoubtedly influences its value.

[24)] In that paper the pseudogap is identified with the decrease in the quasiparticle weight seen in ARPES experiments, the explanation for which is similar to optical transitions in molecules, where in the case of strong coupling with vibrations the intensity of the zero-phonon transition is suppressed in comparison with its phonon wing. From a comparison of the frequency of this Franck–Condon transition with $\varepsilon_F$, the part of the density of states corresponding to polarons is carried over to the region of the multiphonon continuum. It is thought, however, that such observations do not justify the use of the term pseudogap in a situation where the causes of the formation of the gap itself are not apparent (see also Ref. 148). At the same time, we note that if one proceeds from the analogy between the manganites and doped semiconductors, then, as we know,[149] a ''soft'' Coulomb gap can form in the latter near $\varepsilon_F$. Incidentally, that version cannot be considered final either.


[1] G. H. Jonker and J. H. Van Santen, Physica **16**, 337 (1950).
[2] J. H. Van Santen and G. H. Jonker, Physica **16**, 599 (1950).
[3] R. M. Kusters, J. Singleton, D. A. Keen, R. McGreevy, and W. Hayes, Physica B **155**, 362 (1989).
[4] R. M. von Helmholt, J. Wecker, B. Holzapfel, L. Schultz, and K. Samver, Phys. Rev. Lett. **71**, 2331 (1993).
[5] K. Chahara, T. Ohno, M. Kasai, and Y. Kozono, Appl. Phys. Lett. **63**, 1990 (1993).
[6] M. McCormack, S. Jin, T. H. Tiefel, R. M. Fleming, J. M. Phillips, and R. Ramesh, Appl. Phys. Lett. **64**, 3045 (1994).
[7] S. Jin, T. H. Tiefel, M. McCormack, R. A. Fastnacht, R. Ramesh, and L. H. Chen, Science **264**, 413 (1994).
[8] A. Urushibara, Y. Morimoto, T. Arima, A. Asamitsu, G. Kido, and Y. Tokura, Phys. Rev. B **51**, 14103 (1995).
[9] C. W. Searl and S. T. Wang, Can. J. Phys. **47**, 2703 (1969); **48**, 2023 (1970).
[10] S. P. P. Parkin, Annu. Rev. Mater. Sci. **25**, 357 (1995).
[11] A. K. Raychaudhuri, Adv. Phys. **44**, 21 (1995).
[12] V. M. Loktev, Fiz. Nizk. Temp. **22**, 3 (1996) [Low Temp. Phys. **22**, 1 (1996)].
[13] A. Abraham and B. Bleany, *Electron Paramagnetic Resonance of Transition Metals*, Clarendon Press, Oxford (1970).
[14] S. A. Al'tshuler and B. M. Kozyrev, *Electron Paramagnetic Resonance of Compounds of Elements of the Intermediate Groups* [in Russian], Nauka, Moscow (1972).
[15] J. J. Neumeier, M. Hundley, J. D. Thompson, and R. H. Heffner, Phys. Rev. B **52**, R7006 (1995).
[16] T. A. Tyson, J. Mustre de Leon, S. D. Conradson, A. R. Bishop, J. J. Neumeier, H. Röder, and J. Zang, Phys. Rev. B **53**, 13985 (1996).
[17] M. C. Martin, G. Shirane, Y. Endoh, K. Hirota, Y. Morimoto, and Y. Tokura, Phys. Rev. B **53**, 14285 (1996).
[18] P. Dai, J. Zhang, H. A. Mook, S.-H. Liou, P. A. Dowben, and E. W. Plummer, Phys. Rev. B **54**, R3694 (1996).
[19] P. G. Radaelli, M. Marezio, H. Y. Hwang, S.-W. Cheong, and B. Batlogg, Phys. Rev. B **54**, 8492 (1996).
[20] S. J. L. Billinge, R. G. Di Francesco, G. H. Kwei, J. J. Neumeier, and J. D. Thompson, Phys. Rev. Lett. **77**, 715 (1996).
[21] L. Vasiliu-Doloc, J. W. Lynn, A. H. Mouden, A. M. Leon-Guevara, and A. Revcolevsci, Preprint, cond-mat/9806381 (1998).
[22] R. Mahesh and M. Itoh, Aust. J. Phys. **52**, 235 (1999).
[23] K. I. Kugel' and D. I. Khomskiĭ, Usp. Fiz. Nauk **136**, 621 (1982) [Sov. Phys. Usp. **25**, 231 (1982)].
[24] J. B. Goodenough, J. Kafalas, and J. M. Longo, in *Preparative Methods in Solid State Chemistry*, edited by P. Hagenmuller, Academic Press, New York (1972), Ch. 1.
[25] J. B. Goodenough, Aust. J. Phys. **52**, 151 (1999).
[26] H. Y. Hwang, S.-W. Cheong, P. G. Radaelli, M. Marezio, and B. Batlogg, Phys. Rev. Lett. **75**, 914 (1995).
[27] Y. Morimoto, Y. Tomioka, A. Asamitsu, and Y. Tokura, Phys. Rev. B **51**, 3279 (1995).
[28] P. D. Battle, M. A. Green, N. S. Laskey, J. E. Milburn, P. G. Radaelli, M. J. Rosseinsky, S. P. Sullivan, and J. F. Vente, Chem. Mater. **9**, 552 (1997).

[29] D. N. Argurion, J. F. Mitchell, J. D. Jorgensen, J. B. Goodenough, P. G. Radaelli, D. E. Cox, and H. N. Bordallo, Aust. J. Phys. **52**, 279 (1999).
[30] J. A. M. Van Roosmalen and E. H. P. Cordfunke, J. Solid State Chem. **110**, 109 (1994).
[31] M. F. Hundley and J. J. Neumeier, Phys. Rev. B **55**, 11511 (1997).
[32] A. N. Aleksandrovskii, V. B. Esel'son, V. G. Manzhelii, A. V. Soldatov, B. Sundqvist, and B. G. Udovichenko, Fiz. Nizk. Temp. **23**, 1256 (1997) [Low Temp. Phys. **23**, 943 (1997)].
[33] L. J. Terminello, S. M. Mini, H. Ade, and D. L. Perri (eds.), *Applications of Synchrotron Radiation Techniques to Material Sciences III*, Mater. Res. Soc., Pittsburg (1997).
[34] J. B. Goodenough, *Magnetism and the Chemical Bond*, Krieger, Huntington (1976).
[35] A. P. Ramirez, J. Phys.: Condens. Matter **9**, 8171 (1997).
[36] J. B. Goodenough, Phys. Rev. **100**, 564 (1955).
[37] M. D. Struge, in *Solid State Physics*, Vol. 20, edited by F. Seitz, D. Turnbull, and H. Ehrenreich, Academic Press, New York (1967).
[38] J. B. A. A. Elemans, B. Van Laar, K. R. Van der Veen, and B. O. Loopstra, J. Solid State Chem. **3**, 238 (1971).
[39] S. Sathpathy, Z. S. Popovic, and F. Vukajlovic, Phys. Rev. Lett. **76**, 960 (1996).
[40] A. E. Bocquet, T. Mizokawa, T. Saitoh, H. Namatame, and A. Fujimori, Phys. Rev. B **46**, 3771 (1992).
[41] A. Chainani, M. Matthew, and D. D. Sarma, Phys. Rev. B **47**, 15397 (1993).
[42] P. W. Anderson, Phys. Rev. **79**, 350 (1950); **79**, 705 (1950); **115**, 2 (1959).
[43] P. W. Anderson and H. Hasegawa, Phys. Rev. **100**, 675 (1955).
[44] I. E. Dzyaloshinskii, J. Phys. Chem. Solids **4**, 241 (1958).
[45] T. Moriya, Phys. Rev. **120**, 91 (1960).
[46] I. V. Solovyov, N. Hamada, and K. Terakura, Phys. Rev. Lett. **76**, 4825 (1996).
[47] W. E. Pickett and D. J. Singh, Phys. Rev. B **53**, 1146 (1996).
[48] I. V. Solovyov, N. Hamada, and K. Terakura, Phys. Rev. B **53**, 7158 (1996).
[49] E. O. Wollan and W. C. Koehler, Phys. Rev. **100**, 545 (1955).
[50] P. Schiffer, A. P. Ramirez, W. Bao, and S.-W. Cheong, Phys. Rev. Lett. **75**, 3336 (1995).
[51] A. J. Millis, Nature (London) **392**, 147 (1998).
[52] Z. Jirak, S. Krupicka, Z. Simsa, M. Dlouha, and S. Vratislav, J. Magn. Magn. Mater. **53**, 153 (1985).
[53] N. F. Mott, *Metal-Insulator Transition*, Taylor and Francis, London (1990).
[54] V. J. Emery, Physica B **169**, 17 (1991).
[55] J. B. Goodenough, Prog. Solid State Chem. **5**, 145 (1971).
[56] A. Fujimori and F. Minami, Phys. Rev. B **30**, 957 (1984).
[57] J. Zaanen, G. A. Sawatsky, and J. W. Allen, Phys. Rev. Lett. **55**, 418 (1985).
[58] S. Hufner, Z. Phys. B: Condens. Matter **61**, 135 (1985).
[59] T. Saitoh, A. E. Bocquet, T. Mizokawa, H. Namatame, and A. Fujimori, Phys. Rev. B **51**, 13942 (1995).
[60] O. Gunnarson, O. K. Andersen, O. Jepsen, and J. Zaanen, Phys. Rev. B **39**, 1708 (1989).
[61] A. E. Bocquet, T. Saitoh, T. Mizokawa, and A. Fujimori, Solid State Commun. **83**, 11 (1992).
[62] I. H. Park, C. T. Chen, S.-W. Cheong, W. Bao, G. Meigs, V. Chakarian, and Y. U. Idzerda, Phys. Rev. Lett. **76**, 4215 (1996).
[63] P. P. Edwards and C. N. R. Rao (eds.), *Metallic and Non-Metallic States of Matter*, Taylor and Francis, London (1985).
[64] M. Imada, A. Fujimori, and Y. Tokura, Rev. Mod. Phys. **70**, 1039 (1998).
[65] M. Muroi and R. Street, Aust. J. Phys. **52**, 205 (1999).
[66] C. Zener, Phys. Rev. **81**, 440 (1951); **82**, 403 (1951).
[67] Y. Okimoto, T. Katsufuji, T. Ishikawa, A. Urushibara, T. Arima, and Y. Tokura, Phys. Rev. Lett. **75**, 109 (1995).
[68] D. D. Sarma, S. R. Barman, H. Kajueter, and G. Kotliar, Europhys. Lett. **36**, 307 (1996).
[69] K. Kubo and N. Ohata, J. Phys. Soc. Jpn. **33**, 21 (1972).
[70] P. G. de Gennes, Phys. Rev. **118**, 141 (1960).
[71] V. V. Eremenko, *Introduction to the Optical Spectroscopy of Mangets* [in Russian], Naukova Dumka, Kiev (1975).
[72] O. Erikson, R. C. Albers, and A. M. Boring, Phys. Rev. B **43**, 5649 (1991).
[73] M. Isoda, Y. Takahashi, and T. Sakai, J. Magn. Magn. Mater. **140–144**, 1385 (1995).
[74] L. B. Ioffe and A. J. Millis, Usp. Fiz. Nauk **168**, 672 (1998); X. Wang and X.-G. Zhang, Preprint cond-mat/9807244 (1998).
[75] Y. Okimoto, T. Katsufuji, T. Ishikawa, T. Arima, and Y. Tokura, Phys. Rev. B **55**, 4206 (1997).
[76] S. G. Kaplan, U. M. Quijada, H. D. Drew, D. B. Tanner, G. C. Xiong, R. Ramesh, C. Kwon, and T. Venkatesan, Phys. Rev. Lett. **77**, 2081 (1996).
[77] K. H. Kim, J. H. Jung, and T. W. Noh, Preprint cond-mat/9804284 (1998).
[78] I. Inoue and S. Maekawa, Phys. Rev. Lett. **74**, 3407 (1995).
[79] J. Jiang, J. Dong, and D. Y. Xing, Phys. Rev. B **55**, 8973 (1997).
[80] L.-J. Zou, Q. Q. Zheng, and H. Q. Lin, Phys. Rev. B **56**, 13669 (1997).
[81] J. Van der Brink and D. I. Khomskii, Phys. Rev. Lett. **82**, 1016 (1999).
[82] J. C. Slater and G. F. Koster, Phys. Rev. **94**, 1498 (1954).
[83] Y. Nagaoka, Phys. Rev. **147**, 392 (1966).
[84] J. P. Fletcher and X. W. H. Stephens, J. Phys. C **2**, 444 (1969).
[85] A. J. Millis, P. B. Littlewood, and B. I. Shraiman, Phys. Rev. Lett. **74**, 5144 (1995).
[86] H. Roder, J. Zang, and A. R. Bishop, Phys. Rev. Lett. **76**, 1356 (1996).
[87] A. J. Millis, B. I. Shraiman, and R. Mueller, Phys. Rev. Lett. **77**, 175 (1996); D. I. Khomskii and G. A. Sawatsky, Solid State Commun. **102**, 87 (1997).
[88] J. Zang, A. R. Bishop, and H. Röder, Phys. Rev. B **53**, R8840 (1996).
[89] M. C. Martin, G. Shirane, Y. Endoh, K. Hiroda, Y. Morimoto, and Y. Tokura, Phys. Rev. B **53**, 14285 (1996).
[90] H. Kawano, R. Kajimoto, M. Kubota, and H. Yoshikawa, Phys. Rev. B **53**, R14709 (1996).
[91] W. Archibald, J.-S. Zhou, and J. B. Goodenough, Phys. Rev. B **54**, 14445 (1996).
[92] D. Louca and T. Egami, J. Appl. Phys. **81**, 5484 (1997).
[93] J. M. De Teresa, M. R. Ibarra, P. A. Algarabel, C. Ritter, C. Marquina, J. Blasco, J. Garcia, A. del Moral, and Z. Arnold, Nature (London) **386**, 256 (1997).
[94] L.-J. Zou, H. Q. Lin, and Q. Q. Zeng, J. Appl. Phys. **83**, 7363 (1998).
[95] L. P. Gor'kov and V. Z. Kresin, JETP Lett. **67**, 985 (1998); L. P. Gor'kov, Ukr. Fiz. Zh. **168**, 665 (1998).
[96] M. D. Kaplan and G. O. Zimmerman, J. Phys. Chem. Solids **59**, 2218 (1998).
[97] A. Lanzara, N. L. Saini, M. Brunell, F. Natali, A. Biankoni, P. G. Radaelli, and S.-W. Cheong, J. Phys. Chem. Solids **59**, 2220 (1998).
[98] C. H. Booth, E. Bridges, G. H. Kwei, J. M. Lowrence, A. L. Cornelis, and J. J. Neumeier, Phys. Rev. Lett. **80**, 853 (1998).
[99] A. S. Alexandrov and A. M. Bratkovsky, Phys. Rev. Lett. **82**, 141 (1999); Preprint cond-mat/9903217 (1999).
[100] G. M. Zhao, K. Conder, H. Keller, and K. A. Muller, Nature (London) **381**, 676 (1996).
[101] N. A. Babushkina, L. M. Belova, O. Yu. Gorbenko, A. R. Kaul, A. A. Bosak, V. I. Ozhogin, and K. I. Kugel, Nature (London) **391**, 159 (1998).
[102] A. S. Davydov, *Solid State Theory* [in Russian], Nauka, Moscow (1976).
[103] J. M. Coey, M. Viret, L. Ranno, and K. Ounadjela, Phys. Rev. Lett. **75**, 3910 (1995); M. Viret, L. Ranno, and J. M. Coey, Phys. Rev. B **55**, 8067 (1997).
[104] E. L. Nagaev, Aust. J. Phys. **52**, 305 (1999).
[105] E. L. Nagaev, *Physics of Magnetic Semiconductors*, Mir, Moscow (1983).
[106] M. A. Ivanov, V. M. Loktev, Yu. G. Pogorelov, Zh. Éksp. Teor. Fiz. **101**, 596 (1992) [Sov. Phys. JETP **74**, 317 (1992)].
[107] M. A. Ivanov, V. M. Loktev, and Yu. G. Pogorelov, Phys. Rep. **153**, 209 (1987).
[108] W. Bao, C. H. Chen, S. A. Carter, and S.-W. Cheong, Solid State Commun. **98**, 55 (1996).
[109] B. J. Sternlieb, J. P. Hill, U. C. Wildgruber, G. M. Luke, B. Nashumi, Y. Morimoto, and Y. Tokura, Phys. Rev. Lett. **76**, 2169 (1996).
[110] M. A. Ivanov, V. M. Loktev, Yu. G. Pogorelov, and Yu. V. Skripnik, Fiz. Nizk. Temp. **17**, 716 (1991) [Sov. J. Low Temp. Phys. **17**, 377 (1991)].
[111] Y. Tomioka, A. Asamitsu, H. Kuwahara, Y. Morimoto, and Y. Tokura, Phys. Rev. B **53**, R1689 (1996).
[112] I. O. Troyanchuk, D. D. Khalyavin, E. F. Shapovalova, N. V. Kasper, and S. A. Guretskii, Phys. Rev. B **58**, 2422 (1998).
[113] L. M. Rodriguez-Martinez and J. P. Attfield, Phys. Rev. B **58**, 2426 (1998).
[114] J. P. Attfield, A. L. Icharlanov, J. A. Alister, and L. M. Rodriguez-Martinez, MRS Symp. **547**, 15 (1999).
[115] M. Jaime, M. B. Solomon, M. Rubinstein, R. E. Treece, J. S. Horowitz, and D. B. Chrisey, Phys. Rev. B **54**, 11914 (1996).
[116] T. G. Perring, G. Aeppli, S. M. Hayden, S. A. Carter, J. P. Remeika, and S.-W. Cheong, Phys. Rev. Lett. **77**, 711 (1996).
[117] J. Loos and H. Fehske, Preprint cond-mat/9807294 (1998).
[118] Y. Endoh, H. Nojiri, K. Kaneko, K. Hirota, T. Fukuda, H. Kimura,

Y. Murakami, S. Fishihara, S. Maekawa, S. Okamoto, and M. Motokawa, Preprint cond-mat/9812404 (1998).
[119] É. L. Nagaev, Usp. Fiz. Nauk **166**, 833 (1996).
[120] S. V. Vonsovskiĭ, Magnetism [in Russian], Nauka, Moscow (1971).
[121] N. Furukawa, J. Phys. Soc. Jpn. **63**, 3214 (1995); **64**, 3164 (1995); S. Ishihara, J. Inoue, and S. Maekawa, Phys. Rev. B **55**, 8280 (1997); T. Okabe, Prog. Theor. Phys. **97**, 21 (1997).
[122] S. Yunoki and A. Moreo, Phys. Rev. B **58**, 6403 (1998); D. I. Golosov, M. R. Norman, and K. Levin, Phys. Rev. **58**, 8617 (1998).
[123] P. Horsch, J. Jaclic, and F. Mack, Preprint cond-mat/9807255 (1998).
[124] L.-J. Zou and H. Q. Lin, Aust. J. Phys. **52**, 247 (1999).
[125] Yu. B. Gaĭdideĭ, V. M. Loktev, A. F. Prikhot'ko, Fiz. Nizk. Temp. **3**, 549 (1977) [Sov. J. Low Temp. Phys. **3**, 263 (1977)].
[126] P. Mahadevan, I. V. Solovyov, and K. Terakura, Preprint cond-mat/9904369 (1999).
[127] N. B. Perkins and N. M. Plakida, Preprint cond-mat/9901141 (1999); N. B. Perkins and N. M. Plakida, Teor. Mat. Fiz. **120**, 438 (1999).
[128] M. Jaime and M. B. Solomon, Preprint cond-mat/9902284 (1999).
[129] I. F. Lyuksyutov and V. L. Pokrovsky, Phys. Rev. Lett. **81**, 2344 (1998); S. Sergeenkov, H. Bougrine, M. Ausloos, and A. Gilabert, JETP Lett. **70**, 136 (1999).
[130] P. G. Radaelli, D. E. Cox, M. Marezio, and S.-W. Cheong, Phys. Rev. B **55**, 3015 (1997); P. G. Radaelli, D. E. Cox, L. Capogna, S.-W. Cheong, and M. Marezio, Preprint cond-mat/9812366 (1998).
[131] A. A. Mukhin, V. Yu. Ivanov, V. D. Travkin, S. P. Lebedev, A. Pimenov, A. Loidl, and A. M. Balbashov, JETP Lett. **68**, 356 (1998).
[132] S. Mori, C. H. Chen, and S.-W. Cheong, Nature (London) **392**, 473 (1998).
[133] J. M. Tranquada, B. J. Sternlieb, J. D. Axe, Y. Nakamura, and S. Uchida, Nature (London) **375**, 561 (1995).
[134] O. Zacher, S. A. Kivelson, and V. J. Emery, Phys. Rev. B **57**, 1422 (1998).
[135] J. Zaanen, Physica C **317–319**, 217 (1999).
[136] Y. Tomioka, A. Asamatsu, Y. Morimoto, H. Kuwahara, and Y. Tokura, Phys. Rev. Lett. **74**, 5108 (1995).
[137] Y. Morimoto, H. Kuwahara, Y. Tomioka, and Y. Tokura, Phys. Rev. B **55**, 7549 (1997).
[138] H. Kuwahara, Y. Morimoto, Y. Tomioka, A. Asamatsu, M. Kasai, R. Kumai, and Y. Tokura, Phys. Rev. B **56**, 9386 (1998); S. L. Gnatchenko, A. B. Chizhik, I. O. Shklyarevskiĭ, D. N. Merenkov, V. I. Kamenev, Yu. G. Pashkevich, K. V. Kamenev, G. Balakrishnan, and D. McK Paul, Fiz. Nizk. Temp. **25**, 992 (1999) [Low Temp. Phys. **25**, 744 (1999)]; M. Baran, S. L. Gnatchenko, O. Yu. Gorbenko, A. R. Kaul, R. Szymczak, and H. Szymczak, Phys. Rev. B **60**, 9244 (1999).
[139] T. Dagotto and T. M. Rice, Science **271**, 618 (1996).
[140] S. R. White and D. J. Scalapino, Preprint cond-mat/9907375 (1999).
[141] M. Uehara, S. Mori, C. H. Chen, and S.-W. Cheong, Nature (London) **399**, 560 (1999).
[142] P. Littlewood, Nature (London) **399**, 529 (1999).
[143] E. Dagotto, S. Yunoki, and A. Moreo, in Physics of Manganites (*Proc. of the Intern. Conf. on Physics of Manganites, Michigan State University, July 26–29, 1998*), edited by T. A. Kaplan and S. D. Mahanti, Plenum Press, New York (1999).
[144] M. A. Ivanov, V. M. Loktev, Fiz. Nizk. Temp. **25**, 1325 (1999) [Low Temp. Phys. **25**, 996 (1999)].
[145] A. N. Pogorelyi, N. A. Belous, A. I. Tovstolytkin, A. G. Belous, O. Z. Yanchevski, Fiz. Nizk. Temp. **25**, 97 (1999) [Low Temp. Phys. **25**, 74 (1999)].
[146] V. G. Bar'yakhtar, A. N. Pogorilyi, N. A. Belous, and A. I. Tovstolytkin, J. Magn. Magn. Mater. **196–197**, 525 (1999).
[147] D. S. Dessau, T. Saitoh, P. Villella, C. H.-Park, Z.-X. Shen, Y. Moritomo, and Y. Tokura, J. Phys. Chem. Solids **59**, 1917 (1998).
[148] R. Joynt, Science **284**, 777 (1999).
[149] A. L. Efros and B. I. Shklovskii, J. Phys. C **8**, L49 (1974).
[150] N. Mathur, Nature (London) **400**, 405 (1999).

Translated by Steve Torstveit

## LOW-TEMPERATURE MAGNETISM

# The theory of equilibrium magnetic properties of granulated magnetic materials

E. Stefanovskii*

*Department of Physics, Ben-Gurion University of the Negev, Beer-Sheva 84105, Israel*
(Received August 3, 1999)
Fiz. Nizk. Temp. **26**, 262–270 (March 2000)

The present-day analysis of the theoretical adaptation status of the experimental curves of the magnetization and the static magnetic susceptibility as functions of the external parameters H and $T$ (H is an applied external magnetic field and $T$ is a temperature) is made for granulated ferromagnetic systems. Once more it is pointed that the consideration of the energy of magnetic anisotropy of a ferromagnetic material (as against the methods of the adapt used everywhere) play an essential role for the understanding of the magnetic behavior of the systems mentioned above and allow us to investigate the magnetoanisotropic behavior of granulated magnetic systems [at certain granule distribution functions (by their volume and orientation) as regards the external magnetic field]. It is shown that the use of the ''blocking'' concept is not necessary for the investigations of the thermodynamically equilibrium magnetic properties of the above systems. © *2000 American Institute of Physics.* [S1063-777X(00)00203-6]

### 1. INTRODUCTION

Granulated magnetic materials (GMM) have long been subject of intensive and quite successful research. They consist of small ferromagnetic (FM) particles (clusters, granules) in a nonmagnetic (weakly magnetic) matrix. The subject of research can be dielectric materials of the FM component and matrix as well as conducting materials.[1–5]

The renewed interest in GMM-materials is explained by the recent observation of the so-called effect of giant magnetoresistance (GMR) in such conducting systems.[6,7]

It is not hard to understand that the GMR-effect is connected with an additional channel of current carriers scattering on FM granules and is secondarily related to the unique magnetic properties of GMM materials. Therefore, below, as the first stage of research, we limit ourselves to the analysis of the equilibrium magnetic properties of the systems considered above.

### 2. OBJECT OF RESEARCH AND ITS MAIN FEATURES

a) The object under investigation is a solid heterogeneous system (an ensemble of FM particles incorporated into a nonmagnetic solid matrix). As a rule, these are systems with a small (volume) content of the FM component which is essential when interactions between particles of the system are neglected. In other words, FM particles of the GMM-system can neither rotate nor move forward nor change their volume (the state of thermodynamic equilibrium is meant, of course).

b) As is known, the dependence of a magnetic moment or a magnetization (i.e., magnetic moment per unit volume) of a gas of noninteracting paramagnetic (PM) particles on external parameters (absolute temperature $T$ and the value of external magnetic field $H$) within the framework of Langevin's classic theory is described by the function of the same name. Thus, the magnetization $\mu(H,T)$ of a gas of identical magnetic moments $\mu$ can be expressed as (e.g., see [1])

$$\mu(H,T)=N|\mu|L\left(\frac{|\mu|H}{kT}\right), \quad L(x)=\coth(x)-\frac{1}{x}, \qquad (1)$$

where $N$ is the number of atomic magnetic moments $\mu$ in the gas unit volume; $k$ is Boltzmann's constant and $L(x)$ is the Langevin function. It is necessary to note that the description of a magnetic particles system with the help of the Langevin function (as in the present case) is decisively based on the fact that magnetic energy of each particle of the ensemble possesses only one minimum (in its orientation dependence), which corresponds to the orientation of the particle magnetic moment alongside the direction of the applied external magnetic field. It is important that this orientation dependence is described by a function of $\sim \cos\theta$, where $\theta$ is the angle between directions of the magnetic moment and the field.

c) All real FM materials are magnetically anisotropic ones. This means that the magnetic moment of each particle of the ensemble in the absence of external magnetic field tries to orientate itself alongside the so-called directions of ''easy magnetization.'' For reversing the magnetic moment of each of the ensemble particles from one of these directions to another one (under the influence of some external factors), it is necessary to overcome an energy barrier. The value of this barrier is determined by the magnetic anisotropy energy of the particle (and, consequently, by its volume $V$) and external factors.

d) If a GMM system consisted of magnetically isotropic FM particles, i.e., if a corresponding energy barrier did not exist, the description of its magnetic properties would be possible with the help of the Langevin function. In so doing

 

the temperature-field dependence of magnetization [e.g., see Ref. 1] of a system-ensemble of identical volume particles in this case is written as:

$$\mu(H,T)=\mu_s L\left(\frac{\mu_s VH}{kT}\right), \tag{2}$$

where $\mu_s$ is the saturation magnetization of FM substance, $\mu_s V$ is the value of the magnetic moment of the particle with the volume $V$. GMM systems whose magnetization is described by expression (2) (with the addition of ''blocking'' concept) are usually called *superparamagnetics* and these concepts were first introduced into the physics of magnetic phenomena by C. Bean.[8]

e) Even if, with the help of an external magnetic field in the particles of GMM under investigation the energy barrier connected with the energy of magnetic anisotropy is destroyed, the orientation dependence of magnetic energy of system particles is not described by the cos $\theta$-function (except in the limiting case of ''a very strong external magnetic field'' which will be treated below).

f) Thus it can be stated that the GMM systems with granules of real FM material that we consider cannot be, generally speaking, described by the classic theory Langevin. This circumstance was also noted earlier also by L. Néel,[9,10] Yu. Reicher, M. Shliomis[11]

g) Nevertheless, up to now, attempts at describing real GMM systems with the help of the Langevin function have continued to be made (see Refs. 1–5, for example). However, it should be noted that, in order to describe peculiarities relating to magnetic anisotropy of the FM component, the concepts of ''blocking volume'' of particles at a fixed temperature and ''blocking temperature'' of fixed volume of particles were introduced into the physics of magnetic phenomena.

h) In a real GMM system there are FM component particles of different volume, i.e., in the system, there is a certain function of their distribution $f(V)$ by volume $V$. It is evident therewith that the full volume of FM substance in the system is

$$V_{\rm mag}=\int_{V_{\rm min}}^{V_{\rm max}} Vf(V)dV=\sum_i f_i V_i, \tag{3}$$

where $V_{\rm min}$ and $V_{\rm max}$ are the minimum and maximum granule volumes existing in the GMM system, $V_i$ is the volume of the $i$-granule, $f_i$ is the number of granules with volume $V_i$. In Eq. (3) we gave both continuous and discrete description of the subsystem of FM substance granules in the GMM system.

### 3. MAGNETIC ENERGY OF GRANULES, ENERGY BARRIER AND FREE ENERGY OF THE SYSTEM

The object for investigation is placed in an external magnetic field, the direction of which coincides with that of magnetic anisotropy axes. Néel was the first to consider such a geometry of the problem.[10] At the initial stage of research we neglect the interaction of FM component granules with each other. Moreover, all the particles of the GMM system are supposed to be unidomain, i.e., magnetized homogeneously.

It is evident that, when there is no interaction between particles (and only in this case), the full magnetic energy $\varepsilon_i$ of a separate $i$-particle with the volume $V_i$ and saturation magnetization of granules of FM substance $\mu_s$ represents the sum of a magnetic anisotropy energy $\varepsilon_{ai}$ and its Zeeman energy $\varepsilon_{Hi}$ in the external magnetic field, i.e.,

$$\varepsilon_i=\varepsilon_{ai}+\varepsilon_{Hi}. \tag{4}$$

As is known, the expression

$$\varepsilon_{ai}=-K_{\rm eff}V_i(\mu_i,\mathbf{e}_z)^2 \tag{5}$$

can be written for magnetic uniaxial particles, where the constant $K_{\rm eff}$ represents the density of effective uniaxial magnetic anisotropy energy, $M_i=\mu_s V_i$ is the value of magnetic moment of $i$-particle of the ensemble, $\mu_i,\mathbf{e}_z$ are unit vectors along the directions of the magnetic moment $\mathbf{M}_i$ and Cartesian axis $i$ along which the magnetic anisotropy axes of all system particles and external magnetic field are oriented. The Zeeman energy of the $i$-particle is

$$\varepsilon_{Hi}=-\mu_s V_i H(\mu_i,\mathbf{e}_z). \tag{6}$$

In a spherical system of coordinates with the polar axis $\mathbf{e}_z$ we have

$$\mu_i=(\cos\varphi_i\sin\theta_i,\sin\varphi_i\sin\theta_i,\cos\theta_i),$$

$$\mathbf{H}=(0,0,H) \tag{7}$$

and the expression for the full energy of $\varepsilon_i$ particle is written as

$$\varepsilon_i=-\Delta\varepsilon_{ai}(\cos^2\theta_i+2h\cos\theta_i), \tag{8}$$

$$\Delta\varepsilon_{ai}=K_{\rm eff}V_i>0,\quad h=\frac{\mu_s H}{2K_{\rm eff}}=\frac{H}{H_a}.$$

The value of $\Delta\varepsilon_{ai}$ determines the energy barrier in the absence of the external magnetic field that is to be overcome in order to change the orientation of magnetic moment $\mathbf{M}_i$ from one of the ''easy'' directions $\theta_i=0,\ \pi$ to another $\theta_i=\pi,0$.

It is not difficult to show that the value of the energy barrier in the external magnetic field of selected orientation decreases with the increase of $h$ value by the law

$$\Delta\varepsilon_i=\Delta\varepsilon_{ai}(1-h)^2. \tag{9}$$

At last, when the value of the external magnetic field $H$ reaches the value of the so-called magnetic anisotropy field $H_a$, i.e., $h=1$, the energy barrier disappears [see Eq. (10)] and in the energy of the particle $\varepsilon_i$ just one minimum is left at $\theta_i=0$, i.e., the only one equilibrium state. In this external magnetic field, the energy of the particle $\varepsilon_i$ is

$$\varepsilon_i=-\Delta\varepsilon_{ai}[(\cos\theta+1)^2-1]. \tag{10}$$

While the value of the external magnetic field increases further, there is only additional deepening of the single minimum in the particle energy $\varepsilon_i$ at $\theta_i=0$.

Based on the above uncomplicated arguments, the following conclusions (very important ones for further discussion) can be drawn:

1. Granules of different volumes have different values of corresponding energy barriers. This makes it possible, if needed, to introduce the concepts of ''volume'' and ''temperature'' of blocking.

2. Energy barriers in the granules of different volume disappear in one and the same external magnetic field which is equal to the field of magnetic anisotropy $H_a$ [condition $h=1$ from Eq. (9)].

3. Orientational dependence of the energy of $i$ -particle $\varepsilon_i$, even at energy barrier disappearance, is rather far from being $\sim\cos\theta$ [see Eq. (10)]. In other words, even in this case, generally speaking, the Langevin description of the GMM system does not seem to be correct, although all the particles of the system are ''unblocking,'' i.e., they behave in a way resembling a superparamagnetic one.

4. Only in cases (which will be demonstrated below) $T \gg \max\{\Delta\varepsilon_{ai}\}$ and $H \gg H_a$ can one use the Langevin description of the system without doubt.

Thus, the energy of the $i$th particle of the GMM system is described by expression (8). The granule ensemble contains $f_i$ particles with $V_i$ volume, where $f_i$ is the function of granules distribution by volume and the full volume $V_{\text{mag}}$ of the FM component is (3). The full energy of the GMM system (the energy of noninteracting granules ensemble) can be written as

$$E=\sum_i f_i\varepsilon_i, \tag{11}$$

where $\varepsilon_i$ is determined by expression (8).

At finite temperatures the probability of detecting the system (having thermodynamic equilibrium) with energy $E(x_i)$ in the volume element of generalized coordinates $\prod_i dx_i$ is determined by the Boltzmann exponent

$$\exp[-E(x_i)/kT]. \tag{12}$$

In our case, it means that the probability for the $i$-particle (granule) with volume $V_i$ to have the direction of magnetic moment $\mathbf{M}_i$ in the element of space angle $d\Omega_i = \sin\theta_i\, d\varphi_i d\theta$ is

$$d\omega_i = A_i \exp\left[\frac{\Delta\varepsilon_{ai}}{kT}(\cos^2\theta_i + 2h\cos\theta_i)\right] d\Omega_i, \tag{13}$$

where $A_i$ is some constant. It is clear that in this case the corresponding statistical sum $Z$ of the system is determined by an expression

$$Z=\prod_i \left\{A_i\int_{\Omega_i} d\Omega_i \exp\left[\frac{\Delta\varepsilon_{ai}}{kT}(\cos^2\theta_i + 2h\cos\theta_i)\right]\right\}^{f_i} \tag{14}$$

and the free energy $F$ of the system

$$F=-T\ln Z \tag{15}$$

takes the form:

$$F(H,T)=\sum_i f_i F_i(H,T), \tag{16}$$

where

$$F_i(H,T)=-T\ln\left\{A_i\int_{\Omega_i} d\Omega_i \times\exp\left[\frac{\Delta\varepsilon_{ai}}{kT}(\cos^2\theta_i + 2h\cos\theta_i)\right]\right\}.$$

It is necessary to emphasize that additivity of free energy $F$ (16) of the system (and the expression for partition function $Z$ (14) as the product) is conditioned by our neglecting of FM granule interactions with each other. As will be seen below, the magnetic moment of the system will also possess the additivity property. It is mathematically reflected in the independence of some direction of the ***i***th cluster magnetic moment from the state of other system particles.

## 4. MAGNETIC MOMENTS OF SYSTEM AND GRANULES, ITS CONSTITUENTS, MAGNETIZATION AND STATIC MAGNETIC SUSCEPTIBILITY

As is known, the magnetic moment of $M(H,T)$ of the system at temperature differing from absolute zero is expressed by

$$\mathbf{M}(H,T)=-\partial F(H,T)/\partial\mathbf{H}, \tag{17}$$

or, accounting for the geometry and symmetry of our problem,

$$\mathbf{M}(H,T)=M(H,T)e_z,$$
$$M(H,T)=-\partial F(H,T)/\partial H. \tag{18}$$

Taking into account expression (16) for the system free energy, it is easy to obtain from (18)

$$M(H,T)=\sum_i f_i M_i(H,T),$$
$$M_i(H,T)=T\frac{\partial}{\partial H}\ln\left\{A_i\int_{\Omega_i} d\Omega_i \times\exp\left[\frac{\Delta\varepsilon_{ai}}{kT}(\cos^2\theta_i + 2h\cos\theta_i)\right]\right\}. \tag{19}$$

Further on, it will be convenient for us to use the so-called reduced parameters (as regards the internal parameters of the system, namely as regards the value of energy barrier in the absence of external magnetic field and the value of magnetic anisotropy field)

$$a_1^2=\Delta\varepsilon_{ai}/kT=K_{\text{eff}}V_i/kT, \quad h=H/H_a,$$
$$H_a=2K_{\text{eff}}/\mu_s. \tag{20}$$

This is convenient because, e.g., for GMM systems with various FM components (i.e., different values of $K_{\text{eff}}$ and $\mu_s$) but with identical functions of particles distribution by their volume $f(V)$ and identical $V_{\text{mag}}$ and proportion $K_{\text{eff}}V_0/kT$, where $V_0$ is the position of function maximum $Vf(V)$, the curves of reduced magnetization

$$m(a_i^2,h)=\left(\sum_i f_i M_i(H,T)\right)\left(\mu_s\sum_i f_i V_i\right)^{-1} \tag{21}$$

as functions of reduced magnetic field $h$ just coincide.

It is not difficult to show that, when the variables (20) are used, the expression for the system magnetic moment (19) can be written as

$$M(H,T)=\sum_i f_i M_i(a_i^2,h),$$

$$M_i(a_i^2,h)=\frac{a_i^2}{2}\left\{\int_{\Omega_i} d\Omega_i \exp[a_i^2(\cos^2\theta_i + 2h\cos\theta_i)]\right\}^{-1}\frac{\partial}{\partial h}\int_{\Omega_i} d\Omega_i \times\exp[a_i^2(\cos^2\theta_i+2h\cos\theta_i)]. \quad (22)$$

In the case of continuum description

$$m(H,T)=\left(\int_{V_{\min}}^{V_{\max}} Vf(V)\Phi[a^2(V),h]dV\right)\times\left(\int_{V_{\min}}^{V_{\max}} Vf(V)dV\right)^{-1} \quad (23)$$

where $m(H,T)$ is the reduced magnetization ($|m(H,T)\leqslant 1|$), and

$$\Phi(a_i^2,h)=\frac{\exp[a_i^2(1+h)^2]-\exp[a_i^2(1-h)^2]}{\sqrt{\pi}a_i\{\mathrm{erfi}[a_i(1+h)]+\mathrm{erfi}[a_i(1-h)]\}}-h=\frac{1-\exp(-4a_i^2h)}{2a_i\{F_D[a_i(1+h)]+\exp(-4a_i^2h)F_D[a_i(1-h)]\}}-h. \quad (24)$$

In expression (24) for the function $\Phi(a_i^2,h)$ both special functions

$$\mathrm{erfi}(x)=\frac{2}{\sqrt{\pi}}\int_0^x dt\exp(t^2) \quad (25)$$

and the Dawson integral were used

$$F_D(x)=\exp(-x^2)\int_0^x dt\exp(t^2). \quad (26)$$

Thus, from expressions (23)–(26) it is clear that equilibrium curves of magnetization of a real GMM system consisting of magnetic anisotropic FM material granules (in this case of magneto-uniaxial), and, consequently, all equilibrium magnetic parameters of such a system in the whole range of external parameters change ($H$ and $T$) can be described only by the $\Phi(a_i^2,h)$-function and cannot described by the Langevin function $L(2a_i^2h)=L(\mu_s V_i H/kT)$.

There are quite substantial reasons for believing that in real GMM systems the so-called Lifshitz–Slyozov–Wagner logarithmically normal (log-normal) distribution [12,13] of particles by volume is implemented (see, e.g., Refs. 12–14), i.e.,

$$f(V)=\frac{1}{\sqrt{2\pi}V_\sigma}\exp\left\{-\frac{\ln^2(V/V_0)}{2\sigma^2}\right\}. \quad (27)$$

In expression (27): $\sigma$ is dispersion (half-width) of the corresponding distribution while $V_0$ is the volume corresponding to the maximum of the function $Vf(V)$. It is necessary to note that the using of the log-normal distribution function (its properties) gives us the possibility of extending the limits of integrations in (23) to the whole interval of volumes $\{0, \infty\}$.

The temperature parameter $a_i^2$ can be expressed by the so-called blocking temperature. As is known, (see, e.g.,[1–5]), the blocking temperature of the particle with volume $V_i$ in the absence of external magnetic field is determined as

$$T_{\mathrm{bl},i}^0=K_{\mathrm{eff}}V_i/k\ln\left(\frac{\tau}{\tau_0}\right), \quad (28)$$

where $\tau_0$ is relaxation time and $\tau$ is observation time (as a rule, in the usual experiment to measure static magnetic equilibrium properties $\ln(\tau/\tau_0)\approx 25$ is used). Then, it is evident that we have

$$a_i^2=(T_{\mathrm{bl},i}^0/T)\ln\left(\frac{\tau}{\tau_0}\right). \quad (29)$$

However, the following should be noted. The temperature and volume of blocking are introduced into the physics of GMM systems when their equilibrium properties are described in order to break the sums or integrals in the numerators of expression (24) into two parts, the first of which relates to ''blocked'' particles, the second parts relates to ''unblocked'' particles. In so doing, ''blocked'' particles are described as showing ''ferromagnetic'' behavior, while ''unblocked'' ones, with the help of the Langevin function, as showing ''superparamagnetic'' behavior.

The use of the function $\Phi[a_i^2(V),h]$ instead of Langevin's function eliminates all the noted contradictions and complications and we do not think it is necessary to use the concept of blocking (at least when describing thermodynamic equilibrium magnetic properties of the GMM system). The argument of exponent $a_i^2(1-h)^2$ and the argument of functions erfi $[a_i(1-h)]$ and $F_D[a_i(1-h)]$ completely takes into account the competition of heat energy with the full magnetic energy of the particle of any volume at any significant parameters $T$ and $H$. This moment is thought to be quite significant and it is connected with the magnetic anisotropy of granules of the FM material. This more realistic description of magnetic properties of GMM systems was proposed by F. G. West[15] in 1961 (see also, Ref. 16) and was forgotten afterward.

Static magnetic susceptibility of a system is determined as

$$\chi(H,T)=\partial M/\partial H \quad (30)$$

or, taking into account that

$$\frac{\partial}{\partial H}=\frac{\mu_s}{2K_{\mathrm{eff}}}\frac{\partial}{\partial h}, \quad (31)$$

we obtain from Eq. (30)

$$\chi(H,T)=\frac{\mu_s^2}{2K_{\mathrm{eff}}}\sum_i f_i V_i\Psi(a_i^2,h)=\frac{\mu_s^2}{2K_{\mathrm{eff}}}\int_{V_{\min}}^{V_{\max}} Vf(V)\Psi(a^2(V),h)dV, \quad (32)$$

where

$$\Psi(a_i^2,h)=\frac{2a_i}{\sqrt{\pi}}(1+h)\frac{\exp[a_i^2(1+h)^2]-\exp[a_i^2(1-h)^2]}{\mathrm{erfi}[a_i(1+h)]+\mathrm{erfi}[a_i(1-h)]}$$
$$-\frac{\pi}{8}\left\{\frac{\exp[a_i^2(1+h)^2]-\exp[a_i^2(1-h)^2]}{\mathrm{erfi}[a_i(1+h)]+\mathrm{erfi}[a_i(1-h)]}\right\}^2-1. \tag{33}$$

In conclusion of this section we would like to recall that when describing the GMM system as a superparamagnetic one,

$$M(H,T)=\mu_s\sum_i f_iV_iL(2a_i^2h)$$
$$=\mu_s\int_{V_{\min}}^{V_{\max}}Vf(V)L(2a^2(V)h)dV, \tag{34}$$

and the static magnetic susceptibility

$$\chi(H,T)=\frac{\mu_s^2}{2K_{\mathrm{eff}}}\sum_i f_iV_i\Xi(a_i^2,h)$$
$$=\frac{\mu_s^2}{2K_{\mathrm{eff}}}\int_{V_{\min}}^{V_{\max}}f(V)\Xi(a^2(V),h)dV, \tag{35}$$

where

$$2a_i^2h=\frac{\mu_sV_iH}{kT} \tag{36}$$

the argument of the Langevin function corresponding to the Langevin classic theory, while

$$\Xi(a_i^2,h)=\frac{\sinh(2a_i^2h)-4a_i^4h^2}{2a_i^2h^2\sinh(2a_i^2h)}. \tag{37}$$

It not difficult to show that, for example, in the case when the orientation of the applied external magnetic field is perpendicular to the magnetic anisotropy axis of granules the $\Phi(a_i,h)$-function in expression (23) has the form (this case corresponds to $K_{\mathrm{eff}}<0$)

$$\Phi(a_i,h)=\frac{\{\exp[-a_i^2(1+h)^2]-\exp[-a_i^2(1-h)^2]\}}{\sqrt{\pi}a_i[\mathrm{Erf}\{a_i(1+h)\}+\mathrm{Erf}\{a_i(1-h)\}]}+h, \tag{38}$$

$$a_i^2=\frac{|K_{\mathrm{eff}}|V_i}{kT},\quad h=\frac{\mu_sH}{2|K_{\mathrm{eff}}|}, \tag{39}$$

where Erf $(x)$ is the error function.

## 5. SOME SPECIAL CASES. COMPARISON WITH LANGEVIN CLASSIC THEORY

### *a) GMM system with granules of identical sizes*

Under these conditions, it is evident that in a discrete description of the GMM system there is only one value of $f_i$ different from zero that corresponds to the volume of granules $V_0$, and it coincides with the total number of granules in the system. When the GMM system is described in continuum, the distribution function of the system of particles by their volume has the form of the Dirac $\delta$-function

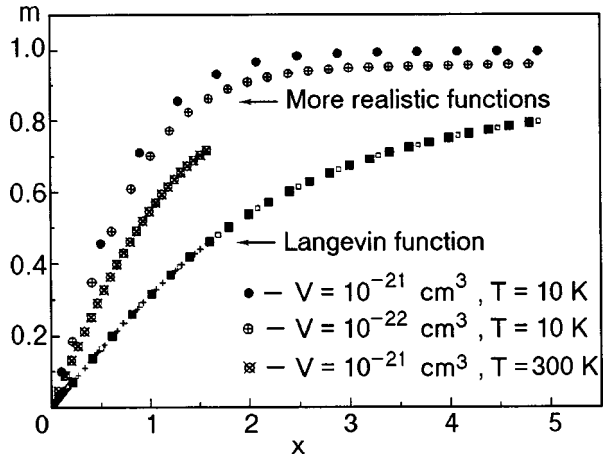


FIG. 1. Dependencies of the magnetization $m=\mu/\mu_s$ of GMM system with identical particles on the Langevin parameter $x=\mu_sVH/kT$ for different volumes of particles and temperatures ($\mu_s=10^3$ Gs, $K_{\mathrm{eff}}=10^8$ erg/cm$^3$). The Langevin description of all GMM systems is the same (the different regions of the lowest curve).

$$f(V)\sim\delta(V-V_0). \tag{40}$$

Here, the reduced magnetization $m(H,T)$ of the GMM system has the form

$$m(H,T)=\Phi(a_0^2,h), \tag{41}$$

and the static magnetic susceptibility

$$\frac{2K_{\mathrm{eff}}}{\mu_s}\chi(H,T)=\Psi(a_0^2,h), \tag{42}$$

where $a_0^2=K_{\mathrm{eff}}V_0/kT$.

Figures 1–4 (as the examples) presents the results of numerical calculation of curves $m(H,T)$ vs the Langevin parameter $2a_i^2h=\mu_sV_0H/kT$ and curves $\chi(h)$ and $\chi(t)$ for a GMM system consisting of *real* FM granules of the same size $V_0$ at different correlations of external and internal parameters of the system. In general, it is seen clearly that these results differ essentially from those that were obtained with the help of the Langevin function. Especially significant to note is a substantial increase in the initial static magnetic susceptibility of the GMM system (as compared to the Langevin one) $\chi(h=0)$ in the range of low temperatures

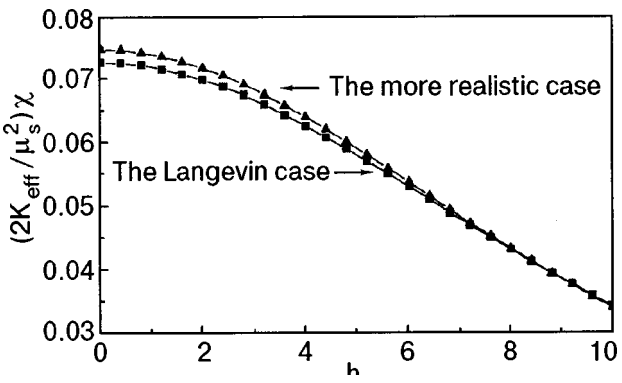


FIG. 2. The static magnetic susceptibility $\chi=dM/dH$ of a GMM system with identical particles as a function of the reduced applied magnetic field $h=H/H_a$ at ''high'' temperatures $t=kT/K_{\mathrm{eff}}V=10\gg1$.

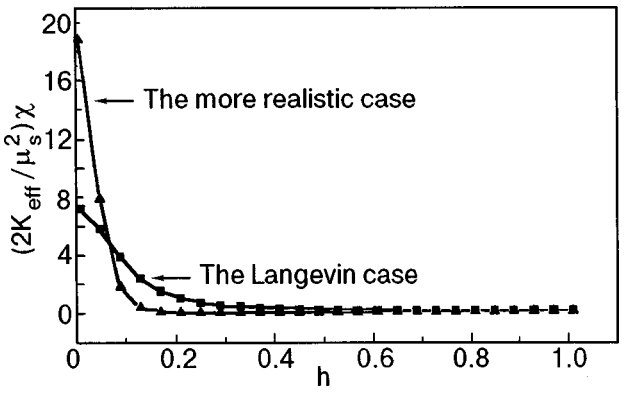


FIG. 3. The static magnetic susceptibility $\chi = dM/dH$ of a GMM system with identical particles as a function of the reduced applied magnetic field $h = H/H_a$ at ''low'' temperatures $t = kT/K_{\text{eff}}V = 0.1 \ll 1$.

$K_{\text{eff}} V_0/kT \gg 1$. This can be essential when GMM objects are used in devices to record and read out an information.

b) The case $f_i V_i = \text{const}(Vf(V) = \text{const})$ is a specific distribution of the system particles when particles of any size contribute equally to the magnetic component volume of the GMM system.

It is not difficult to show that, in these cases, the reduced magnetization of the system can be expressed in the form

$$m(H,T) = \frac{1}{V_{\max} - V_{\min}} \int_{V_{\min}}^{V_{\max}} \Phi[a^2(V),h]dV. \tag{43}$$

Using the theorem of integral calculation on the average

$$\int_{V_{\min}}^{V_{\max}} \Phi[a^2(V),h]dV = (V_{\max} - V_{\min})\Phi[a^2(\hat{V}),h] \tag{44}$$

we come to the expression

$$m(H,T) = \Phi[a^2(\hat{V}),h], \tag{45}$$

where $\hat{V}$ is some value of the volume from the range $[V_{\min}, V_{\max}]$, i.e., $V_{\min} \leqslant \hat{V} \leqslant V_{\max}$.

In other words, this GMM system with such a distribution function behaves as a GFM system consisting of identical granules with the volume $V$. Considered below are some limit cases for values of the system's external parameters $H$ and $T$.

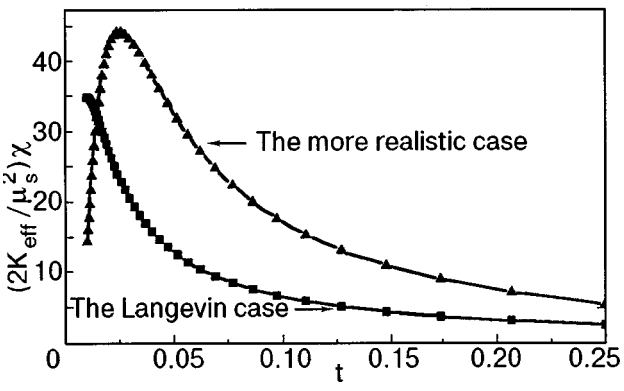


FIG. 4. The static magnetic susceptibility $\chi = dM/dH$ of a GMM system with identical particles as a function of the reduced temperature $t = kT/K_{\text{eff}}V$ at ''weak'' external magnetic field $h = H/H_a = 0.01 \ll 1$.

c) $H \gg H_a (h \gg 1)$.

In these conditions, taking into account that $|\cos\theta| \leqslant 1$ and neglecting the unity as compared to $h$ in expressions (13), (14), (16), (19), and (22), we come to the Langevin classic theory. And this is not surprising as it is under these conditions that the energy barrier in all the particles of the GMM system disappears and the orientation dependence of full magnetic energy of the system [see Eq. (9)] becomes quite near $\sim \cos\theta$.

The same result can be obtained by using asymptotic expressions for the above mentioned special functions at the corresponding conditions.

d) $h = 0$.

In accordance with the general postulates of equilibrium thermodynamics, in this situation, at any temperatures, the system under investigation must be demagnetized, i.e., $m = 0$. It is this result that comes out of the expression for the function $\Phi(a_i^2,h)$ [see (24)] at $h = 0$, as the numerator of the first term is equal to zero, its denominator is equal to $2\sqrt{\pi}$ erfi $(a_i)$ and the second term is equal to zero.

e) Let us consider now the region of temperatures which are so ''high'' that one can think that, for $a_i$ parameters of all the system particles the conditions $a_i \ll 1$, $a_i^2 \ll 1$ are fulfilled and the region of values of the external magnetic field is such that $a_i^2 h \ll 1$ (this corresponds to the case of $\mu_s V_i H/kT \ll 1$, $K_{\text{eff}} V_i/kT \ll 1$). Using expansions

$$\exp[a_i^2(1 \pm h)^2] = 1 + a_i^2(1 \pm h)^2 + \frac{1}{2}a_i^4(1 \pm h)^4 + \ldots \tag{46}$$

and

$$\text{erfi}[a_i(1 \pm h)] = a_i(1 \pm h) + \frac{1}{3}a_i^3(1 \pm h)^3 + \ldots$$

it is not difficult to obtain

$$\Phi(a_i^2,h) = \frac{1}{3}2a_i^2 h = \frac{1}{3}\frac{\mu_s V_i H}{kt} \tag{47}$$

which coincides with the expansion of the Langevin function when $2a_i^2 h = \mu_s V_i H/kT \ll 1$. Accidentally, it also follows from this that at any temperature differing from $T = 0$ at $h \to 0$ the magnetization of each FM granule (and therefore of the whole GMM system) tends to zero.

Thus under these conditions, every granule of the GMM system and the system as a whole can be described by the classic Langevin theory, i.e., the phenomenon of superparamagnetism takes place.

The above expressions show that when the conditions $a_i^2 \ll 1$, $2a_i^2 h \ll 1$ are implemented, the presence of the energy barrier in the GMM system granules is not essential (it can use the Langevin description).

## 6. CONCLUSIONS

It has been shown that, in a general case, real GMM systems with a magnetic anisotropic FM component cannot be described with the help of the Langevin classic theory, i.e., their thermodynamic equilibrium magnetization and static magnetic susceptibility cannot be described by the Langevin function and its derivatives.

The function has been found (substituting the Langevin function) which describes, in a universal way, the competition of full magnetic energy of a GMM system particle of any volume (without separating them into the so-called ''blocked'' and ''unblocked'') with their heat energy. It has been ascertained that the use of the concept of ''blocking'' is not necessary when the thermodynamic equilibrium properties of GMM are described. In addition to it, the use of such universal description for all the particles of a system and a system as a whole makes it possible to avoid such artificial and ambiguous models, one of which, for instance is used in.[17]

The regions of changing external parameters $H$ and $T$ have been indicated (relating to internal parameters of an FM component of a GMM system) where classic Langevin description of investigated objects is possible. In GMM systems with a known function of granule distribution by their volume $f(V)$, magnetization curves $m(h)$ and curves of static magnetic susceptibility $\chi(h)$, registered at different temperatures, may be used both for determining the value of effective constant of magnetic anisotropy $K_{\text{eff}}$ and for clarifying the peculiarity of its temperature dependence. And conversely, the knowledge of the temperature dependence of the effective magnetic anisotropy constant $K_{\text{eff}}$ may allow one to reconstruct the volume distribution function $f(V)$ of the GMM system particles. The corresponding investigations of both the soft-magnetic and hard-magnetic ferromagnetic components of the different GMM systems will be published later.

The author would like to thank the Israel Ministry of Absorption (the Department of Science Absorption) for financial support, Prof. Gad Gorodetsky from the Ben-Gurion University of the Negev (Israel, Beer-Sheva) for the possibility of working in the region of magnetic properties of GMM systems and the extremely useful discussions and Dr. Victor Meerovich for the help in the work.

*E-mail: stefan@bgumail.bgu.ac.il

[1] S. V. Vonsovsky, Magnetism, Wiley, New York (1974).
[2] C. P. Bean, and J. D. Livingston, J. Appl. Phys. **30**, 1209 (1959).
[3] I. S. Jacobs and C. P. Bean, *Fine Particles, Thin Films and Exchange Anisotropy*, in Magnetism, v. III, G. T. Rado and H. Suhl (eds.), Academic Press (1963), p. 231.
[4] B. D. Cullity, *Introduction to Magnetic Materials*, Addison-Wesley Publishing Company (1972).
[5] *Magnetic Properties of Fine Particles*, edited by J. L. Dormann and D. Fiorani, North Holland (1992).
[6] A. E. Berkovitz, J. R. Mitchell, M. J. Carey, A. P. Young, S. Zhang, F. E. Spada, T. Parker, A. Hutten, and G. Thomas, Phys. Rev. Lett. **68**, 3745 (1992).
[7] J. Q. Xiao, J. S. Jiang, and C. L. Chien, Phys. Rev. Lett. **68**, 3749 (1992).
[8] C. P. Bean, J. Appl. Phys. **26**, 1381 (1955).
[9] L. Neel, Compt. Rend. **228**, 664 (1949).
[10] L. Neel, Ann. Geophys. **5**, 99 (1949).
[11] Yu. L. Reichel, and M. I. Shliomis, Sov. Phys. JETP **40**, 526 (1974).
[12] V. V. Slezov, *Theory of Diffusive Decomposition of Solid Solutions*, Physics Review, Soviet Scientific Reviews/Section A, I. M. Khalatnikov (ed.), Harwood Academic Publishers, v. 17, part 3 (1995).
[13] I. M. Lifshitz and V. V. Slyozov, J. Phys. C **19**, 35 (1961).
[14] M. H. Mathon, F. Maury, F. Dunstetter, N. Lorenzelli, C.-H. de Novion, and F. Boue, J. Phys. (Paris) **3**, 279 (1993).
[15] F. G. West, J. Appl. Phys. **32**, Suppl., 249S (1961).
[16] *Magnetism and Metallurgy*, v. 1, edited by A. E. Berkowitz and E. Kneller, Academic Press, NY and London (1969), p. 421.
[17] B. Dieny, S. R. Teixeira, B. Rodmacq, C. Cowache, S. Auffret, O. Redon, and J. Pierre, JMMM **130**, 197 (1994).

Published in English in the original Russian journal. Reproduced here with stylistic changes by the Translation Consultant.

# Phase diagram of a strongly anisotropic biaxial ferromagnet and the spectra of coupled magnetoelastic waves

Yu. N. Mitsaĭ, Yu. A. Fridman, and O. V. Kozhemyako

*V. I. Vernadskiĭ Tavricheskiĭ National University, ul. Yaltinskaya 4, 95035 Simferopol, Ukraine**

(Submitted August 19, 1999; revised September 16, 1999)
Fiz. Nizk. Temp. **26**, 271–278 (March 2000)

The spectral and thermodynamic properties of a biaxial ferromagnetic crystal are investigated at different temperatures. It is shown that, depending on the direction of the external magnetic field, in the case of a large single-ion anisotropy (much greater than the exchange interaction) there can be both a reorientation phase transition and a transition involving a decrease in the modulus of the magnetization vector. In the first case the elastic and magnetic subsystems actively interact, which leads to the softening of a transverse polarized phonon mode at the point of the orientational phase transition; in the second case the magnon and phonon branches do not interact, and the phase transition takes place through a magnon mode. The phase diagram of a highly anisotropic biaxial ferromagnet is constructed for an arbitrary orientation of the external magnetic field and for arbitrary temperatures. © *2000 American Institute of Physics.* [S1063-777X(00)00303-0]

## 1. INTRODUCTION

The most popular theoretical model for studying magnetic systems is that of a uniaxial magnet. Its popularity is due to the transparency of the results and the relative simplicity of the mathematical description of this model (see, e.g., Ref. 1). However, technological progress has led to the creation of a number of new magnetic materials with anisotropies more complicated than the uniaxial. These materials are mainly low-temperature magnets in which the single-ion anisotropy is comparable to or even greater than the exchange interaction constant (e.g., the singlet magnet $Cs_3Cr_2Br_9$ (Refs. 2 and 3) and a number of others).

Such magnets can exhibit purely quantum effects,[4–6] the presence of which can have a substantial influence on both the dynamics of the system and on its phase states. In particular, they can have phases with a tensor order parameter—so-called quadrupole-ordered (QO) phases (see Refs. 1, 7, and 8).

The onset of QO phases in these systems is due to a change of the ground state and inversion of the energy levels. The latter depends substantially on the orientation of the external magnetic field relative to the crystallographic axes.[1]

In addition, taking the magnetoelastic interaction into account leads to a number of interesting results, e.g., to a fundamental change of the spectral properties in the neighborhood of the orientational phase transitions, specifically, to a softening of the phonon branch of excitations and the appearance of a magnetoelastic gap in the magnon spectrum.[4,9]

In this paper we construct a microscopic theory of coupled magnetoelastic waves in a biaxial ferromagnet (FM); this theory is able to take into account the large single-ion anisotropy and the magnetoelastic coupling for an arbitrary orientation of the external magnetic field and over a wide temperature interval. The phase diagram of these magnets is obtained and investigated for different relationships of the material constants, an arbitrary orientation of the external magnetic field, and a wide range of temperatures.

## 2. DISPERSION RELATION OF A BIAXIAL FERROMAGNET

As a model system we consider a biaxial Heisenberg ferromagnet in an external magnetic field **H** directed parallel to the $0Z$ axis. The Hamiltonian of the system is written

$$\mathcal{H}=-H\sum_n S_n^z+\frac{\beta_1}{2}\sum_n (S_n^z)^2+\frac{\beta_2}{2}\sum_n (S_n^y)^2 + \frac{\beta_3}{2}\sum_n (S_n^x)^2-\frac{1}{2}\sum_{n,n'} J(n-n')\mathbf{S}_n\mathbf{S}_{n'} + v_0\sum_n (S_n^i)^2 u_{ii}(n)+v_1\sum_n S_n^i S_n^j u_{ij}(n) + \int dr\left\{\frac{\lambda}{2}\sum_i u_{ii}^2+\mu\sum_{i,k} u_{ik}^2\right\}, \quad (1)$$

where $\beta_i$ are the single-ion anisotropy constants, $J(n-n')>0$ is the exchange integral, $v_i$ are the magnetoelastic coupling constants, $u_{ij}$ are the components of the strain tensor, and $\lambda$ and $\mu$ are elastic constants.

The calculations are done in terms of the Hubbard operators.[10,11] For simplicity we assume that the spin of the magnetic ion $S=1$. However, the proposed calculational scheme is also valid for $S>1$.

Separating out in the exchange part of (1) the mean field $\langle S^z\rangle$ due to the ordering of the magnetic moment, we obtain the one-site Hamiltonian $\mathcal{H}_0(n)$, which in terms of the Hubbard operators has the form[11]

$$\mathcal{H}_0=\sum_n\left(\sum_M A_M H_n^M+\sum_\alpha A_\alpha X_n^\alpha\right). \quad (2)$$

Here $X_n^\alpha=X_n^{M'M}=|\Psi_n(M')\rangle\langle\Psi_n(M)|$ are the Hubbard operators describing the transition of a magnetic ion from the state $M'$ to the state $M(M=-1,0,1)$; $H_n^M\equiv X_n^{MM}$; $\alpha$ are are

 

the corresponding root vectors; $\Psi_n(M)$ are the eigenfunctions of Hamiltonian (2). For a magnet with $S=1$ the general form of the functions $\Psi_n(M)$ was established in Ref. 6. Solving the Schrödinger equation with Hamiltonian (2) we obtain the energy levels of the magnetic ion with allowance for the magnetoelastic interaction:

$$E_1=\frac{2\beta_1+\beta_2+\beta_3}{4}+\frac{v_0}{2}(u^0_{xx}+u^0_{yy}+2u^0_{zz})-\frac{\chi}{2},$$

$$E_0=\frac{\beta_2+\beta_3}{2}+v_0(u^0_{xx}+u^0_{yy}), \tag{3}$$

$$E_{-1}=\frac{2\beta_1+\beta_2+\beta_3}{4}+\frac{v_0}{2}(u^0_{xx}+u^0_{yy}+2u^0_{zz})+\frac{\chi}{2},$$

$$\chi^2=[2\chi_0-v_0(u^0_{xx}-u^0_{yy})\sin 2\theta]^2+v_0^2(u^0_{xx}-u^0_{yy})^2\cos^2 2\theta,$$

$$\chi_0^2=\overline{H}^2+\tilde{\beta}^2,\quad \tilde{\beta}=\frac{\beta_3-\beta_2}{4}, \tag{4}$$

$$\cos\theta=-\frac{\tilde{\beta}}{\sqrt{2\chi_0(\chi_0-\overline{H})}},\quad \overline{H}=H+J(0)\langle S^z\rangle.$$

The spontaneous strains $u^0_{ij}$ are determined from the condition that the free energy density be minimum.

The spin operators and the Hubbard operators are related by

$$S_b^+=\sqrt{2}\cos\tilde{\theta}(X_n^{10}-X_n^{0-1})+\sqrt{2}\sin\tilde{\theta}(X_n^{-10}+X_n^{01}),$$

$$S_n^-=(SS_n^+)^+, \tag{5}$$

$$S_n^z=\cos 2\tilde{\theta}(H_n^1-H_n^{-1})+\sin 2\tilde{\theta}(X_n^{1-1}+X_n^{-11}),$$

$$\tilde{\theta}=\theta-\delta,$$

$$\cos\delta=\frac{v_0(u_{xx}-u_{yy})\cos 2\theta}{\sqrt{2\chi[\chi-2\chi_0+2(u_{xx}-u_{yy})\sin 2\theta]}}.$$

Representing the components of the strain tensor in the form $u_{ij}=u^0_{ij}+u^{(1)}_{ij}$, where $u^{(1)}_{ij}$ is the dynamic part of the strain tensor, which describes the vibrations of the crystal lattice, and quantizing the dynamic part in the standard way,[12] we obtain from Hamiltonian (2) a Hamiltonian describing the processes of transformation of magnons into phonons and back:

$$\mathcal{H}_{tr}=\sum_n\left(\sum_M \tilde{P}_M Y_n^M+\sum_\alpha \tilde{P}_\alpha Y_n^\alpha\right),$$

where

$$\tilde{P}_{M(\alpha)}=\sum_{k,\lambda}(b_{k,\lambda}+b^+_{-k,\lambda})T_n^{M(\alpha)}(k,\lambda)/\sqrt{N};$$

$b^+_{-k,\lambda}$ and $b_{k,\lambda}$ are the creation and annihilation operators for phonons with polarization $\lambda$, $T_n^{M(\alpha)}(k,\lambda)$ are the transform amplitudes, and $N$ is the number of sites in the crystal lattice.

The spectrum of elementary excitations is determined by the poles of the Green function, which in our case has the form

$$G^{\alpha,\alpha'}(n,\tau,n',\tau')=-\langle T\tilde{Y}_n^\alpha(\tau)\tilde{Y}_{n'}^{-\alpha'}(\tau')\rangle. \tag{6}$$

Here $T$ is the Wick operator, $\tilde{Y}_n^\alpha(\tau)$ is the Hubbard operator in the Heisenberg representation, and the averaging is done using the total Hamiltonian $\mathcal{H}$. All the calculations below will be done in the mean-field approximation.

The equation for the Green function (6) has the form of Larkin's equation.[13] Solving it, we obtain the dispersion relation for coupled magnetoelastic waves:

$$\det\|\delta_{ij}+\frac{J(k)}{2}G_0^\alpha(\omega_n)b(\alpha)a_{ij}(\alpha)+\frac{J(k)}{2}B_0T^{-\alpha}(k,\lambda)G_0^\alpha(\omega_n)b(\alpha)T^\beta(-k,\lambda')\times G_0^\beta(\omega_n)b(\beta)a_{ij}(\alpha,\beta)\|=0. \tag{7}$$

In Eq. (7) we have introduced the following notation:

$$B_0=\frac{D_\lambda(k,\omega_n)}{1-Q_{\lambda\lambda'}D_{\lambda'}(k,\omega_n)},\quad Q_{\lambda\lambda'}=T^\alpha(-k,\lambda)G_0^\alpha(\omega_n)b(\alpha)T^{-\alpha}(k,\lambda),$$

$$a_{ij}(\alpha,\beta)=\begin{pmatrix} 2\gamma_\parallel(\alpha)\gamma_\parallel(-\beta) & \gamma_\parallel(\alpha)\gamma_\perp^*(\beta) & \gamma_\parallel(\alpha)\gamma_\perp(-\beta)\\ 2\gamma_\perp(\alpha)\gamma_\parallel(-\beta) & \gamma_\perp(\alpha)\gamma_\perp^*(\beta) & \gamma_\perp(\alpha)\gamma_\perp(-\beta)\\ 2\gamma_\perp^*(-\alpha)\gamma_\parallel(-\beta) & \gamma_\perp^*(-\alpha)\gamma_\perp^*(\beta) & \gamma_\perp^*(-\alpha)\gamma_\perp(-\beta)\end{pmatrix}.$$

The functions $\gamma_{\perp(\parallel)}(\alpha)$ are determined from the relation between the spin operators and Hubbard operators.[11]

Dispersion relation (7) is valid over a wide temperature interval, and also for arbitrary values of the material constants $\beta_i$ and $J_0$.

### 3. SPECTRA OF COUPLED MAGNETOELASTIC WAVES

Let us analyze Eq. (7) for the most interesting case, when the wave vector $\mathbf{k}\|0Y$. In this geometry the nonzero components of the phonon polarization unit vector are $e_l^y$, $e_\tau^x$, and $e_\tau^z$, and dispersion relation (7) decomposes into two equations, which determine the spectra of the ''longitudinal'' and ''transverse'' vibrations, respectively:

$$(1+x_{11})\begin{vmatrix}1+x_{22} & x_{23}\\ x_{32} & 1+x_{33}\end{vmatrix}=0, \tag{8}$$

where

$$x_{ij}=\frac{J(k)}{2}[G_0^{\alpha}b(\alpha)a_{ij}(\alpha)+B_0G_0^{\alpha}T^{-\alpha}(k)b(\alpha)G_0^{\beta}T^{\beta}\times(-k)b(\beta)a_{ij}(\alpha,\beta)].$$

This ''decoupling'' of Eq. (7) is possible because in our case $\gamma_{\perp}(\alpha)\gamma_{\parallel}(\beta)=0$ for all $\alpha$, $\beta$.

At low temperatures ($T\to 0$) we only need to consider the lowest energy level.

The ferromagnetic (FM) phase in which the system under study may be found is stable in two cases: 1) $\beta_3>\beta_1>\beta_2$; 2) $\beta_1>\beta_3>\beta_2$. These cases actually correspond to a rotation of the magnetic field: in the first case the field is perpendicular to the easy axis, and in the second case it is perpendicular to the easy plane. This can easily be seen by representing the energy of the single-ion anisotropy in Hamiltonian (1) as $(\beta_1-\beta_3)(S^z)^2/2+(\beta_2-\beta_3)(S^y)^2/2$, using the well-known quantum-mechanical identity $(S^x)^2+(S^y)^2+(S^z)^2=S(S+1)$.

Let us consider these cases in more detail. If the single-ion anisotropy constants are related as $\beta_3>\beta_1>\beta_2$, then the magnetic field **H** is parallel to the ''medium'' magnetization axis. Solving the dispersion relation (8), we obtain the spectra of the ''longitudinal'' and ''transverse'' branches of excitations, which in our geometry have the form

$$\varepsilon_{\parallel}(k)=\sqrt{E_{1-1}(E_{1-1}+2J(k)\sin^2 2\tilde{\theta})};$$

$$\omega_{\parallel}^2(k)=\omega_l^2(k)\frac{E_{1-1}+2J(k)\sin^2 2\tilde{\theta}+2a_0\cos^2 2\tilde{\theta}}{E_{1-1}+2J(k)\sin^2 2\tilde{\theta}};\qquad(9)$$

$$\varepsilon_{\perp}(k)=\sqrt{[E_{10}+J(k)(1+\sin 2\tilde{\theta})][E_{10}+J(k)(1-\sin 2\tilde{\theta})]};$$

$$\omega_{\perp}^2(k)=\omega_{\tau}^2(k)\frac{E_{10}+J(k)(1-\sin 2\tilde{\theta})+a_1(1+\sin 2\tilde{\theta})}{E_{10}+J(k)(1-\sin 2\tilde{\theta})};\qquad(10)$$

where $E_{ij}=E_i-E_j(i,j=1,0,-1)$; $a_0=v_0^2/2\mu$, $a_1=v_1^2/2\mu$; $\omega_l(k)$ and $\omega_{\tau}(k)$ are the spectra of longitudinally and transversely polarized noninteracting acoustic waves, respectively.

In the case when the largest parameter of the system under study is the exchange interaction constant ($J_0\gg\beta_i, a_iH$), i.e., in the case of small single-ion anisotropy, the system undergoes a reorientation phase transition from the FM to the tilted phase. The soft mode in this case is a transversely polarized quasiphonon branch, and a magnetoelastic gap appears in the quasimagnon spectrum. This corresponds to the known results for uniaxial magnets[4,9] when the corresponding renormalizations are taken into account.

The most interesting situation is when the single-ion anisotropy constants are comparable to or even greater than the exchange interaction constant. In that case (see, e.g., Refs. 1, 4, and 5) the system can manifest purely quantum effects such as the ''quantum contraction of the spin.''

If $\tilde{\beta}>J_0, H$, then the mean value of the magnetization, as follows from Eq. (5), is smaller than the maximum possible value $\langle S^z\rangle=1$ and is given by

$$\langle S^z\rangle\approx\frac{H}{\tilde{\beta}}.$$

This decrease is due to the fact that the ground state of the crystal is a superposition of the states $|1\rangle$ and $|-1\rangle$ of the operator $S^z$. The larger the value of $\tilde{\beta}$, the larger the contribution from the $|-1\rangle$ state, and that leads to a decrease in $\langle S^z\rangle$.

As an analysis of the spectra of coupled magnetoelastic waves shows, in this case there do not exist values of the magnetic field for which the quasiphonon branch would soften. This means that the system does not undergo an orientational phase transition, and $\langle S^z\rangle$ remains always parallel to the $0Z$ axis and decreases in modulus as the magnetic field $H$ is decreased.

Let us now consider the second case, when the single-ion anisotropy constants are related as $\beta_1>\beta_3>\beta_2$. Here the magnetic field is parallel to the ''hard'' magnetization axis. The case of small single-ion anisotropy leads to results that are analogous to the case $\beta_3>\beta_1>\beta_2$.

Let us now examine the spectra of coupled magnetoelastic waves in a highly anisotropic biaxial FM ($\beta_i\gg J_0$).

As was shown in Refs. 1, 4, and 5, in the case when the single-ion anisotropy energy becomes equal to the exchange energy, besides the FM and quadrupole-ferromagnet (QFM) phases there can be phases with a tensor order parameter (QO phases).

We assume that at the fields $H_{c2}$ and $H_{c3}$ there occur orientational phase transitions from the QO phase, characterized by a tensor order parameter, to the QFM (tilted) phase and from the QFM phase to the FM phase, in which the magnetic moment is directed along the field.

Let us study the spectra of the coupled magnetoelastic waves in the field intervals $H>H_{c3}$ and $H<H_{c2}$.

For $H>H_{c3}$ the mean magnetization is directed along the field. The ground state in this case is $\tilde{\Psi}_n(1)$, and the lowest energy level is $E_1$. The mean magnetic moment $\langle S\rangle\approx 1$.

The spectrum of quasiphonons in this phase is

$$\omega_{\perp}^2(k)=\omega_{\tau}^2(k)\frac{\alpha k^2+H-H_{c3}}{\alpha k^2+H-H_{c3}+a_1}\qquad(11)$$

and it softens in the low-wavelength limit for $H=H_{c3}=\beta=(2\beta_1-\beta_3=\beta_2)/4$. A magnetoelastic gap $\varepsilon\perp(0)=\sqrt{2a_1J_0\tilde{\beta}/\beta}$ appears in the quasimagnon spectrum (at $H=H_{c3}$).

Let us consider the spectrum of magnetoelastic waves for $H<H_{c2}$. In this field interval there occurs an inversion of the energy levels and, as follows from Eq. (4), the lowest level of the magnetic ion is $E_0$, and the ground state is described by the function $\Psi_n(0)$.

It follows from Eq. (7) that the $l$- and $\tau$-polarized acoustic modes do not interact with the magnetic subsystem, and for the spectrum of $\tau$-polarized quasiphonons we have

$$\omega_{\perp}^2(k)=\omega_{\tau}^2(k)\frac{\alpha k^2+H_{c2}^2-H^2}{\alpha k^2+H_{c2}^2-H^2+\tilde{a}_1},\qquad(12)$$

where

$$\tilde{a}_1 = 2a_1(\beta - \tilde{\beta} - 2J_0),$$

$$H_{c2} = \sqrt{(\beta + \tilde{\beta} - 2a_1)(\beta - \tilde{\beta} - 2J_0)}.$$

At $H = H_{c2}$ a magnetoelastic gap appears in the quasimagnon spectrum, with the value

$$\varepsilon_\perp(0) = \sqrt{2a_1 J_0 \tilde{\beta}(\beta - \tilde{\beta})}/\beta.$$

Analogous results have been obtained[4,5] for uniaxial ferromagnets with large single-ion anisotropy. As we see from Eqs. (11) and (12), at $H = H_{c3}$ the system undergoes a phase transition from the FM to the QFM phase, and at $H = H_{c2}$, from the QFM to the QO phase.

Let us examine the behavior of the system at arbitrary temperatures. Suppose we start in the FM phase near the line of the orientational phase transition from the FM to the QFM phase. At first glance it seem that in this phase the change in behavior of the system will be determined solely by the temperature dependence of $\langle S \rangle$, which leads to a decrease in $\langle S^z \rangle$ with increasing temperature. However, in addition to this there are purely quantum effects at work. Indeed, if at low temperatures the lowest energy level in the FM phase is $E_1$, then as the temperature increases, the level $E_1$ increases, while $E_0$ decreases. At fields

$$H_{\text{inv}} \cong \left( \beta - \frac{J_0}{2} \right) \sqrt{1 - (\tilde{\beta}/\beta)^2} \tag{13}$$

the energy levels $E_1$ and $E_0$ become equal, and the mean spin at $H = H_{\text{inv}}$ has the value

$$\langle S^z \rangle_{H = H_{\text{inv}}} \cong \frac{1}{2} \sqrt{1 - (\tilde{\beta}/\beta)^2}.$$

This decrease is due not to the temperature dependence of $\langle S^z \rangle$ but to the inversion of the energy levels in the FM phase for $H \leqslant H_{\text{inv}}$.

With further decrease in the magnetic field and increase in temperature the value of $\langle S^z \rangle$ decreases, and at $H = H_{\text{cr}}$ and $T = T_{\text{cr}}$ it goes to zero: $\langle S^z \rangle = 0$. The values of the critical field and temperature are determined from the spectra of elementary excitations and the equation for $\langle S^z \rangle$:

$$H_{\text{cr}} = \sqrt{(\beta - \tilde{\beta})(\beta + \tilde{\beta} - 2J_0)}. \tag{14}$$

If we set $\beta_2 = \beta_3 = 0$, then expression (14) goes over to the corresponding result of Ref. 14, which was obtained for an easy-plane FM with a large single-ion anisotropy.

From the relation (5) between the spin operators and Hubbard operators it follows that

$$\langle S^z \rangle = \cos 2\tilde{\theta} \frac{\exp(-E_1/T) - \exp(-E_{-1}/T)}{\exp(-E_1/T) + \exp(-E_0/T) + \exp(-E_{-1}/T)}. \tag{15}$$

From the condition $\langle S^z \rangle = 0$ at $H = H_{\text{cr}}$ and $T = T_{\text{cr}}$ and with allowance for (14), we obtain an equation for finding $T_{\text{cr}}$:

$$\tilde{J}_0 \exp \frac{2\beta - \tilde{J}_0}{T_{\text{cr}}} - (2\beta - \tilde{J}_0) \exp \frac{\tilde{J}_0}{T_{\text{cr}}} = 4(\beta - J_0), \tag{16}$$

where $\tilde{J}_0 = J_0(\beta + \tilde{\beta})/\beta$.

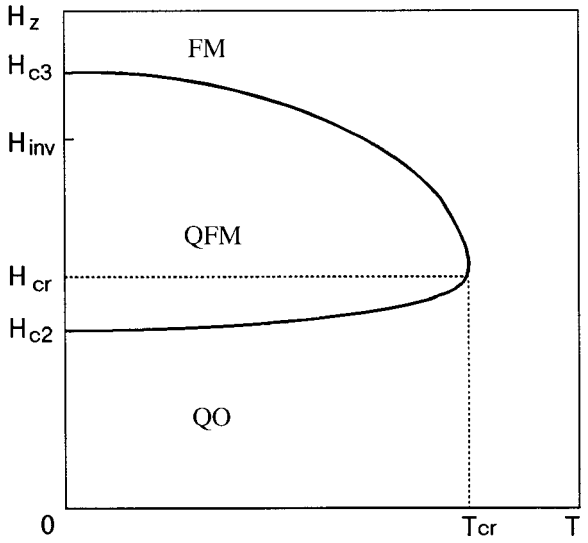


FIG. 1. Phase diagram of a biaxial ferromagnet for $\mathbf{H} \| 0Z$.

It is not possible to solve Eq. (16) exactly in the arbitrary case. However, in the case of large single-ion anisotropy ($\beta \gg \tilde{J}_0$)

$$T_{\text{cr}} = \frac{\tilde{J}_0}{3} \frac{A}{\ln(A-5)}; \quad A = 6\frac{\beta}{\tilde{J}_0}. \tag{17}$$

The phase diagram corresponding to the situation considered above is shown in Fig. 1.

Analogous phase diagrams are obtained for easy-plane FMs with large single-ion anisotropy (see, e.g., Refs. 1, 5, and 14). However, in those papers there is no inversion of the energy levels in the FM phase.

We note that the line $H_{c2}$ separating the QO and QFM phases depends very weakly on temperature, and it is only in the neighborhood of $T_{\text{cr}}$ that this dependence is noticeable. This is because of the weak temperature dependence of the quadrupolar order parameter $q = 3\langle (S^z)^2 \rangle - S(S+1)$.

## 4. PHASE DIAGRAM OF A BIAXIAL FERROMAGNET

Let us consider the case $\beta_1 > \beta_2 > \beta_3$, when the magnetic field lies in the plane $Z0X$ at an angle $\alpha$ to the $0Z$ axis, and we construct the phase diagram of the investigated system. The limiting cases of this geometry are considered above ($\alpha = 0$, $\alpha = \pi/2$). We assume that the single-ion anisotropy is large ($\tilde{\beta} > J_0$).

We rotate the coordinate system around the $0Y$ axis by an angle $\alpha$ such that the new quantization axis $0Z'$ ($0Z' \| \mathbf{H}$) is parallel to the magnetization vector. In this local coordinate system we introduce the new spin operators $\tilde{S}_n^x, \tilde{S}_n^y, \tilde{S}_n^z$, in terms of which the one-site Hamiltonian (2) without allowance for the magnetoelastic coupling has the form

$$\mathcal{H}_0(n) = -\bar{H}\tilde{S}^z + \frac{B_1}{2}(\tilde{S}^z)^2 + \frac{\beta_2}{2}(\tilde{S}^y)^2 + \frac{B_3}{2}(\tilde{S}^x)^2 + \frac{\beta_3 - \beta_1}{4} \sin 2\alpha (\tilde{S}^z \tilde{S}^x + \tilde{S}^x \tilde{S}^z), \tag{18}$$

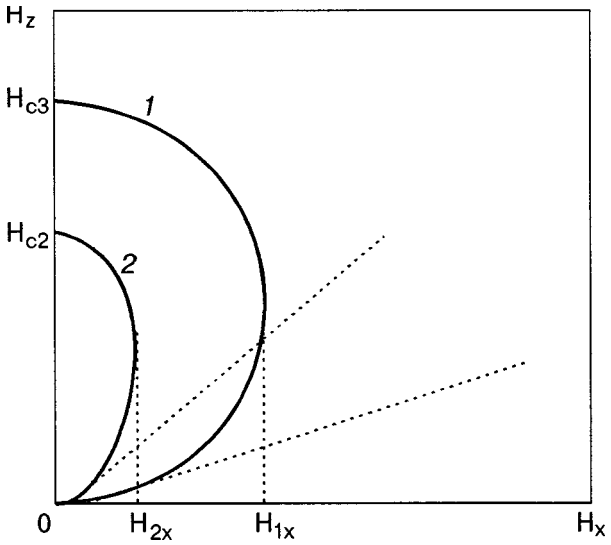


FIG. 2. Phase diagram of a biaxial ferromagnet for an arbitrary orientation of the external magnetic field in the plane $Z0X(T\to 0)$.

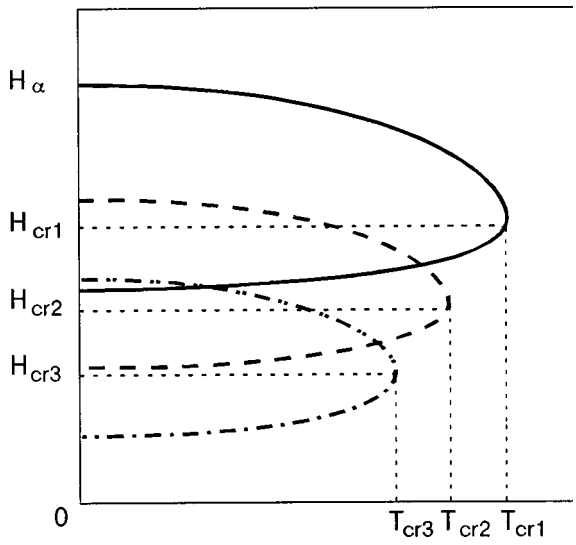


FIG. 3. Phase diagram of a biaxial ferromagnet for an arbitrary orientation of the external magnetic field in the plane $Z0X$ and for arbitrary temperatures.

where

$$B_1=\beta_1\cos^2\alpha+\beta_3\sin^2\alpha;$$

$$B_3=\beta_1\sin^2\alpha+\beta_3\cos^2\alpha. \tag{19}$$

Expression (18) differs formally from the one-site Hamiltonian without allowance for the magnetoelastic coupling by the presence of the last term, proportional to $\sin 2\alpha$. Therefore, if we limit consideration to the cases $\alpha\to 0$ and $\alpha\to\pi/2$, then we will return to the situation considered previously (see Sec. 3) with the replacements $\beta_1\to B_1$ and $\beta_3\to B_3$. The phase diagram of the system at low temperatures $(T\to 0)$ in this case is presented in Fig. 2.

Line *1*, which separates the FM and QFM phases, passes through the points $H_{c3}$ [see Eq. (11)] and $H_{1x}=4/9(H_{c3})^{3/2}$, and the tangent to this line at the point 0 is determined by the equation $\cos 2\alpha=-J_0/\beta'$, where $\beta'=(\beta_1-\beta_3)/4$.

In the case when $\cos 2\alpha<-J_0/\beta'$, the system is found in the FM phase, and only at the point 0 does it undergo a transition to the QO phase, and not by a rotation of the magnetization vector but by a decrease of its modulus to zero.

Line *2*, which separates the QFM and QO phases, passes through the points $H_{c2}$ [Eq. (12)] and

$$H_{2x}=\left\{p\left[\frac{\beta_1(1-p)\beta_3 p-\beta_2}{2}-4a_1\right][\beta'(1-2p)-J_0]\right\}^{1/2},$$

$$p=\frac{1}{8}\,\frac{\beta_1+\beta_3-2\beta_2}{\beta_1-\beta_2},$$

and the equation of the tangent to line 2 at the point 0 has the form $\cos 2\alpha=J_0/\beta'$.

If the angle $\alpha$ satisfies the inequality $-J_0/\beta'<\cos 2\alpha<J_0/\beta'$, then the system can be found in the FM or in the QFM phase, depending on the value of the external magnetic field.

If, however, $\cos 2\alpha>J_0/\beta'$, then the system can be found in any of three phases (FM, QFM, and QO), depending on the value of the field. It should be noted that on lines 1 and 2 (Fig. 2) the system undergoes second-order phase transitions, with the unstable (''soft'') mode being the transversely polarized quasiphonon branch, and a magnetoelastic gap appears in the quasimagnon branch of excitations.

Based on what we have said, in the case of finite temperatures the result can be presented in the form of a phase diagram in the coordinates $(H_\alpha,T)$, where $H_\alpha=Hf(\alpha)$, several cross sections of which are shown in Fig. 3. For the $\alpha=0$ cross section the form of the phase diagram was given previously in Fig. 1 and corresponds to the situation considered in Sec. 3. Increasing the angle $\alpha$ leads to a change in the values of the critical fields and temperature. Thus the values of $H_{c2}$, $H_{c3}$, $H_{\rm cr}$, and $T_{\rm cr}$ in this case are functions of the angle $\alpha$, which specifies the direction of the external magnetic field **H**. Their explicit form is determined by the following expressions:

$$H_{c2}=2\sqrt{[\beta\cos^2\alpha+\tilde\beta\sin^2\alpha-a_1][(\beta-\tilde\beta)\cos 2\alpha-J_0]};\quad H_{c3}=3\beta\cos^2\alpha-\beta-\tilde\beta;$$

$$H_{\rm cr}=2\sqrt{[\beta\cos^2\alpha+\tilde\beta\sin^2\alpha+b(\alpha_3)a_1][(\beta-\tilde\beta)\cos 2\alpha+b(a_3)J_0]};\quad T_{\rm cr}=\frac{2H_{c3}}{\ln(A-5)};\quad A=\frac{3H_{c3}^2}{\beta\cos^2\alpha+\tilde\beta\sin^2\alpha}. \tag{20}$$

Using these expressions, one can easily trace the evolution of the system as the angle $\alpha$ is increased. As we see from Eq. (20), as the angle $\alpha$ is increased, the corresponding expressions for $H_{c2}$, $H_{c3}$, $H_{\rm cr}$, and $T_{\rm cr}$ decrease, i.e., the diagram is shifted downward and is compressed in temperature. For $\alpha$ satisfying the equation $\cos\alpha=\{1+J_0/[2(\beta-\tilde{\beta})]\}/\sqrt{2}$, the field $H_{c2}=0$, and the QO phase degenerates to the line $H_\alpha=0$.

## 5. CONCLUSION

This studies have shown that biaxial FMs have a number of peculiar features. Of particular interest is the case of highly anisotropic magnets. In that case, as we have shown above, phases with a tensor order parameter can arise. Depending on the relationship between the single-ion anisotropy constants, this phase can be realized in different ways. The phase diagram of such systems does not have any analogs among uniaxial magnets.

The obtained phase diagrams for biaxial ferromagnets can be used to determine the existence regions of the FM, QFM, and QO phases for different magnitudes and directions of the external magnetic field and for different values of the temperature.

By taking the magnetoelastic interaction into account, one can find out what relationships of the material constants of the system and what magnitudes and directions of the external magnetic field correspond to phase transitions of the reorientation type or to phase transitions occurring by a decrease in the modulus of the magnetization vector.

*E-mail: man@expl.cris.crimea.ua

[1] V. M. Loktev and V. S. Ostrovskiĭ, Fiz. Nizk. Temp. **20**, 983 (1994) [Low Temp. Phys. **20**, 775 (1994)].
[2] B. Leunberger, H. U. Gudel, R. Horne, and A. J. Duyneveldt, J. Magn. Magn. Mater. **49**, 131 (1985).
[3] B. Leunberger, A. Stables, H. U. Gudel, R. Feile, and J. K. Kjems, Phys. Rev. B **28**, 6300 (1984).
[4] Yu. N. Mitsaĭ and Yu. A. Fridman, Fiz. Tverd. Tela (Leningrad) **32**(8), 361 (1990) [Sov. Phys. Solid State **32**, 1345 (1990)].
[5] F. P. Onufrieva, Fiz. Tverd. Tela (Leningrad) **26**, 3435 (1984) [Sov. Phys. Solid State **26**, 2062 (1984)].
[6] V. M. Loktev, V. S. Ostrovskiĭ, Fiz. Tverd. Tela (Leningrad) **20**, 3086 (1978) [Sov. Phys. Solid State **20**, 1779 (1978)].
[7] Yu. N. Mitsaĭ, Yu. A. Fridman, O. V. Kozhemyako, and O. A. Kosmachev, Fiz. Nizk. Temp. **25**, 690; (1999) [Low Temp. Phys. **25**, 513 (1999)].
[8] Yu. N. Mitsay, Yu. A. Fridman, O. V. Kozhemyako, and M. S. Kochmanski, Acta Phys. Pol. A **96**, 363 (1999).
[9] E. A. Turov and V. G. Shavrov, Usp. Fiz. Nauk **140**, 429 (1983) [Sov. Phys. Usp. **26**, 593 (1983)].
[10] R. O. Zaĭtsev, Zh. Éksp. Teor. Fiz. **68**, 207 (1975) [Sov. Phys. JETP **41**, 100 (1975)].
[11] Yu. N. Mitsaĭ, Yu. A. Fridman, Teor. Mat. Fiz. **89**, 207 (1989).
[12] L. D. Landau and E. M. Lifshitz, *Statistical Physics*, 3rd ed. [Pergamon Press, Oxford (1980); Nauka, Moscow (1975)].
[13] Yu. A. Izyumov and Yu. N. Skryabin, *Statistical Mechanics of Magnetically Ordered Systems* [in Russian], Nauka, Moscow (1987).
[14] Yu. V. Pereverzev and V. G. Borisenko, Fiz. Nizk. Temp. **13**, 1185 (1987) [Sov. J. Low Temp. Phys. **13**, 670 (1987)].

Translated by Steve Torstveit

## PHYSICAL PROPERTIES OF CRYOCRYSTALS

# On the mechanism of transformation of icosahedral rare-gas clusters into fcc aggregations

S. I. Kovalenko, D. D. Solnyshkin, and É. T. Verkhovtseva

*B. Verkin Institute for Low Temperature Physics and Engineering, National Academy of Sciences of Ukraine, pr. Lenina 47, 61164 Kharkov, Ukraine**

(Submitted August 6, 1999)
Fiz. Nizk. Temp. **26**, 279–282 (March 2000)

The experimental diffraction patterns from Kr cluster beams are compared with the diffraction functions calculated for rare-gas clusters with dimensions of $3\times10^3$ and $1\times10^4$ atoms/cluster. The experimental results are found to correlate well with the calculation if it is assumed that the clusters have a face-centered cubic structure with a constant number of intersecting stacking faults. Additional confirmation is obtained for the decisive role of the kinetic factor in the formation of the crystalline phase of the clusters. Conjectures are offered concerning the possible reasons why the densitometer traces presented by M-F. de Feraudy, G. Torchet, and B. W. van de Wall at the conference ISSPIC (1998) showed no substantial changes when the cluster size was increased by more than an order of magnitude. © *2000 American Institute of Physics.* [S1063-777X(00)00403-5]

Theoretical calculations based on the maximization of the particle binding energy indicate that a noncrystalline phase in rare-gas clusters is stable all the way to sizes of $\sim10^5$ atoms/cluster. This makes it difficult to explain the mechanism of transition of the non-crystalline phase to the characteristic face-centered cubic (fcc) structure of massive samples, since in large atomic aggregations such a restructuring would require an expenditure of energy comparable to the heat of fusion of the crystal. Particular attention is paid to the idea that the kinetic factor plays a key role in the formation of the crystalline phase of the cluster. According to the ideas developed in the theoretical papers,[1,2] the coalescence or intergrowth of icosahedral clusters during the growth of a rare-gas cluster creats regions having an fcc lattice with stacking faults. The presence of intersecting stacking faults gives rise to atomic steps on the surface of the cluster which are not overgrown during the growth, the these steps promote the subsequent rapid and defect-free growth of the fcc phase. As a result, the density of stacking faults $\alpha$ decreases as the cluster grows. This hypothesis has been confirmed experimentally in Refs. 3 and 4, in which stacking faults were detected in clusters of heavy rare gases and the density of these stacking faults was found to decrease during growth of the aggregation. In a recent report[5] the diffraction functions calculated for Ar clusters with $N=10^4$ atoms/cluster were presented. A simulation was carried out for clusters both with stacking faults of various configurations and without stacking faults. Previously a similar calculation was carried out for Ar clusters with $N\approx3\times10^3$ atoms/cluster.[1,2]

In the present study we compare the different patterns obtained in an electron-diffraction study of krypton cluster beams with the model diffraction functions given in Refs. 1, 2, and 5 in order to further test the theoretical ideas developed in Refs. 1 and 2.

A study of the structure of Kr clusters which are free from a substrate was carried out on an apparatus consisting of an supersonic cluster-beam generator and a high-energy electron diffraction device. A description of the experimental apparatus, geometry, and procedures is given in Refs. 4 and 6. Figure 1 shows the diffraction patterns from Kr cluster beams with average cluster sizes of $\bar{N}=2\times10^3$ and $1.5\times10^4$ atoms/cluster. For clarity the curves have been shifted along the vertical. Plotted along the abscissa are values of the diffraction vector $s=4\pi\sin\Theta/\lambda$, where $\lambda$ is the electron wavelength and $\Theta$ is the Bragg diffraction angle, and along the ordinate, in arbitrary units, is the diffraction intensity $I(s)$ multiplied by $s^3$. In the experiment the diffraction intensity $I(s)$ was determined. It was then multiplied by $s^3$ for convenience in comparing the experimental curves with the calculation.

The simulated diffraction functions are presented in Fig. 2. Curves a and c were calculated for defect-free fcc rare-gas clusters containing 3281 and $1\times10^4$ atoms/cluster, respectively. Curves b and d were calculated for the same cluster sizes but with two intersecting stacking faults. It follows from a comparison of Figs. 1 and 2 that the diffraction patterns observed in the electron-diffraction experiment are substantially different from diffraction functions a and c in Fig. 2, which were calculated for clusters with a defect-free fcc structure. Whereas on the model functions the fcc peaks are completely resolved, this is not the case for the experimental diffraction patterns in the interval of $s$ values investigated. On the diffraction pattern for clusters with $\bar{N}\sim2\times10^3$ atoms/cluster (curve a in Fig. 1) the close-lying peaks, such as 111/200, 311/222, and 331/420, are practically unresolved. When the average cluster size is increased to $\bar{N}=1.5\times10^4$ atoms/cluster (curve b in Fig. 1) these peaks (except for 331/420) are noticeably split, but the degree of

 

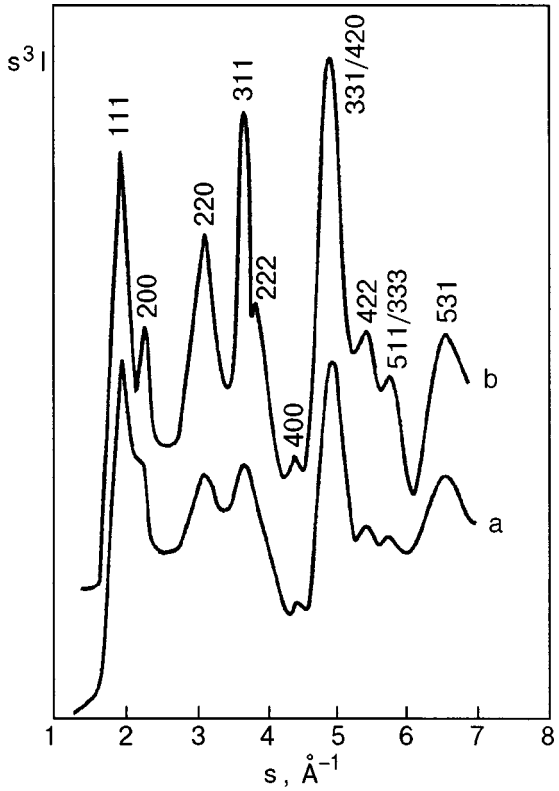


FIG. 1. Diffraction patterns from Kr cluster beams with an average cluster size $\bar{N}$, atoms/cluster: $2\times10^3$ (a); $1.5\times10^4$ (b).

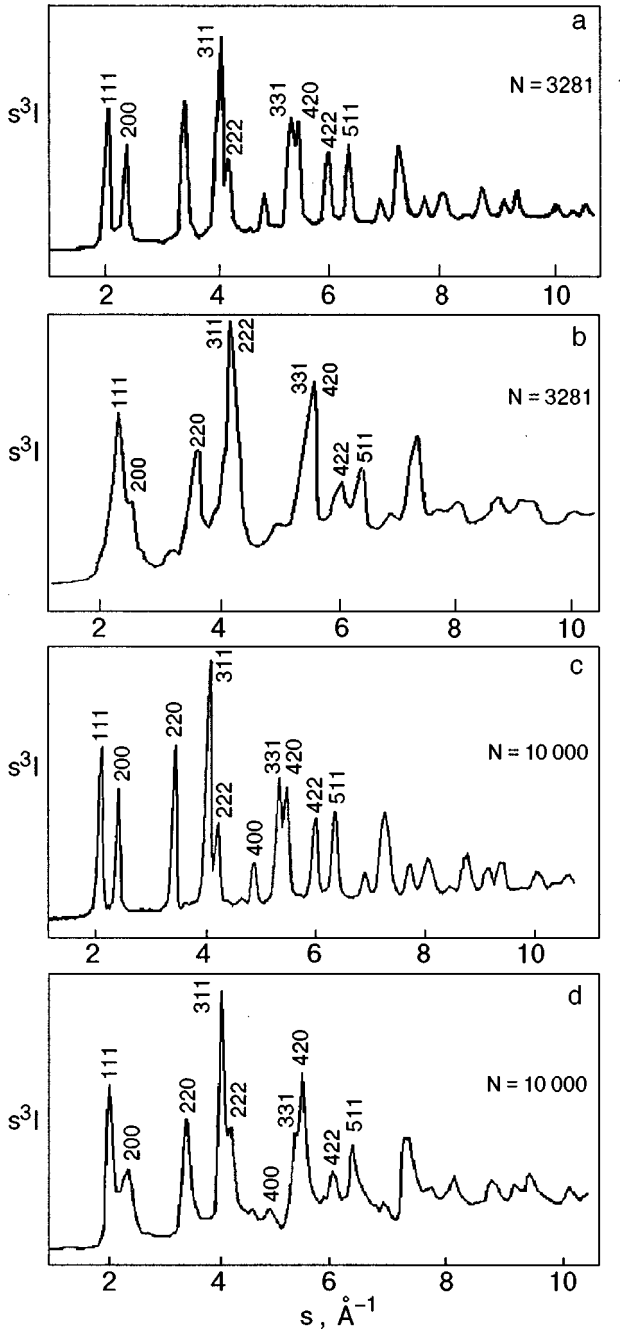


FIG. 2. Simulated diffraction functions calculated for the case of defect-free fcc clusters with $N=3281$ atoms/clusters[1,2] (a) and 10 000 atoms/cluster[5] (c) and for fcc clusters containing two intersecting stacking faults, with $N=3281$ atoms/clusters[1,2] (b) and 10 000 atoms/clusters[5] (d).

their resolution is much lower than for the curve calculated for defect-free clusters with $N=1\times10^4$ atoms/cluster (curve c in Fig. 2). Thus it becomes perfectly obvious that the structure of the clusters formed in a supersonic jet do not have a defect-free fcc structure. This conclusion is confirmed by a comparison of the experimental diffraction patterns with the model functions b and d in Fig. 2, which were calculated under the assumption that the clusters had two intersecting stacking faults. It follows from a comparison of the experimental and theoretical curves that the degree of splitting of the peaks on the diffraction patterns is similar to that on the corresponding calculated curves. It should be noted, however, that there is some disagreement between the heights of the individual peaks on the experimental and calculated curves. For example, on the model curve d in Fig. 2 ($N=1\times10^4$ atoms/cluster) the 331/420 peak is considerably lower than the 311 peak, and the 422 peak is lower than the 511/333 peak, whereas on diffraction pattern b in Fig. 1 ($N=1.5\times10^4$ atoms/cluster) the height of the 331/420 peak is greater than that of the 311 peak, and the 422 peak is higher than the 511/333 peak. This discrepancy is most likely due to the following circumstance. The simulation of the diffraction function was carried out for a cluster of definite size, without allowance for the influence on the diffraction pattern of the scattering of electrons on monomers, which were always present in the supersonic jet in our experiments. It follows from Ref. 7 that the scattering curve for the electrons on monomers in the coordinates $s^3I$-$s$ is bell-shaped. The position of the maximum of this curve nearly coincides with the position of the 331/420 peak. On account of the summation of the scattering intensities, the height of the 331/420 peak on the resultant diffraction pattern is increased substantially, and it becomes higher than the 311 peak. The different contribution to the heights of the diffraction peaks from the monomer component also accounts for the raising of the 422 peak above the 511/333 peak.

Thus, a comparison of the experimental data with the results of the calculation confirms that Kr clusters with $N=2\times10^3$ and $1.5\times10^4$ atoms/cluster have an fcc structure with intersecting stacking faults. The somewhat weaker (as it appears to us) splitting of the 111 and 200 peaks and the 311 and 222 peaks on the diffraction patterns in comparison with the simulated functions may be due to the presence of more than two stacking faults in the clusters. This is confirmed by

the data of Ref. 4, according to which the number of ''defect'' planes in rare-gas clusters is equal to four.

An analysis of the results obtained in this study raises the question of the reasons for the absence of splitting of the 111/200 and 311/222 peaks on the densitometer traces from Ar clusters as the cluster size was increased from $N=3\times10^3$ to $8\times10^4$ atoms/cluster (these traces are shown in Ref. 5). It is possible that in that case the resolution of the diffraction patterns was poor, for a number of reasons: 1) the short distance from the diffraction zone to the detector; 2) those authors did not directly measure the intensity of the diffraction peaks but the blackening $S$ of a photoemulsion by the beams. In the case of electrons, however, the relation $S\sim I\tau$ (where $\tau$ is the exposure time) does not hold in practice for the majority of photoemulsions, but instead $S=k\log I\tau$, where the coefficient $k$ depends on the electron energy and the type of photoemulsion. In addition, it is possible that the defect structure of the clusters is influenced by the conditions of their formation in the jet, which was produced by a sonic nozzle in Ref. 5 and by a supersonic nozzle in Ref. 4.

*E-mail: sktb@ilt.kharkov.ua

[1] B. W. van de Waal, Phys. Rev. Lett. **76**, 1083 (1996).
[2] B. W. van de Waal, J. Cryst. Growth **158**, 153 (1996).
[3] S. I. Kovalenko, D. D. Solnyshkin, E. T. Verkhovtseva, and V. V. Eremenko, Chem. Phys. Lett. **250**, 309 (1996).
[4] S. I. Kovalenko, D. D. Solnyshkin, E. A. Bondarenko, and É. T. Verkhovtseva, Fiz. Nizk. Temp. **23**, 190 (1997) [Low Temp. Phys. **23**, 140 (1997)].
[5] M.-F. de Feraudy, G. Torchet, and B. W. van de Waal, in *Proceedings of the International Symposium on Small Particles and Inorganic Clusters ISSPIC-98*, *Lozanna* (*1998*).
[6] S. I. Kovalenko, D. D. Solnyshkin, É. T. Verkhovtseva, and V. V. Eremenko, Fiz. Nizk. Temp. **20**, 961 (1994) [Low Temp. Phys. **20**, 758 (1994)].
[7] B. Raoult and J. Farges, Rev. Sci. Instrum. **44**, 430 (1973).

Translated by Steve Torstveit

## LATTICE DYNAMICS

# Crowdion dynamics in a nonuniformly deformed three-dimensional crystal

V. D. Natsik*

*B. Verkin Institute for Low Temperature Physics and Engineering, National Academy of Sciences of Ukraine, pr. Lenina 47, 61164 Kharkov, Ukraine*

E. I. Nazarenko**

*Kharkov State University, pl. Svobody 4, 61047 Kharkov, Ukraine*

(Submitted September 8, 1999)
Fiz. Nizk. Temp. **26**, 283–293 (March 2000)

The problem of crowdion motion is formulated and analyzed as a dynamical problem of a three-dimensional crystal lattice formed by atoms of several kinds, which interact with each other by means of short-range pair potentials. It is explained that in order for the the crowdion excitations of the close-packed atomic rows to be distinguishable against the background of small dynamic deformations of the crystal as a whole, the microscopic parameters of the crystal structure must meet certain stated requirements. The equation of motion of a crowdion in an arbitrary elastic strain field of the crystal is derived in the Lagrangian formalism. Expressions are obtained which relate the effective mass and the rest energy of a crowdion with the geometric and force parameters of the crystal lattice. © *2000 American Institute of Physics.* [S1063-777X(00)00503-X]

### INTRODUCTION

Many rather complex crystal structures contain close-packed atomic rows relatively weakly coupled with their surrounding environment. An intrinsic interstitial atom in such a row forms a specific configuration—a smeared clump called a crowdion, and the vacancy also becomes delocalized, forming a smeared rarefaction region that can be called an anti-crowdion. These defects move rather easily along the close-packed rows; the motion of crowdions is essentially of a cooperative nature and is fundamentally different from the diffusive motion of localized interstitial atoms or vacancies.

Crowdions can play an important role in the dynamics and kinetics of radiation defects, in diffusion processes, and in several other inelastic deformation phenomena in crystals.[1–7] In the physics of crystals a great deal of importance is placed on the widely discussed and physically rich analogy between a crowdion and the elementary carrier of plasticity—the dislocation.[3,8,9] In addition, the displacements of the atoms of a close-packed row during the motion of crowdions is an example of a soliton (nonlinear solitary wave), and the mathematical description of crowdions dynamics therefore has a direct relation to the problems of modern nonlinear mechanics and its applications.[8–11]

For a qualitative description of the basic properties of a crowdion, the Frenkel–Kontorova model of a one-dimensional crystal is widely used in the physics of crystals. This model is a chain of mutually strongly interacting atoms which undergoes one-dimensional motion in a relatively weak static periodic potential.[12] Various aspects of the nonlinear dynamics in the Frenkel–Kontorova model are discussed in a recent review.[13] In comparing this model with a real crystal, it is assumed that the mobile chain corresponds to a close-packed row of atoms and that the periodic potential models the interaction of this row with the other atoms of the crystal, which are assumed immobile. The properties of a crowdion as a solitary wave of displacements in a three-dimensional crystal have been analyzed in a series of papers by Kosevich and Kovalev and their co-workers.[14–17] They proposed and analyzed a model in which a close-packed atomic row is embedded in a highly anisotropic elastic continuum. One of the main results of those papers is the conclusion that the strain field of the crowdion in a three-dimensional elastic medium is substantially delocalized in comparison with the exponentially localized deformations created by a soliton in a one-dimensional Frenkel–Kontorova crystal. The second interesting result was a description of the acoustic emission from a moving crowdion into the bulk of a crystal.[14,15]

However, a discussion of the question of the relationship between the properties of a crowdion in a three-dimensional deformable crystal and the properties of a soliton (dislocation) in the Frenkel–Kontorova model meets with certain complexities.[14,15] It it not at all clear whether it is possible to distinguish a crowdion excitation from the other excitations of the crystal: free harmonic vibrations (phonons) or forced deformations of the crystal lattice.

A special discussion and analysis is warranted for the problem of deriving the equation of motion of a crowdion and describing the interaction of a crowdion with dynamic and static deformations created by other defects or excitations of the crystal and by external forces. A soliton in a Frenkel–Kontorova crystal behaves like a particle with effective values of the self-energy and mass, and the motion of its center in the field of forces acting on the mobile chain of atoms is governed by an equation analogous to the one-dimensional equation of motion in the classical

 

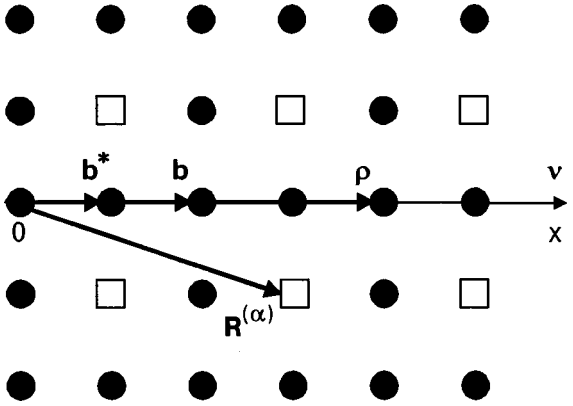


FIG. 1. Fragment of a crystal structure with a close-packed row of atoms (two-dimensional diagram): **b*** and **b** are respectively the elementary vectors of translations inside and along the distinguished row; $\boldsymbol{\rho}$ and $\mathbf{R}^{(\alpha)}$ are the corresponding equilibrium positions of the atoms of the distinguished row and the crystal matrix surrounding it; 0 is the coordinate origin.

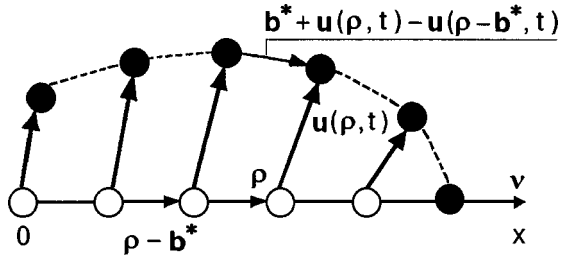


FIG. 2. Bending of a close-packed row of atoms as a result of elastic deformations of the crystal: ○—equilibrium positions of the atoms in the undeformed crystal; ●—instantaneous positions of the atoms in the deformed crystal; $\mathbf{b}^*+\mathbf{u}(\boldsymbol{\rho},t)-\mathbf{u}(\boldsymbol{\rho}-\mathbf{b}^*,t)$ is the vector specifying the direction of the crowdion displacement at the site $\boldsymbol{\rho}$.

mechanics.[9,13,18] However, a rigorous derivation of the equation of motion of a crowdion in a three-dimensional deformed crystal, something similar to Kosevich's derivation of the equation of motion of a dislocation,[19] has not yet been given.

In this paper we formulate and analyze the problem of crowdion motion as a dynamical problem of a three-dimensional crystal lattice. We consider a rather general case of crystal structure, formed by atoms of several different kinds, interacting with one another by means of short-ranged pair potentials. We formulate the requirements on the parameters of the crystal geometry and interatomic interaction which permit one to distinguish the crowdion excitations of the close-packed atomic rows against the background of small dynamic deformations of the crystal as a whole. We obtain expressions relating the self-energy and the effective mass of a crowdion with the microscopic parameters of the crystal. We derive an equation of motion for the center of a crowdion in an arbitrary elastic strain field of the crystal.

## 1. STATEMENT OF THE MODEL, THE DYNAMICAL VARIABLES, AND THE LAGRANGIAN FUNCTION

Let us consider a complex multiatomic crystal lattice in which a close-packed row of identical atoms can be identified. The chemically different species of atoms are enumerated by an index $\alpha$, and we assume for the sake of definiteness that the atoms of the distinguished row have index $\alpha=1$. The spatial orientation of the distinguished atomic row and the period of translations within it are specified by the vector **b***, while the vector of translations of the crystal in this direction is denoted by **b**; in complex crystal structures these vectors can differ in modulus. The equilibrium positions of the atoms in the ideal crystal structure are specified by a set of vectors **R**, and we separate it into sets of vectors of two types: $\mathbf{R}=\{\boldsymbol{\rho},\mathbf{R}^{(\alpha)}\}$, where $\boldsymbol{\rho}$ and $\mathbf{R}^{(\alpha)}$ are, respectively, the equilibrium positions of the atoms of the distinguished row and of the crystal matrix surrounding it. The origin of the coordinate system for the vectors $\boldsymbol{\rho}$ and $\mathbf{R}^{(\alpha)}$ is conveniently chosen to lie at one of the atoms of the distinguished row, that for which the energy of coupling with the lattice is maximum (Fig. 1).

We assume that the interatomic interaction in the crystal is described by a set of short-ranged pair potentials $U_{\alpha\alpha'}(\mathbf{r}-\mathbf{r}')$ ($\mathbf{r}$ and $\mathbf{r}'$ are the coordinates of two arbitrary atoms), and each individual atom with coordinate $\mathbf{r}$ can also be acted on by time-varying external forces, which correspond to potentials $U_\alpha^{(e)}(\mathbf{r},t)$.

We note that all of the main results obtained in an analysis of the model described above carry over without substantial limitations to the case of ordered rows of impurity atoms inside a crystal or to rows of adsorbed atoms on the surface of a crystal, and also to the case of two-dimensional crystals or quasi-one-dimensional structures of the double-polymer chain type. In the case of molecular structures the ''atoms'' of the model will of course be molecules or relatively ''rigid'' monomers of the molecular chains, the internal degrees of freedom of which can be neglected.

The atomic displacements $\boldsymbol{\eta}(\mathbf{R},t)$ from the equilibrium positions in the ideal crystal are written in the form

$$\eta(\mathbf{R},t)=\mathbf{u}(\mathbf{R},t)+\frac{bz(\boldsymbol{\rho},t)}{b^*}[\mathbf{b}^*+\mathbf{u}(\boldsymbol{\rho},t)-\mathbf{u}(\boldsymbol{\rho}-\mathbf{b}^*,t)]\delta_{\mathbf{R}\boldsymbol{\rho}}. \tag{1}$$

Here $\delta_{ik}$ is the Kronecker delta; $\mathbf{u}(\mathbf{R},t)$ are arbitrary small displacements satisfying the condition $|\mathbf{u}(\mathbf{R},t)-\mathbf{u}(\mathbf{R}',t)| \ll |\mathbf{R}-\mathbf{R}'|$; $z$ stands for additional dimensionless displacements describing the propagation of a crowdion excitation along the distinguished atomic row $\mathbf{R}=\boldsymbol{\rho}$. It is important here that the crowdion displacements described by the second term in (1) are directed at all times along the vector $\mathbf{b}^*+\mathbf{r}(\boldsymbol{\rho},t)-\mathbf{u}(\boldsymbol{\rho}-\mathbf{b}^*,t)$, i.e., along the tangent to the instantaneous configuration axis of the distinguished atomic row, which is bent by the elastic displacements $\mathbf{u}(\mathbf{R},t)$ away from its configuration $0x$ in the ideal crystal (Fig. 2). The nucleation and motion of a crowdion are accompanied by changes in the dimensionless displacement $z$ by an amount $|z|\leqslant 1$.

We believe that the displacement structure specified by relation (1) best reflects the physical meaning of a crowdion and makes it possible to separate correctly the nonlinear crowdion excitations from the linear natural or forced deformations of the crystal.

We denote the mass of the atoms by $m_\alpha$ and start by considering the total displacements $\boldsymbol{\eta}(\mathbf{R},t)$ and velocities $\dot{\boldsymbol{\eta}}(\mathbf{R},t)\equiv\partial\boldsymbol{\eta}(\mathbf{R},t)/\partial t$ as the dynamical variables. Using the notation introduced above for the interatomic interaction potentials $U_{\alpha\alpha'}(\mathbf{r}-\mathbf{r}')$ and the potentials of the external fields

$U_\alpha^{(e)}(\mathbf{r},t)$ and taking into account the special role of the distinguished row of atoms, we write a general expression for the Lagrangian of the problem in the form

$$\mathcal{L}=\frac{1}{2}\sum_{\alpha,\mathbf{R}^{(\alpha)}} m_\alpha[\dot{\mathbf{u}}(\mathbf{R}^{(\alpha)},t)]^2+\frac{1}{2}\sum_{\rho} m_1[\dot{\boldsymbol{\eta}}(\boldsymbol{\rho},t)]^2$$
$$-\frac{1}{2}\sum_{\alpha,\mathbf{R}^{(\alpha')}}\sum_{\alpha',\mathbf{R}^{(\alpha')}} U_{\alpha\alpha'}[\mathbf{R}^{(\alpha)}-\mathbf{R}^{(\alpha')}+\mathbf{u}(\mathbf{R}^{(\alpha)},t)$$
$$-\mathbf{u}(\mathbf{R}^{(\alpha')},t)]-\frac{1}{2}\sum_{\boldsymbol{\rho}}\sum_{\boldsymbol{\rho}'} U_{11}[\boldsymbol{\rho}-\boldsymbol{\rho}'+\boldsymbol{\eta}(\boldsymbol{\rho},t)$$
$$-\boldsymbol{\eta}(\boldsymbol{\rho}',t)]-\sum_{\rho}\sum_{\alpha,\mathbf{R}^{(\alpha)}} U_{1\alpha}[\boldsymbol{\rho}-\mathbf{R}^{(\alpha)}+\boldsymbol{\eta}(\boldsymbol{\rho},t)$$
$$-\mathbf{u}(\mathbf{R}^{(\alpha)},t)]-\sum_{\alpha,\mathbf{R}^{(\alpha)}} U_\alpha^{(e)}[\mathbf{R}^{(\alpha)}+\mathbf{u}(\mathbf{R}^{(\alpha)},t),t]$$
$$-\sum_{\boldsymbol{\rho}} U_1^{(e)}[\boldsymbol{\rho}+\boldsymbol{\eta}(\boldsymbol{\rho},t),t]. \tag{2}$$

This way of writing the Lagrangian is convenient in that there are separate expressions for the kinetic and potential energies of the matrix (the first and third terms) and of the distinguished atomic row (the second and fourth terms) and for the interaction energy of the atomic row with the matrix (the fifth term). In expression (2) it is relatively easy to make appropriate simplifications for the problem under study, without which further analysis would not be possible.

## 2. SIMPLIFIED LAGRANGIAN

Let us begin by discussing the main approximation of crowdion theory, without the use of which it would be altogether impossible to introduce correctly the concept of a crowdion excitation: the qualitative assumption that the energy of interaction of the atoms within the distinguished row [the fourth term in (2)] is large compared to the energy of interaction of this row with the external matrix [the fifth term in (2)]. In our model this postulate allows us to assume that, like the elastic strains of the crystal, the crowdion deformations are also small, i.e., we have the two simultaneous inequalities:

$$|\mathbf{u}(\mathbf{R},t)-\mathbf{u}(\mathbf{R}',t)|\ll|\mathbf{R}-\mathbf{R}'|,$$
$$b^*|z(\boldsymbol{\rho},t)-z'(\boldsymbol{\rho}',t)|\ll|\rho-\rho'|. \tag{3}$$

A quantitative criterion which refines the conditions under which the second of inequalities (3) holds, will be written below [see Eq. (20)]. We also note that the satisfaction of equations (3) is reliant on the requirement that the potentials of the external forces [the last two terms in (2)] be small and have a sufficiently smooth dependence on space and time.

Satisfaction of inequalities (3), as we know, allows one to pass from a discrete (lattice) to a continuum approximation in the description of the dynamical processes or static deformations in a crystal, by replacing the finite differences of the displacements by derivatives:

$$u_i(\mathbf{R},t)-u_i(\mathbf{R}',t)=(R_k-R_k')u_{ik}(\mathbf{R},t),$$
$$u_{ik}(\mathbf{R},t)=\frac{\partial u_i(\mathbf{R},t)}{\partial R_k};$$
$$z(\boldsymbol{\rho},t)-z(\boldsymbol{\rho}',t)=(\boldsymbol{\rho}_i-\boldsymbol{\rho}_i')v_i z'(\boldsymbol{\rho},t),$$
$$z'\equiv\frac{\partial}{\partial x}z,\quad \boldsymbol{\rho}=vx. \tag{4}$$

Here $u_{ik}(\mathbf{R},t)$ is the tensor of elastic distortions of the crystal, $b^*z'$ is the local crowdion deformation of the distinguished atomic row, and $\boldsymbol{\nu}$ is the unit vector in the direction of that row; summation over repeated coordinate indices is implied. We note that the use of relations (4) means that we are neglecting the higher-order spatial derivatives of the displacements $\mathbf{u}$ and $z$, i.e., we are neglecting spatial dispersion effects in the equations of motion of the crystal lattice. Clearly equations (3) are equivalent to the inequalities

$$|u_{ik}|\ll 1,\quad b^*|z'|\ll 1. \tag{5}$$

The above-formulated requirements on the external forces allow us to consider the time derivatives as well as the spatial derivatives of the displacements to be small, which is equivalent to neglecting effects of retardation of the acoustic waves in the dynamical processes under consideration:

$$|\dot{\mathbf{u}}|\ll c,\quad b^*|\dot{z}|\ll c, \tag{6}$$

where $c$ is the characteristic sound velocity.

The short-range character of the interatomic potentials and the smallness of the deformations allow us to represent the Lagrangian (2) in the form of a Taylor series expansion in the derivatives $u_{ik}$, $z'$, $\dot{u}_i$, and $\dot{z}$ or the finite differences corresponding to them. The main approximation of the dynamical theory of crystals corresponds, as we know, to taking into account the quadratic terms in this expansion. This accuracy is also acceptable for solving the problem which we are addressing here, although, in doing the expansion, we must take into account that in the presence of a crowdion excitation the difference of the displacements of the atoms of the distinguished row and of the crystal matrix surrounding it contain the term $\mathbf{b}z$, which cannot be considered to be a small quantity:

$$\boldsymbol{\eta}_i(\boldsymbol{\rho},t)-u_i(\mathbf{R}^{(\alpha)},t)=b_i z(\boldsymbol{\rho},t)+u_i(\boldsymbol{\rho},t)-u_i(\mathbf{R}^{(\alpha)},t)$$
$$+\frac{b}{b^*}z(\boldsymbol{\rho},t)[u_i(\boldsymbol{\rho},t)-u_i(\boldsymbol{\rho}-\mathbf{b}^*,t)]$$
$$=b_i z(\boldsymbol{\rho},t)+[\boldsymbol{\rho}_k-R_k^{(\alpha)}$$
$$+b_k z(\boldsymbol{\rho},t)]u_{ik}(\boldsymbol{\rho},t). \tag{7}$$

The potential of the external forces acting on the atoms of the distinguished row can be simplified by taking into account that $|z|\leqslant 1$ and assuming that $b^*|z|\ll|\boldsymbol{\rho}+\mathbf{u}|$:

$$U_1^{(e)}[\boldsymbol{\rho}+\boldsymbol{\eta}(\boldsymbol{\rho},t),t]\approx U_1^{(eZ)}[\boldsymbol{\rho}+\mathbf{u}(\boldsymbol{\rho},t),t]$$
$$-b_i F_i^{(e\alpha)}[\boldsymbol{\rho}+\mathbf{u}(\boldsymbol{\rho},t),t]z(\boldsymbol{\rho},t),$$
$$\mathbf{F}^{(e\alpha)}(\mathbf{r},t)=-\frac{\partial}{\partial\mathbf{r}}U_\alpha^{(e)}(\mathbf{r},t). \tag{8}$$

In this expansion we have neglected terms of order $F^{(e1)}u_{ik}$, since we have stipulated that the external forces $F^{(e1)}$ are small.

Expanding expression (2) in the derivatives $u_{ik}$, $z'$, $\dot{u}_i$, and $\dot{z}$ to terms of second order, taking into account the consequences of the translational symmetry of the crystal, and regrouping the terms for our future convenience, we obtain

$$\mathcal{L}=\frac{1}{2}\sum_{\alpha,\mathbf{R}} m_\alpha[\dot{\mathbf{u}}(\mathbf{R},t)]^2-\frac{1}{2}\sum_{\alpha,\mathbf{R}}\sum_{\alpha',\mathbf{R}'} A_{ik}^{(\alpha\alpha')}$$
$$\times(\mathbf{R}-\mathbf{R}')u_i(\mathbf{R},t)u_k(\mathbf{R}',t)-\sum_{\alpha,\mathbf{R}} U_\alpha^{(e)}[\mathbf{R}+\mathbf{u}(\mathbf{R},t),t]$$
$$+\frac{1}{2}\sum_{\rho}\{m_1b^2[\dot{z}(\rho,t)]^2-wb^2[z'(\boldsymbol{\rho},t)]^2-2\Phi[z(\boldsymbol{\rho},t)]\}$$
$$+\sum_{\rho}\{m_1b_i\dot{u}_i(\boldsymbol{\rho},t)\dot{z}(\boldsymbol{\rho},t)-bw_{ik}u_{ik}(\boldsymbol{\rho},t)z'(\boldsymbol{\rho},t)$$
$$-u_{ik}(\boldsymbol{\rho},t)\Phi_{ik}[z(\boldsymbol{\rho},t)]+b_iF_i^{(e1)}[\boldsymbol{\rho}+\mathbf{u}(\mathbf{R},t),t]z(\boldsymbol{\rho},t)\}. \tag{9}$$

In writing expression (9) we have used the following notation:

$$A_{ik}^{(\alpha\alpha')}(\mathbf{R})=-\frac{\partial^2U_{\alpha\alpha'}(\mathbf{R})}{\partial R_i\partial R_k},$$
$$w=-\frac{1}{2}\sum_{\rho} A_{ik}^{(11)}(\boldsymbol{\rho})\rho_i\rho_k,$$
$$w_{ik}=-\frac{1}{2}\sum_{\boldsymbol{\rho}} A_{ni}^{(11)}(\boldsymbol{\rho})\rho_n\rho_k,$$
$$\Phi(z)=\sum_{\alpha,\mathbf{R}^{(\alpha)}}[U_{1\alpha}(\mathbf{R}^{(\alpha)}+\mathbf{h}z)-U_{1\alpha}(\mathbf{R}^{(\alpha)})],$$
$$\Phi_{ik}(z)=\sum_{\alpha,\mathbf{R}^{(\alpha)}}\left[\frac{\partial U_{1\alpha}(\mathbf{R}^{(\alpha)}+\mathbf{h}z)}{\partial(R_i^{(\alpha)}+b_iz)}(R_k^{(\alpha)}+b_kz)\right.$$
$$\left.-\frac{\partial U_{1\alpha}(\mathbf{R}^{(\alpha)})}{\partial R_i^{(\alpha)}}R_k^{(\alpha)}\right]. \tag{10}$$

In expression (9) we have neglected terms of second order in the small deformations,

$$\left|\sum_{\alpha,\mathbf{R}^{(\alpha)}}[A_{ik}^{(1\alpha)}(\mathbf{R}^{(\alpha)}+\mathbf{h}z)-A_{ik}^{(1\alpha)}(\mathbf{R}^{(\alpha)})]u_{in}u_{km}\right|$$
$$\ll|hw_{ik}u_{ik}z'|,$$

assuming the stipulated smallness of the interaction of the distinguished row of atoms with the crystal matrix:

$$\left|\sum_{\alpha,\mathbf{R}^{(\alpha)}} A_{ik}^{(1\alpha)}(\mathbf{R}^{(\alpha)})R_n^{(\alpha)}R_m^{(\alpha)}\right|\ll|w_{ik}|.$$

Turning to a discussion of the expression (9) which we have obtained for $\mathcal{L}$, we recall that the lattice vector $\mathbf{R}=\{\mathbf{R}^{(\alpha)},\boldsymbol{\rho}\}$ runs over all equilibrium positions of the atoms of the complex crystal lattice, and that the quantity $A_{ik}^{(\alpha\alpha')}\times(\mathbf{R})$ is the force matrix of the crystal. Therefore, the first three terms in (9) describe the dynamics of an ideal harmonic crystal with allowance for the effects of external forces on it.

The fourth term in (9) is analogous to the Lagrangian of a one-dimensional Frenkel–Kontorova crystal. However, the dynamical variable $z$ has a more general meaning than the displacement of the atoms in the Frenkel–Kontorova model, since in the general case $z$ describes the displacements along a bent close-packed atomic row. Furthermore, as compared with the Frenkel–Kontorova model, the parameter $w$ and the lattice potential $\Phi(z)$ also acquire a more general meaning: $w$ is no longer determined only by the interaction of nearest neighbors, and the periodic function $\Phi(z)$ can be very different from the sinusoidal dependence $\Phi(z)\sim\sin^2\pi z$ used in Ref. 12. We note that the different features that arise in the nonlinear dynamics of a one-dimensional crystal when a complex form of the potential $\Phi(z)$ is used are discussed in the aforementioned review.[13]

Finally, the last term in Eq. (9) describes effects due to the interaction of linear and nonlinear (quadrupole) excitations of the crystal and the influence of external forces on the motion of a crowdion. It is clear that the possibility of effectively separating these excitations arises in those case when the last term in (9) can be regarded as a small correction to the other terms.

We conclude this Section with a discussion of the salient properties of the lattice parameters and the functions (10) from the standpoint of the analysis below.

1. The most important property of the parameter $w$ characterizing the interatomic interaction within the distinguished close-packed atomic row is its positive definiteness ($w>0$), which ensures the stability of the crystal structure. The function $\Phi(z)\geqslant 0$ is also positive definite, as is ensured by the choice of the reference point for the measurement of the interaction energy of an individual atom of the distinguished row with the crystal matrix (see Sec. 1).

2. A direct consequence of the symmetry properties of the crystal and of formulas (10), which define these functions, is their periodicity, their vanishing at the points $z=n=0,\pm1,\pm2,...$, and their evenness:

$$\Phi(z+n)=\Phi(z),\quad \Phi_{ik}(z+n)=\Phi_{ik}(z);$$
$$\Phi(n)=0,\quad \Phi_{ik}(n)=0;$$
$$\Phi(z)=\Phi(-z),\quad \Phi_{ik}(z)=\Phi_{ik}(-z). \tag{11}$$

3. A consequence of the properties listed above is that the first derivatives of $\Phi(z)$ and $\Phi_{ik}(z)$ go to zero at the points $z=n$, and the validity of the following expansions in the neighborhoods of these points (for $|z-n|\ll1$):

$$\Phi(z)=\frac{1}{2}\kappa(z-n)^2+\ldots,\quad \kappa=\left.\frac{\partial^2\Phi(z)}{\partial z^2}\right|_{z=n}>0; \tag{12a}$$
$$\Phi_{ik}(z)=\frac{1}{2}\kappa_{ik}(z-n)^2+\ldots,\quad \kappa_{ik}=\left.\frac{\partial^2\Phi_{ik}(z)}{\partial z^2}\right|_{z=n}. \tag{12b}$$

4. In the particular case of centrosymmetric interatomic potentials $U_{\alpha\alpha'}(\mathbf{r})=U_{\alpha\alpha'}(\mathbf{r})$ the matrices $w_{ik}$ and $\Phi_{ik}(z)$ are symmetric with respect to the coordinate indices:

$$w_{ik}=w_{ki}=w\nu_i\nu_k,\quad \Phi_{ik}(z)=\Phi_{ki}(z). \tag{13}$$

## 3. CROWDION IN A RIGID CRYSTAL MATRIX

In the previous Section we saw that in a crystal capable of undergoing elastic deformations ($\mathbf{u}(\mathbf{R},t)\equiv0$), the field of

the nonlinear displacements $z(\boldsymbol{\rho},t)$ cannot be rigorously separated from the linear excitations of the crystal. One can only hope that such a separation can be done using perturbation theory,[14,15] provided that there exist small parameters that permit one to treat the last term in (9) as a small perturbation. Therefore, as a zeroth approximation of perturbation theory it is natural to treat the crowdion as a topological soliton on the distinguished row of atoms in the absence of external forces ($\mathbf{F}^{(e\alpha)}(\mathbf{r})\equiv 0$), assuming that the crystal matrix is absolutely rigid ($\mathbf{u}(\mathbf{R},t)\equiv 0$). This approximation corresponds to the Lagrangian

$$\mathcal{L}_0=\frac{1}{2}\sum_{\rho}\,[m_1b^2(\dot{z})^2-wb^2(z')^2-2\Phi(z)] \tag{14}$$

and the equation of motion that follows from it:

$$m_1b^2\ddot{z}-wb^2z''+\frac{d}{dz}\Phi(z)=0. \tag{15}$$

The topological soliton of interest is a solution of equation (15) in the form $z(\boldsymbol{\nu}x,t)=z_s[\boldsymbol{\nu}(x-x_s)]$ ($x_s=v_st$, $v_s=\text{const}$), which satisfies the following boundary conditions at the ends of the atomic row:

$$z_s(-\infty)\equiv 0,\quad z_s(\infty)=s,\quad z_s'(\pm\infty)\equiv 0. \tag{16}$$

The symbol $s=\pm 1$ denotes the sign of the soliton (crowdion): the value $s=1$ corresponds to a delocalized vacancy, and $s=-1$ to a delocalized interstitial in the atomic row. The procedure of integrating Eq. (15) is well known and is described in detail in the literature: if the function $\Phi(z)$ is even [$\Phi(sz)=\Phi(z)$], positive definite, and satisfies the condition $\Phi(0)=\Phi(s)=0$, then the first and second integrals can be written in the form of the following relations (see Refs. 8 and 13):

$$z_s'=s\left[\frac{c_0^2}{c_0^2-v_s^2}\,\frac{2\Phi(z_s)}{b^2w}\right]^{1/2},\quad c_0^2=\frac{w}{m_1}; \tag{17}$$

$$\int_{1/2}^{sz_s}\frac{dz}{\sqrt{2\Phi(z)}}=\left[\frac{c_0^2}{(c_0^2-v_s^2)w}\right]^{1/2}\frac{x-x_s}{b},\quad x_s=v_st. \tag{18}$$

Relation (18) defines the center of the crowdion as the point $x=x_s$ at which the displacement $z_s(0)=s/2$.

In what follows we will consider only comparatively slow (''nonrelativistic'') crowdions $v_s\ll c_0$, since, according to Eq. (17), for $v_s\to c_0$ the basic initial assumption $b^*|z'|\ll 1$ is violated, and we can no longer use the simplified expression (9) for the Lagranian. Since at large distances from the center of the crowdion, $x-x_s\to\pm\infty$, according to conditions (16) the value of the potential $\Phi(z)$ can be replaced by the expansion (12a), from relation (18) we easily obtain the asymptotic expressions for the displacements $z_s[\boldsymbol{\nu}(x-x_s)]$ for the slow crowdion:

$$sz_s[\nu(x-x_s)]=\begin{cases}\dfrac{1}{2}\exp\left(\dfrac{x-x_s}{\lambda_s}\right), & x<x_s-\lambda_s;\\[2ex] 1-\dfrac{1}{2}\exp\left(-\dfrac{x-x_s}{\lambda_s}\right), & x>x_s+\lambda_s,\end{cases}$$

$$\lambda_s=b\left(\frac{w}{\kappa}\right)^{1/2}. \tag{19}$$

The parameter $\lambda_s$ has the meaning of the half-width of the crowdion: the relative local deformation of the atomic row, $b^*z_s'[\boldsymbol{\nu}(x-x_s)]$ is appreciably different from zero only near its center, on an interval $x_s\pm\lambda_s$, and reaches its maximum value at the center of the crowdion:

$$\max|b^*z_s'|=\frac{b^*}{\lambda_s}=\frac{b^*}{b}\left(\frac{\kappa}{w}\right)^{1/2}.$$

This relation, together with (10) and (12), enables us to write the basic condition for the existence of crowdions, $b^*|z'|\ll 1$, in terms of the lattice parameters:

$$(b^*)^2\kappa=-(b^*)^2\sum_{\alpha,\mathbf{R}^{(\alpha)}}A_{ik}^{(1\alpha)}(\mathbf{R}^{(\alpha)})b_ib_k\ll b^2w$$

$$=-\frac{b^2}{2}\sum_{\rho}\,A_{ik}^{(11)}(\rho)\rho_i\rho_k. \tag{20}$$

The additional energy of the atomic row due to the appearance in it of a crowdion wave $z_s[\boldsymbol{\nu}(x-x_s)]=z_s(\boldsymbol{\rho}-\boldsymbol{\rho}_s)$, where $\boldsymbol{\rho}_s=\boldsymbol{\nu}x_s=\boldsymbol{\nu}v_st$, is given by

$$E_0=\frac{1}{2}\sum_{\rho}\,\{m_1b^2[\dot{z}_s(\rho-\rho_s)]^2+wb^2[z_s'(\rho-\rho_s)]^2$$

$$+2\Phi[z_s(\rho-\rho_s)]\}. \tag{21}$$

In performing the summation over the vector $\boldsymbol{\rho}$ below, we will just use the continuum approximation:

$$\sum_{\rho}\,(\ldots)=\int_{-\infty}^{\infty}\frac{dx}{b^*}(\ldots).$$

In this approximation the energy $E_0$ takes the form[1)]

$$E_0=\frac{1}{2}m_{s0}v_s^2+\varepsilon_{s0};$$

$$\varepsilon_{s0}=\frac{b}{b^*}\int_0^1[2w\Phi(z)]^{1/2}dz,\quad m_{s0}=m_1\frac{\varepsilon_{s0}}{w}. \tag{22}$$

The parameters $\varepsilon_{s0}$ and $m_{s0}$ have the meaning of the self-energy and the effective mass of the crowdion, and the center of the crowdion can be treated as a pseudoparticle endowed with those properties. When inequality (20) holds we have $\lambda_s\gg b^*$, $\varepsilon_{s0}\ll w$, and $m_{s0}\ll m_1$.

## 4. CROWDION AS A SOURCE OF ELASTIC FIELDS

In the last Section we saw that a close-packed atomic row placed in an absolutely rigid (undeformable) crystal matrix can support a crowdion whose center moves with an arbitrary constant velocity $v_s$. We shall assume that the interaction of such a crowdion with a deformable crystal matrix and a system of sufficiently weak external forces preserves the soliton properties of the crowdion excitation but can lead to changes in the shape of the crowdion and disrupt the steady motion of its center, i.e., it can lead to a change in the velocity $v_s$ of the crowdion during its motion. This assumption allows us to consider the coordinate of the center of the crowdion to be some, in general nonlinear, function of time $x_s(t)$ and to consider, in addition to the elastic displacements $\mathbf{u}(\mathbf{R},t)$, velocities $\dot{\mathbf{u}}(\mathbf{R},t)$, and distortions $u_{ik}(\mathbf{R},t)$, the functions $x_s(t)$ and $v_s(t)=\dot{x}_s(t)$ as dynamical variables

of the crystal. The formal substitution of the soliton $z = z_s[\boldsymbol{\rho} - \boldsymbol{\rho}_s(t)]$ described in the previous Section into the function (9) converts it to a function of the set of dynamical variables indicated above:

$$\mathcal{L} = \mathcal{L}_{cs}\{\mathbf{u}(\mathbf{R},t), \dot{\mathbf{u}}(\mathbf{R},t), u_{ik}(\mathbf{R},t), x_s(t), v_s(t)\}.$$

The expression thus obtained will be considered as the Lagrangian of a crystal containing a crowdion and will determine the combined space-time evolution of the elastic displacements of the atoms of the crystal $\mathbf{u}(\mathbf{R},t)$ and of the crowdion center $x_s(t)$.

Treating the motion of the center of the crowdion as specified and using $\mathcal{L}_{cs}$, we can obtain a Lagrangian equation of motion for the crystal:[20]

$$\frac{d}{dt}\left(\frac{\partial \mathcal{L}_{cs}}{\partial \dot{u}_i}\right) + \frac{\partial}{\partial R_k}\left(\frac{\partial \mathcal{L}_{cs}}{\partial u_{ik}}\right) - \frac{\partial \mathcal{L}_{cs}}{\partial u_i} = 0. \tag{23}$$

The transition from this equation to the equation of motion for the displacements $\mathbf{u}(\mathbf{R},t)$ in Newtonian form for the slow-crowdion case under consideration can be done in an approximation linear in the velocity $v_s$, neglecting terms of order $v_s^2/c^2 \ll 1$ and effects of retardation of the elastic waves. In this approximation the following relations are valid:

$$\dot{z}_s = -v_s z_s', \quad \ddot{z}_s = -\dot{v}_s z_s'. \tag{24}$$

Substituting $z = z_s[\boldsymbol{\rho} - \boldsymbol{\rho}_s(t)]$ into Eq. (9) and using Eqs. (23) and (24), we obtain

$$m_\alpha \ddot{u}_i(\mathbf{R},t) + \sum_{\alpha',\mathbf{R}'} A_{ik}^{(\alpha\alpha')}(\mathbf{R}-\mathbf{R}')u_k(\mathbf{R}',t) = F_i^{(e\alpha)}[\mathbf{R}+\mathbf{u}(\mathbf{R},t),t] + F_i^{(s)}(\mathbf{R},t), \tag{25}$$

$$F_i^{(s)} = \delta_{\mathbf{R}\boldsymbol{\rho}}\left\{ m_1 b_i \dot{v}_s z_s'(\boldsymbol{\rho}-\boldsymbol{\rho}_s) + \frac{\partial}{\partial \rho_k}\Phi_{ik}[z_s(\boldsymbol{\rho}-\boldsymbol{\rho}_s)] + b w_{ik}\frac{\partial}{\partial \rho_k} z_s'(\boldsymbol{\rho}-\boldsymbol{\rho}_s)\right\}. \tag{26}$$

On the right-hand side of Eq. (25) are the external forces $\mathbf{F}^{(e\alpha)}$ and also the force $\mathbf{F}^{(s)}$, which determines the additional elastic deformation of the crystal under the influence of the crowdion. In writing this force we have neglected the term $z b_k \partial F_k^{(e1)}/\partial R_i$, which takes into account the above-stipulated long-wavelength character of the external forces.

The long-wavelength character of the forces $\mathbf{F}^{(e\alpha)}$ and the relatively small values of the phonon and crowdion displacements allow us to assume that $\mathbf{F}^{(e\alpha)} \approx \mathbf{F}^{(e\alpha)}[\mathbf{R}+\mathbf{u}^{(e)} \times (\mathbf{R},t),t]$. In this approximation the general solution of equation (25) can be written in the form of a superposition of three types of displacements:

$$\mathbf{u} = \mathbf{u}^{(\mathrm{ph})} + \mathbf{u}^{(e)} + \mathbf{u}^{(s)}. \tag{27}$$

Here $\mathbf{u}^{(\mathrm{ph})}$ are the free vibrations of the crystal (acoustical and optical phonons), $\mathbf{u}^{(e)}$ are the displacements under the influence of the external forces $\mathbf{F}^{(e\alpha)}$, and $\mathbf{u}^{(s)}$ are the displacements arising as a result of the presence of the crowdion in the crystal.

In this Section we are mainly interested in the displacement field $\mathbf{u}^{(s)}(\mathbf{R},t)$. In the quasistatic approximation (i.e., not including the retardation of the elastic waves) these displacements are the decaying (at distances far from the center of the crowdion) solution of the equation

$$\sum_{\alpha',R'} A_{ik}^{(\alpha\alpha')}(\mathbf{R}-\mathbf{R}')u_k^{(s)}(\mathbf{R}',t) = F_i^{(s)}(\mathbf{R},t).$$

Assuming the (tensor) Green function $G_{ik}^{(\alpha\alpha')}(\mathbf{R})$ is known for the equation of equilibrium of the crystal, one can write the displacement field $\mathbf{u}^{(s)}(\mathbf{R},t)$ in the form[2)]

$$u_i^{(s)}(\mathbf{R},t) = \sum_{\alpha',\mathbf{R}'} G_{ik}^{(\alpha\alpha')}(\mathbf{R}-\mathbf{R}')F_k^{(s)}(\mathbf{R}',t).$$

After substituting expression (26) into this formula and doing some straightforward manipulations, we can write the displacement $\mathbf{u}^{(s)}$ in the form

$$u_i^{(s)}(\mathbf{R},t) = \sum_{\rho'}\left\{ m_1 \dot{v}_s z_s'(\boldsymbol{\rho}'-\boldsymbol{\rho}_s) b_k G_{ik}^{(\alpha 1)}(\mathbf{R}-\boldsymbol{\rho}') + [b w_{kn} z_s'(\boldsymbol{\rho}'-\boldsymbol{\rho}_s) + \Phi_{kn}[z_s(\boldsymbol{\rho}'-\boldsymbol{\rho}_s)]] \times \frac{\partial}{\partial R_n} G_{ik}^{(\alpha 1)}(\mathbf{R}-\rho')\right\}. \tag{28}$$

An explicit relation between these displacements and the coordinate and velocity of the center of the crowdion can be obtained at distances $|\mathbf{R}-\boldsymbol{\rho}_s| \gg \lambda_s$, taking into account the exponential localization of the functions $z_s'(\boldsymbol{\rho}-\boldsymbol{\rho}_s)$ and $\Phi_{ik}[z_s(\boldsymbol{\rho}-\boldsymbol{\rho}_s)]$ on the $0x$ axis around the center of the crowdion $\boldsymbol{\rho}_s$ [see the asymptotic expressions (12b) and (19)] and the smooth (power-law) character of the coordinate dependence of the Green function and its derivative:

$$u_i^{(s)}(\mathbf{R},t) = q_s m_1 v_k G_{ik}^{(\alpha 1)}(\mathbf{R}-\boldsymbol{\rho}_s)\dot{v}_s + (q_s w_{kn} + \varphi_{kn})\frac{\partial}{\partial R_n} G_{ik}^{(\alpha 1)}(\mathbf{R}-\boldsymbol{\rho}_s), \tag{29}$$

$|\mathbf{R}-\rho_s| \gg \lambda_s$;

$$q_s = \frac{sb}{b^*} = b\sum_\rho z_s'(\rho), \quad \varphi_{ik} = \frac{b w^{1/2}}{b^*}\int_0^1 \frac{\Phi_{ik}(z)}{\sqrt{2\Phi(z)}}dz.$$

In the absence of phonons and external forces, the total displacements of the atoms of the distinguished row in which the crowdion is located are described, according to Eq. (1), by the formula

$$\eta_i^{(s)}(\boldsymbol{\rho},t) = u_i^{(s)}(\boldsymbol{\rho},t) + [b_i + b_k u_{ik}^{(s)}(\boldsymbol{\rho},t)]z_s(\rho-\boldsymbol{\rho}_s). \tag{30}$$

From formulas (28)–(30) we obtain a qualitatively new feature of the deformation fields generated by a crowdion in a three-dimensional crystal in comparison to the crowdion (soliton) deformations in a Frenkel–Kontorova crystal. The components of the distortion tensor $u_{ik}^{(s)}(\mathbf{R},t)$ that correspond to the displacements (29), both in the bulk of the crystal ($\mathbf{R} = \mathbf{R}^{(\alpha)}$) and inside the distinguished atomic row ($\mathbf{R} = \boldsymbol{\rho}$) fall off with distance from the center of the crowdion $\boldsymbol{\rho}_s$ as the spatial derivatives of the components of the Green function, i.e., by a power law, whereas in a one-dimensional

crystal the crowdion creates only exponentially localized deformations $z_s'(\boldsymbol{\rho}-\boldsymbol{\rho}_s)$. We note that the conclusion that the elastic fields created by the crowdion fall off by a power law far from the center was first stated in Refs. 14–17.

## 5. CROWDION EQUATION OF MOTION

Expression (27) uniquely determines the deformation of the crystal if the law of motion $\boldsymbol{\rho}_s(t)$ of the center of the crowdion is known. However, in order that the description of the dynamics of a crystal containing a crowdion be completely self-consistent and closed, it is also necessary to give the equation determining the function $\boldsymbol{\rho}_s(t)$ at specified elastic deformations of the crystal, i.e., the equation of motion for the center of the crowdion.

A crowdion in a three-dimensional crystal, as in a Frenkel–Kontorova model crystal, is a self-trapped collective excitation of the atomic displacement field, and its equation of motion will therefore be of a field origin. The method of obtaining field equations of motion was developed by Lorentz in a derivation of the equation of motion of the electron, and in the physics of crystals it was used effectively by Kosevich[19] in a derivation of the equation of motion of a dislocation. We will also use a variant of this method for the solution of the problem of interest to us here.

We consider a crowdion as a particle whose motion in the bulk of the crystal can be described by the dynamical variables $\boldsymbol{\rho}_s=\boldsymbol{\nu}x_s(t)$ and $\dot{\boldsymbol{\rho}}_s=\boldsymbol{\nu}v_s$. We assume that the crystal contains free vibrations (acoustical and optical phonons) $\mathbf{u}^{(\mathrm{ph})}(\mathbf{R},t)$ and driven displacements excited by external forces, $\mathbf{u}^{(e)}(\mathbf{R},t)$, and we treat these fields as specified functions of the coordinates and time. Substituting the expression $z=z_s(\boldsymbol{\rho}-\boldsymbol{\rho}_s)$, the general expression for the displacement fields (27), and the expression for the displacement field created by the crowdion (28) into the Lagrangian (9), we can separate off from it the last two terms as a separate unit $\mathcal{L}_s$, which will depend on the dynamical variables of the crowdion and will include the external fields and forces as parameters. Some of the terms of this separate unit can be interpreted as the energy of interaction of a crowdion with the external fields, while the terms due to the displacements $\mathbf{u}^{(s)}$ describe its self-effect. The quantity $\mathcal{L}_s$ assumes the usual form of the Lagrangian of a particle in classical mechanics, $\mathcal{L}_s=\mathcal{L}_s\{x_s,v_s;\mathbf{u}^{(\mathrm{ph})}+\mathbf{u}^{(e)},\mathbf{F}^{(e1)}\}$, if it is constructed in the quadratic approximation in the velocities $v_s$ and the terms proportional to the acceleration $\dot{v}_s$ in (28) are neglected in the description of the self-effect.

Taking into account the self-effect of the crowdion through a crystal having a finite elastic compliance leads to a renormalization of the bare values of the effective mass $m_{s0}$ and rest energy $\varepsilon_{s0}$:

$$\mathcal{L}_s=\frac{1}{2}m_s v_s^2-\varepsilon_s-\sum_{\rho}\{m_1 v_s b_i[\dot{u}_i^{(\mathrm{ph})}(\boldsymbol{\rho},t)+\dot{u}_i^{(e)}\times(\boldsymbol{\rho},t)]z_s'(\boldsymbol{\rho}-\boldsymbol{\rho}_s)+[u_{ik}^{(\mathrm{ph})}(\boldsymbol{\rho},t)+u_{ik}^{(e)}(\boldsymbol{\rho},t)]\times[bw_{ik}z_s'(\boldsymbol{\rho}-\boldsymbol{\rho}_s)+\Phi_{ik}(z_s)]+b_iF_i^{(e)}[\boldsymbol{\rho}+\mathbf{u}^{(e)}\times(\boldsymbol{\rho},t),t]z_s(\boldsymbol{\rho},t)\}. \tag{31}$$

$$m_s=m_{s0}+2m_1b\sum_{\boldsymbol{\rho},\boldsymbol{\rho}'}\frac{\partial^2 G_{ik}^{(11)}(\boldsymbol{\rho}-\boldsymbol{\rho}')}{\partial\rho_n\partial\rho_m}v_iv_mz_s'(\boldsymbol{\rho})\times\{bw_{kn}z_s'(\boldsymbol{\rho}')+\Phi_{kn}[z_s(\boldsymbol{\rho}')]\}; \tag{32}$$

$$\varepsilon_s=\varepsilon_{s0}+\sum_{\boldsymbol{\rho},\boldsymbol{\rho}'}\frac{\partial^2 G_{ik}^{(11)}(\boldsymbol{\rho}-\boldsymbol{\rho}')}{\partial\rho_n\partial\rho_m}\{bw_{im}z_s'(\boldsymbol{\rho})+\Phi_{im}[z_s(\boldsymbol{\rho})]\}\{bw_{kn}z_s'(\boldsymbol{\rho}')+\Phi_{kn}[z_s(\rho')]\}. \tag{33}$$

Analysis of these expressions shows that renormalization due to the self-effect is not weak: the additional terms in (32) and (33), generally speaking, are quantities of the same order as $m_{s0}$ and $\varepsilon_{s0}$. In order for the renormalization effects to be weak, it is necessary that the properties of the crystal meet certain special requirements in order that the components of the Green function tensor $G_{ik}^{(11)}$ be anomalously small (in the terminology of Refs. 14 and 15—strong anisotropy).

Expression (31) is the Lagrangian of a crowdion executing a slow motion in specified external fields. Having $\mathcal{L}_s$ and following the general rules of the Lagrangian formalism, we can write the equation of motion of a crowdion in the form

$$\frac{d}{dt}\left(\frac{\partial\mathcal{L}_s}{\partial v_s}\right)-\frac{\partial\mathcal{L}_s}{\partial x_s}=0. \tag{34}$$

In going from (34) to the Newtonian form of the equation of motion it is helpful to take into account the exponentially ''sharp'' character of the functions $z_s'(\boldsymbol{\rho}-\boldsymbol{\rho}_s)$ and $\Phi_{ik}[z_s'(\boldsymbol{\rho}-\boldsymbol{\rho}_s)]$ against the background of the smooth coordinate dependences of the external fields, as this was done in the derivation formula (29). This lets us take the values of the external fields at the point $\boldsymbol{\rho}=\boldsymbol{\rho}_s$ out from under the summation over $\boldsymbol{\rho}$. As a result, the equation of motion of the crowdion takes the final form

$$m_s\dot{v}_s=q_sv_iF_i^{(e1)}[\boldsymbol{\rho}_s+\mathbf{u}^{(e)}(\boldsymbol{\rho}_s,t),t]+q_sm_1v_i\frac{\partial^2}{\partial t^2}[u_i^{\mathrm{ph}}(\boldsymbol{\rho}_s,t)+u_i^{(e)}(\boldsymbol{\rho}_s,t)]-(q_sw_{ik}+\varphi_{ik})\frac{\partial}{\partial x_s}[u_{ik}^{\mathrm{ph}}(\boldsymbol{\rho}_s,t)+u_{ik}^{(e)}(\boldsymbol{\rho}_s,t)]. \tag{35}$$

Expressions for the constants of the lattice-crowdion interaction $w_{ik}$ and $\varphi_{ik}$ are given in (10) and (29).

Now turning to a discussion of the equations obtained, let us mention a few of the important features of the influence exerted on the crowdion by fields and forces external to it.

1. The main part of the terms on the right-hand side of the equation of motion (35) is proportional to the parameter $q_s=bs/b^*$, which plays the role of an effective ''charge'' of the crowdion with respect to the external fields. Thus the directions of the corresponding forces are different for positive ($s=1$) and negative ($s=-1$) crowdions. In addition, there is also a force component due to the elastic distortions of the crystal, which does not depend on the sign of the crowdion. It should be noted, however, that this force is comparatively small, since in the model under study the constants of the crowdion-deformation interaction satisfy the inequality $|\varphi_{ik}|\ll|w_{ik}|$.

2. For quasistatic deformations of the crystal a crowdion is acted on by the deformation-related forces only in the presence of gradients of the elastic distortions. If the interatomic interaction is not centrosymmetric ($w_{ik} \neq w_{ki}, \varphi_{ik} \neq \varphi_{ki}$), then forces arise under the influence of both nonuniform deformations $u_{ik}^{(e)} + u_{ki}^{(e)}$ and nonuniform rotations $u_{ik}^{(e)} - u_{ki}^{(e)}$.

3. The deformation of the crystal in an essentially dynamic regime gives rise to specific forces of an inertial origin, proportional to $\partial^2 \mathbf{u}^{(e)}/\partial t^2$. The appearance of these forces is completely natural, since the crowdion excitation moves within an atomic row, which, in turn, moves under the influence of the external fields.

4. One should also note an important feature of the coordinate-time dependences of the force $\mathbf{F}^{(e1)}$. Even for small deformations of the crystal $|u_{ik}^{(e)}| \ll 1$ the corresponding displacements $\mathbf{u}^{(e)}$ of individual parts of the crystal can be rather large. Therefore, in the description of the influence of external fields on the crowdion it is necessary to take into account the possible large movements of its center in space together with the corresponding parts of the crystal.

Let us conclude with a discussion of another important question that has direct bearing on the dynamical properties of a crowdion. The equation of motion (35) obtained above takes into account only forces of elastic origin (so-called conservative forces). In real situations various nonconservative (frictional) forces are present and can play an important role. These include phonon and electron drag, radiative losses, etc. Taking the frictional forces into account will give rise to additional terms in the equation of motion (35), and these will be analyzed in separate publications.

In addition, in certain cases an important role in the crowdion dynamics can be played by a conservative force not included in (35)—the Peierls force, which arises when the discreteness and translational symmetry of the crystal is taken into account in greater detail (see footnote 1 from Sec. 3).

## CONCLUSIONS

We have constructed a microscopic theory of the dynamical properties of crowdions—specific nonlinear excitations of a crystal structure which arise on close-packed atomic rows that interact relatively weakly with the crystal matrix.

The problem of the crowdion motion is formulated and analyzed as a dynamical problem of a three-dimensional crystal lattice formed by atoms of several kinds with a short-range interatomic pair interaction. We have elucidated the microscopic meaning of the parameters used in the phenomenological models of crowdions.

We have stated the requirements on the force and geometric parameters of the crystal that must be satisfied in order for it to be possible to distinguish the crowdion excitations against the background of the dynamic elastic deformations of the crystal as a whole.

We have derived the equation of motion of a crowdion in a nonuniformly deformed crystal in the framework of the Lagranian formalism and have discussed the physical nature of the forces acting on the crowdion.

We have obtained equations relating the self-energy and effective mass of a crowdion with the microscopic parameters of the crystal.

The authors thank A. M. Kosevich and A. S. Kovalev for helpful discussions and constructive criticism which led to a deeper understanding of the issues touched upon in this paper.

*E-mail: natsik@ilt.kharkov.ua
**E-mail: nazarenko@ilt.kharkov.ua

[1)] Taking the discreteness into account leads to a correction to the crowdion energy which is periodic in the coordinate $x_s = v_s t$ and is analogous to the Peierls energy for a dislocation.[8,13]

[2)] The static Green function of the crystal in the lattice approximation is determined by the equation $\sum_{\alpha'',\mathbf{R}''} A_{in}^{(\alpha\alpha'')}(\mathbf{R}-\mathbf{R}'') G_{nk}^{(\alpha''\alpha')}(\mathbf{R}''-\mathbf{R}') = \delta_{\alpha\alpha'}\delta_{\mathbf{R}\mathbf{R}'}\delta_{ik}$ and by the natural condition that its components go to zero at $|\mathbf{R}-\mathbf{R}'| \to \infty$.

[1] H. R. Paneth, Phys. Rev. **80**, 708 (1950).
[2] L. Tewordt, Phys. Rev. **109**, 61 (1958).
[3] J. Friedel, *Dislocations* [Pergamon Press, Oxford (1964); Mir, Moscow (1967)].
[4] J. R. Manning, *Diffusion Kinetics for Atoms in Crystals* [Van Nostrand, New York (1968); Mir, Moscow (1971)].
[5] A. Seeger, Phys. Status Solidi **38**, 235 (1970).
[6] L. M. Brown, Scr. Metall. **8**, 1045 (1974).
[7] C. H. Wao and W. Frank, J. Nucl. Mater. **137**, 7 (1985).
[8] A. M. Kosevich, *Physical Mechanics of Real Crystals* [in Russian], Naukova Dumka, Kiev (1981).
[9] A. M. Kosevich, *Theory of the Crystal Lattice* [in Russian], Vishcha Shkola, Kharkov (1988).
[10] G. L. Lamb Jr., *Elements of Soliton Theory* [Wiley (1980); Mir, Moscow (1983)].
[11] A. S. Davydov, *Solitons in Molecular Systems*, 2nd ed. [Kluwer, Dordrecht (1992); Naukova Dumka, Kiev (1988)].
[12] Ya. I. Frenkel' (J. Frenkel), *Introduction to the Theory of Metals* [in Russian], Nauka, Leningrad (1972).
[13] O. M. Braun and Yu. S. Kivshar, Phys. Rep. **306**, No. 1–2 (1998).
[14] A. M. Kosevich and A. S. Kovalev, ''Theory of dynamic crowdions,'' *Materials of the School on Radiation and Other Defects in Solids*, Vol. 1 [in Russian], Izd. Inst. Fiz. AN GSSR, Tbilisi (1974).
[15] A. M. Kosevich and A. S. Kovalev, ''Theory of the dynamic crowdion in in a strongly anisotropic three-dimensional medium,'' in *Dynamics of Dislocations* [in Russian], Naukova Dumka, Kiev (1975).
[16] A. S. Kovalev, A. D. Kondratyuk, A. M. Kosevich, and A. I. Landau, Phys. Rev. B **48**, 4122 (1993); Phys. Status Solidi B **177**, 117 (1993).
[17] A. L. Landau, A. S. Kovalev, and A. D. Kondratyuk, Phys. Status Solidi B **179**, 373 (1993).
[18] V. A. Slyusapev, I. A. Bupakhovich, and M. A. Stpzhemechnyĭ, ''Theory of dynamic crowdions in classical and quantum crystals'' [in Russian], Preprint FTINT AN USSR (1973).
[19] A. M. Kosevich, *Dislocations in the Theory Elasticity* [in Russian], Naukova Dumka, Kiev (1978); Usp. Fiz. Nauk **84**, 579 (1964) [Sov. Phys. Usp. **7**, 837 (1965)].
[20] H. Goldstein, *Classical Mechanics* [Addison–Wesley, Reading, Mass. (1950); GITTL, Moscow (1957)].

Translated by Steve Torstveit

## LOW-TEMPERATURE PHYSICS OF PLASTICITY AND STRENGTH

# Dislocation-related inelastic phenomena at different damping levels

V. Ya. Beloshapka and V. G. Gur'yanov

*P. D. Osipenko Berdyansk State Pedagogical Institute, ul. Shmidta 4, 71440 Berdyansk, Ukraine*

V. Ya. Platkov

*Kharkov State Technical University of Agriculture, ul. Artema 44, 61002 Kharkov, Ukraine*
(Submitted December 18, 1998; revised January 31, 1999)
Fiz. Nizk. Temp. **26**, 294–303 (March 2000)

A numerical investigation is made into the dynamics of steady-state oscillations of an isolated dislocation loop over a wide interval of forced oscillation frequencies and at different levels of damping. The dependence of the dislocation-related strain and power dissipation on the external stress is found for different levels of damping. The amplitude dependences of such integral characteristics of the dynamics of dislocation motion as the internal friction, the elastic-modulus defect, and the ratio of the two are investigated. A critical value of the damping level of the dislocation loop is found at which the dislocation hysteresis begins to lose its static character and starts to take on dynamic traits. The features of the formation of dislocation hysteresis under conditions of its transformation from a static to a dynamic type are established.
 [S1063-777X(00)00603-4]

The quasiviscous drag on dislocations when a pulse of some kind of elementary excitation is applied is sharply reduced on going to the low-temperature region. This change is especially strong for superconductors at the *NS* transition. In turn, the quasiviscous drag, which is characterized by a damping coefficient $B$, has a substantial influence on the process by which dislocation loops overcome local pinning centers and, hence, on the dislocation-related inelastic properties of crystals (elastic-modulus defect, internal friction).[1–12] One expects that increasing the frequency $\omega$ of the external force will not only lead to quantitative changes but will qualitatively alter the way in which the inelastic properties are formed. In this connection it is important to study the dislocation-related inelastic phenomena over wide ranges of values of $B$ and $\omega$. In particular, studies of this kind can yield information about the influence of the forced oscillation frequency on the change in the dislocation-amplitude-dependent internal friction at the *NS* transition and also about the change in the dynamic characteristics of a dislocation as the electronic viscosity coefficient decreases. A theoretical analysis of the influence of viscosity on the dynamics of dislocations and the dislocation-related internal friction[1–12] shows that the physical picture of the phenomenon in the general case is complicated. In particular, it is found that a viscosity-related renormalization of the depinning stress of dislocation segments occurs, that the depinning process does not always have a catastrophic character, that the influence of the viscosity is a substantially nonlinear effect, and that the dislocation hysteresis loses its static character and begins to take on dynamic traits as the damping level increases.[12] The results of the well-known Granato-Lücke[13] and Rogers[14] theories, which describe the amplitude-dependent losses, turn out to be valid only in the particular limiting case of weak damping of the dislocation loop. We note that the influence of the level of damping of the dislocation loop on the internal friction was investigated analytically in Ref. 12, but the complexity of the equations of motion did not permit a detailed analysis of the phenomenon or a determination of all the characteristics of the internal friction. The influence of the viscosity on the dislocation-amplitude-dependent internal friction was investigated by numerical methods in Refs. 15 and 16 for the case of pinning centers distributed over the entire glide plane. In Ref. 15 the results of the simulation were presented only for one frequency, $\nu = 10^5$ Hz, and four values of $B$; consequently, there was no systematic analysis of the influence of the damping level on the internal friction. We note that in Ref. 15, unlike Ref. 13, the dislocation loop did not have sites of rigid attachment, and for this reason the linear tension exerted no restoring force. Thus the model of Ref. 15 does not correctly reflect the connection between the level of damping and the dislocation-related losses in the amplitude-dependent region. In Ref. 16 the decrement was calculated in the quasistatic approximation for a zero effective frequency of the external stress. For this reason, in Ref. 16, as in Refs. 13 and 14, the treatment of the energy losses in the amplitude-dependent region did not include the cases of practical importance.

The goal of the present study was to carry out a numerical analysis of the dynamics of oscillation of a dislocation loop and of inelastic effects over a wide range of oscillation frequency and viscosity.

### COMPUTATIONAL MODEL AND PROCEDURES

We analyzed the behavior of an isolated dislocation loop of length $L_N$ with rigidly fixed ends and and having weak pinning centers along its initially rectilinear position. The

 

coordinates of these centers along the dislocation line was specified by a pseudo-random number generator, which led to an exponential distribution law for the dislocation segments $L_c$ with respect to lengths ($L_c$ is the distance between weak centers). The analysis was carried out in the well-known linear-tension approximation for an activationless depinning of the dislocations from the weak centers; $L_N$ was varied over the interval $10^{-6}$–$10^{-4}$ m, and the ratio $L_N/L_c$ was varied from 10 to 150. For the computations a shear modulus $G=10^{10}$ Pa was adopted, along with a Burgers vector $b=3\times10^{-10}$ m, a linear tension of the dislocation $C=10^{-9}$ N/m, and a linear effective mass density of the dislocation $A=10^{-15}$ kg/m. The viscosity was varied over the interval $10^{-8}\,\mathrm{N\cdot s/m^2}<B<10^{-3}\,\mathrm{N\cdot s/m^2}$ (typical values in most materials range from $10^{-7}$ to $10^{-4}\,\mathrm{N\cdot s/m^2}$).[4] The external stress varied as $\sigma=\sigma_0\sin(\omega t)$, where $\sigma_0$ is the amplitude of the alternating stress, and $\omega=2\pi\nu$ was varied over an interval corresponding to frequencies $10^3\,\mathrm{Hz}<\nu<2\times10^6$ Hz. The flexure of the dislocation loop always remained much smaller than its length. The equation of the oscillations of the dislocation loop had the form

$$A\partial^2u/\partial t^2+B\partial u/\partial t+C\partial^2u/\partial x^2=b\sigma_0\sin(\omega t)+b\sum_{i=1}^{n}\tau_i[(x-x_i)/x_0,(u-u_i)/u_0], \tag{1}$$

where $\tau_i$ is a term describing the stress arising as a result of the interaction of the dislocation with the pinning center at the coordinates $(x_i,u_i)$ and $x_0$ and $u_0$ are the characteristic dimensions of the interaction region of a pinning center with a dislocation in the $x$ and $u$ directions (they had a value $10^{-9}$–$10^{-7}$ m). For a description of the interaction of a dislocation with a pinning center we used the approximation[16]

$$\tau(u)\begin{cases}\tau_0 s(1-s)^n & \text{for } |s|\leqslant 1,\\ 0 & \text{for } |s|>1\end{cases} \tag{2}$$

for $n=2$ and $n=500$, where $s=(u-u_i)/u_0$. The maximum interaction force of a dislocation with a pinning center was always much smaller than the linear tension $C$, and the ''angle of attack'' did not exceed $\pi/10$.

In the framework of the above model we calculated the dynamic characteristics of a dislocation loop during its oscillations with various amplitudes and also the integral characteristics of the loop, such as the hysteretic internal friction and the elastic-modulus defect. We investigated the following relationships describing the dynamics of a dislocation loop:

the dependence of the shape $u(x)$ of the dislocation loop on time and on the external stress $\sigma$;

the dependence of the phase shift of the displacements of different parts of the dislocation loop (with respect to the phase of the external stress) on the damping level;

the dependence of the mean dislocation strain $\varepsilon$ on $\sigma$;

the dependence on $\sigma$ of the power $P$ dissipated by the dislocation loop.

For integration of the equation of motion (1) we used three numerical methods which gave good agreement: Masso's method,[17] and explicit and implicit finite-difference methods.[18] The main results were obtained by an implicit finite-difference method which permitted working with the largest time step. Whenever possible, the results obtained by the numerical methods for steady-state oscillations of the loop were compared with the data from an analytical treatment. The calculated characteristics were not affected by changes in the initial conditions in Eq. (1) and remained constant in any subsequent oscillation period for $t>t_0$, where $t_0$ is the time required for the transient oscillations to die out. The value of $t_0$ depended on the values of $\omega$ and $B$ and was found by an empirical method. The maximum velocity of the segments of the loop did not exceed 800 m/s. The energy $\Delta W$ dissipated by the dislocation loop over an oscillation period $T$ was estimated as the area of the $\sigma(\varepsilon)$ hysteresis loop:

$$\Delta W=\int_{t_i}^{t_i+T}\sigma(t)d\varepsilon(t). \tag{3}$$

The dislocation-related strain was determined from the area of the figure under the dislocation loop:

$$\varepsilon=\overline{u}bL_N, \tag{4}$$

where

$$\overline{u}=(1/L_N)\int_0^{L_N}u(x)dx. \tag{5}$$

The following expressions were used for the logarithmic damping decrement $\delta$ and the modulus defect $\Delta G/G$:

$$\delta=\Delta WG/\sigma_0^2, \tag{6}$$

$$\Delta G/G=G/(\pi\sigma_0)\int_0^{2\pi}\varepsilon(\sigma)\sin(\omega t)d(\omega t). \tag{7}$$

For presenting the results in a compact form it is helpful to transform to normalized dimensionless parameters. Since the individual results were to be compared with the data of Refs. 12–14, and also because of the form of Eq. (1) and its boundary conditions, we chose the following normalized coordinates $\xi$ and $\eta$ and normalized time $\theta$:

$$\xi=x/L_N;\ \eta=u/L_N;\ \theta=(t/L_N)(C/A)^{1/2}.$$

Equation (1) in the normalized coordinates has the form

$$\frac{1}{4}\partial^2\eta/\partial\theta^2+\gamma\partial\eta/\partial\theta-\frac{1}{4}\partial\eta^2/\partial\xi^2=S+\sum_{i=1}^{n}\phi[(\xi-\xi_i)/\xi_0,(\eta-\eta_i)/\eta_0], \tag{8}$$

where $\gamma=BL_N/[4(AC)^{1/2}]$ is the normalized viscosity, $S=b\sigma L_N/(4C)$ is the normalized stress, $\phi=(bL_N/4C)\tau[(\xi-\xi_i)/\xi_0,(\eta-n_i)/\eta_0]$ is the force law of the interaction between a weak pinning center and the dislocation in the normalized coordinates, and $\xi_0$ and $\eta_0$ are the normalized dimensions of the interaction region of a pinning center with the dislocation in the $\xi$ and $\eta$ directions. The expression for the normalized frequency has the form $\Omega=\omega L_N(A/C)^{1/2}$. With this normalization of the variables the dimensionless quantity $\gamma\Omega$ determines the level of damping of the dislocation loop and matches the analogous parameter used in Ref. 12. Although the characteristics of the inelasticity and dislo-

cation dynamics are presented as functions of the normalized variables, in the discussion of the results we will also use the real values of these variables.

## RESULTS

The oscillations of the dislocation loop and the inelastic phenomena at different damping levels were investigated in the amplitude interval $0<S_0<5S_{0c}$, where $S_{0c}$ is the normalized critical stress amplitude above which the activationless depinning of the dislocation loop begins. The following relationships were established. It was found that the depinning of the dislocation loop always had a catastrophic character, both in the initial state of the loop along the pinning centers and in the repinned state during the motion. The depinning started at the pinning center with the maximum sum of the lengths of the adjacent segments and then propagated along the whole length of the loop. The propagation time of the depinning was always less than a quarter of the oscillation period except for the case with the largest values of the product $\gamma\Omega$. The shape of the dislocation loop $\eta(\xi)$, the amplitude dependence of the internal friction $\delta(S_0)$, and the modulus defect $\Delta G/G(S_0)$ changed qualitatively as $\gamma$ and $\Omega$ were varied but remained constant under the condition $\gamma\Omega=\text{const}$. This was observed in the entire interval of $S_0$, including in the amplitude-dependent region, and therefore the data on the influence of $B$ and $\omega$ on the investigated characteristics are presented as functions of the product of $\gamma\Omega$.

As $L_N/L_c$ was varied, the functions $\delta(S_0)$ and $\Delta G/G(S_0)$ did not undergo any qualitative or substantial quantitative changes, and they are therefore presented for a fixed value of $L_N/L_c$. Thee quantitative relationships describing the influence of $L_N/L_c$ on the amplitude dependences will be given separately. Figure 1 shows the amplitude dependences of $\delta$, $\Delta G/G$, and of their ratio $r$ for various values of $\gamma\Omega$ in the interval $2.5\times10^{-3}<\gamma\Omega<25$ for $L_N/L_c=20$. For $L_N/L_c>12$ in the entire amplitude-independent region $\delta_i$ increases in proportion to $\gamma\Omega$. The character of the influence of $\gamma\Omega$ on the amplitude dependences of $\delta$ and $\Delta G/G$ attests to the existence of a critical damping level $(\gamma\Omega)_c=0.025$ such that under the condition $\gamma\Omega<(\gamma\Omega)_c$ the internal friction is independent of $\gamma$ and $\Omega$.

The values of the critical amplitude $S_{0c}$ obtained from the functions $\delta(S_0)$ and $\Delta G/G(S_0)$ at the same value of $\gamma\Omega$ are equal. As $\gamma\Omega$ increases, the critical amplitude $S_{0c}$ increases (Fig. 2). Although for values in the region $\gamma\Omega<(\gamma\Omega)_c$ the damping level $\gamma\Omega$ does not affect the functions $\delta(S_0)$ and $\Delta G/G(S_0)$, for $\gamma\Omega>(\gamma\Omega)_c$ they change substantially and behave in qualitatively different ways. For $\gamma\Omega>(\gamma\Omega)_c=0.025$ the $\delta(S_0)$ curves become more gradual with increasing $\gamma\Omega$, and the maxima on these curves are shifted to larger $S_0$, and the value of $\delta$ at the maximum of the $\delta(S_0)$ curve increases with increasing $\gamma\Omega$, reaching its highest value at $\gamma\Omega\approx2.5$. At larger $\gamma\Omega$ the maximum on the $\delta(S_0)$ curve gives way to a plateau region on which $\delta$ remains unchanged all the way out to the maximum values of $S_0$. The plateau begins for $S_0>(1.5-2)S_{0c}^0$, where $S_{0c}^0$ is the value of $S_{0c}$ for $\gamma\Omega<(\gamma\Omega)_c$. The value of $\delta$ on the plateau region decreases with increasing $\gamma\Omega$.

In contrast to $\delta(S_0)$, the $\Delta G/G(S_0)$ curves are monotonic, and they shift to larger $S_0$ and become more gradual

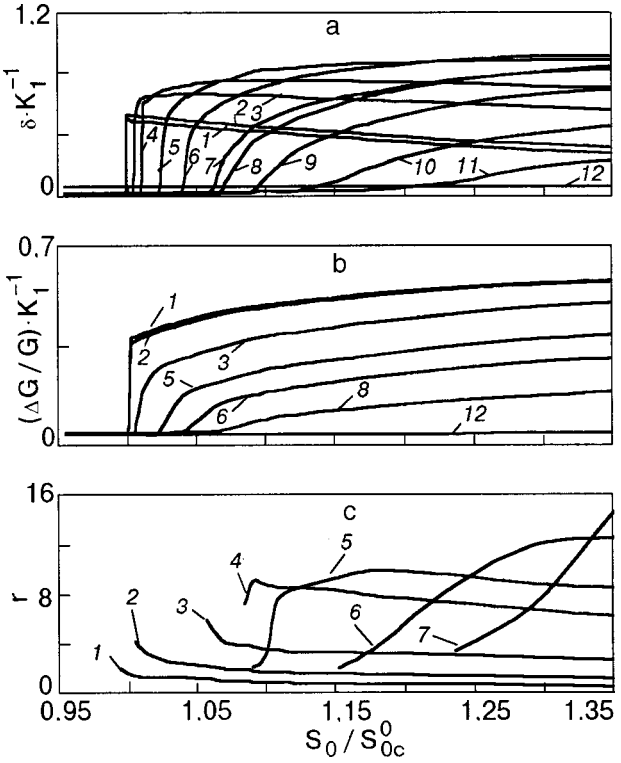


FIG. 1. Amplitude dependence of the damping decrement (a), modulus defect (b), and their ratio $r=\delta_h/(\Delta G/G)$ (c) for different values of the product $\gamma\Omega$: 0.000031 (*1*), 0.031 (*2*), 0.31 (*3*), 0.53 (*4*), 0.95 (*5*), 1.2 (*6*), 2.0 (*7*), 3.1 (*8*), 4.1 (*9*), 6.2 (*10*), 9.3 (*11*), 14 (*12*) (*a,b*); <0.025 (*1*), 0.25 (*2*), 1 (*3*), 2.5 (*4*), 3.25 (*5*), 5 (*6*), 7.5 (*7*) (c). $K_1=(4\Lambda Gb^2L_N^2)/(\pi^3C)$, where $\Lambda$ is the length of the dislocation lines per unit volume.

with increasing $\gamma\Omega$ (Fig. 1b). For $S_0>1.5S_{0c}^0$ the $\Delta G/G(S_0)$ curves exhibit a plateau. The modulus defect and the decrement decrease monotonically with increasing $\gamma\Omega$ on this part of the curves.

The values of the ratio $r(S_0)$ obtained for $\gamma\Omega<(\gamma\Omega)_c$ do not depend on $\gamma\Omega$ and have a maximum value of 1.8–1.9, and $r$ decreases with increasing $S_0$ (Fig. 1c). However, as $\gamma\Omega$ increases, for $\gamma\Omega>(\gamma\Omega)_c$, the maximum value of $r$ increases, reaching 14.0–16.0, and the position of the maximum on the $r(S_0)$ curve is shifted to larger values of $S_0$.

For detailed analysis of the influence of the damping level $\gamma\Omega$ on the amplitude-dependent inelastic phenomena we studied $\delta(\gamma\Omega)_{S_0=\text{const}}$ and $\Delta G/G(\gamma\Omega)_{S_0=\text{const}}$ at fixed values of $S_0$ (Fig. 3). These curves were obtained for different values $S_0=\text{const}$ from the whole range of stress amplitudes. With increasing $S_0$ the maximum on the $\delta(\gamma\Omega)_{S_0=\text{const}}$ curves initially shifted to larger values of $\gamma\Omega$, but above $S_0\geqslant1.5S_{0c}^0$ the position of the maximum along the $\gamma\Omega$ axis

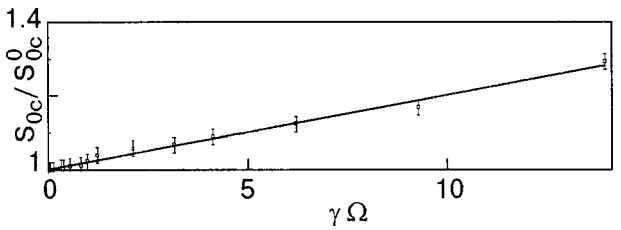


FIG. 2. Normalized critical amplitude of the external stress corresponding to the onset of depinning versus the damping level $\gamma\Omega$.

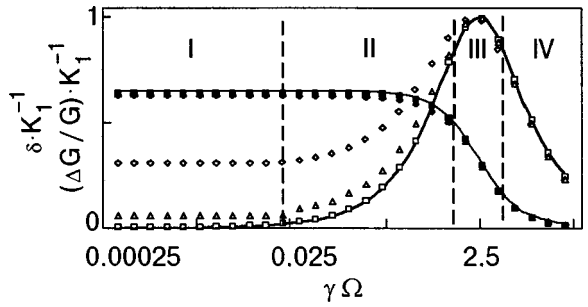


FIG. 3. Damping decrement and elastic modulus defect (at fixed values of the amplitude of the external stress) versus the damping level $\gamma\Omega$: □,△—the decrement for $S_0/S_{0c}^0=1.5$ and 3, respectively; ▲,■—the defect modulus for $S_0/S_{0c}^0=1.5$ and 3, respectively; ◇—the decrement in the absence of pinning centers on the loop; the lines ——and ——correspond to the defect modulus and decrement calculated according to the Granato-Lücke theory in the absence of pinning centers on the dislocation loop.

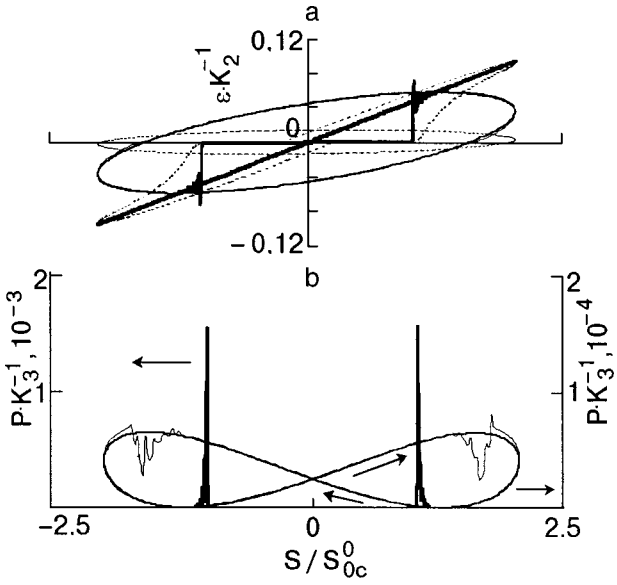


FIG. 4. The dependence of the dislocation-related strain $\epsilon$ (a) and the power $P$ dissipated by a dislocation loop (b) on the normalized external stress, at a fixed amplitude $S_0/S_{0c}^0=2$ and various values of $\gamma\Omega$: 0.03 (——), 0.3 (— — —); 3, in the absence of pinning centers on the dislocation loop (——), and 15 (· · · ·). $K_2=(\Lambda b L_N)$, $K_3=(4C^{3/2})/(L_N A^{1/2})$.

remained unchanged. For $S_0 \geqslant 1.5S_{0c}^0$ the value of the decrement in the region of the maximum and in the entire region to the right of the maximum was unaffected by changes in the fixed values of $S_0$ at which the curves of $\delta(\gamma\Omega)_{S_{0=\text{const}}}$ were obtained. Similarly, increasing $S_0$ in the region $S_0 > 1.5S_{0c}^0$ had no effect on $\Delta G/G(\gamma\Omega)_{S_{0=\text{const}}}$ in this same range of $\gamma\Omega$ values. Figure 3 shows a semilogarithmic plot of the curves $\delta(\gamma\Omega)_{S_{0=\text{const}}}$ and $\Delta G/G(\gamma\Omega)_{S_{0=\text{const}}}$, obtained for two values of $S_0$, and the curve for the decrement in the absence of pinning centers on the dislocation loop. This last curve did not change as $S_0$ was increased. At values of $\gamma\Omega$ corresponding to the region of the maximum and to the right of the maximum it corresponds to the $\delta(\gamma\Omega)_{S_{0=\text{const}}}$ curves obtained in the presence of pinning centers on the dislocation loop. The curves of $\Delta G/G(\gamma\Omega)_{S_{0=\text{const}}}$ are monotonically decreasing, and the region of their most rapid fall always coincides with the position of the maximum on the analogous curve of the decrement.

Increasing $L_N/L_c$ from 10 to 150 led to changes in $\delta(\gamma\Omega)_{S_{0=\text{const}}}$ and $\Delta G/G(\gamma\Omega)_{S_{0=\text{const}}}$ only in the region to the left of the maximum on the curve of the decrement ($\gamma\Omega < 2.5$), and the greatest changes in the curves were observed for $\gamma\Omega < (\gamma\Omega)_c$, but these changes were not important. For example, increasing $L_N/L_c$ from 10 to 150 caused $\delta$ to increase by only a factor of 1.2.

Figure 3 shows the four characteristic regions. In region *I* the decrement is practically independent of $\gamma\Omega$, and $\delta(S_0)$, after reaching a maximum, falls off as $S_0^{-2}$. In region *II* the $\delta(\gamma\Omega)_{S_{0=\text{const}}}$ curve is close to linear, and in region *III* it has a maximum. Region *IV* corresponds to the interval of $\gamma\Omega$ values to the right of the maximum, and here the loss is inversely proportional to $\gamma\Omega$.

Figure 4 shows the dislocation-related strain $\epsilon$ and the power $P$ dissipated by the dislocation loop as functions of the external stress $S$. These curves, which were obtained for different values of $\gamma\Omega$ but at the same amplitude $S_0$, have the form of hysteresis loops. The character of the hysteresis loop changes qualitatively as $\gamma\Omega$ is increased. At values of $\gamma\Omega$ corresponding to region *I* in Fig. 3 the function $\epsilon(S)$ during the unloading part of the oscillation period is practically linear. The dislocation loop, as it returns to its initial position, approaches the line of pinning centers at zero values of $S$ with nearly its linear equilibrium shape. As $S$ increases further, the dislocation loop, after its complete depinning, always executes damped oscillations with a frequency close to the natural frequency $v_0=(2L_N)^{-1}(C/A)^{1/2}$. The $P(S)$ plot shown in Fig. 4b indicates that the dissipation of energy by the dislocation loop occurs predominantly at the time immediately following its depinning and arrival at the equilibrium position. Increasing the amplitude $S_0$ to the maximum values in the indicated range did not alter the aforementioned features of all the curves for values of $\gamma\Omega$ corresponding to region *I*.

For values of $\gamma\Omega$ corresponding to region *II* in Fig. 3 the $\varepsilon(S)$ curve has a qualitatively different form (Fig. 4a). The dislocation loop returns to the pinning centers at nonzero values of the stress. At a fixed $S_0$ the stress at which the dislocation loop returns to the centers increases with increasing $\gamma\Omega$, and the extent of the region of direct proportionality on the $\varepsilon(S)$ curve near $S_{0c}$ becomes shorter. For $S_0$ not much greater than $S_{0c}$, this part of the $\varepsilon(S)$ curve becomes shorter as $\gamma\Omega$ increases, but it does not vanish completely even at the largest values of $\gamma\Omega$. As $S_0$ increases, however, this part does vanish completely for $\gamma\Omega > (\gamma\Omega)_c$ (Fig. 5a). Here the hysteresis loop becomes elliptical, and with increasing $\gamma\Omega$ the ellipse rotates in such a way that the angle between its semimajor axis and the stress axis decreases. The elliptical hysteresis loops obtained at fixed values of $\gamma\Omega$ but for different $S_0$ have parallel orientations of their semiaxes. On going to regions *III* and *IV* the continuing growth of $\gamma\Omega$ at fixed $S_0$ causes further changes in the elliptical hysteresis loop: its area and the angle between the semimajor axis and the stress axis decreases (Fig. 4a). It was found that at all $\gamma\Omega$ for which the dislocation loop at $S \approx S_{0c}$ returns to the pinning centers the curves of $\delta(\gamma\Omega)_{S_{0=\text{const}}}$ and $\Delta G/G(\gamma\Omega)_{S_{0=\text{const}}}$ coincide with the analogous curves ob-

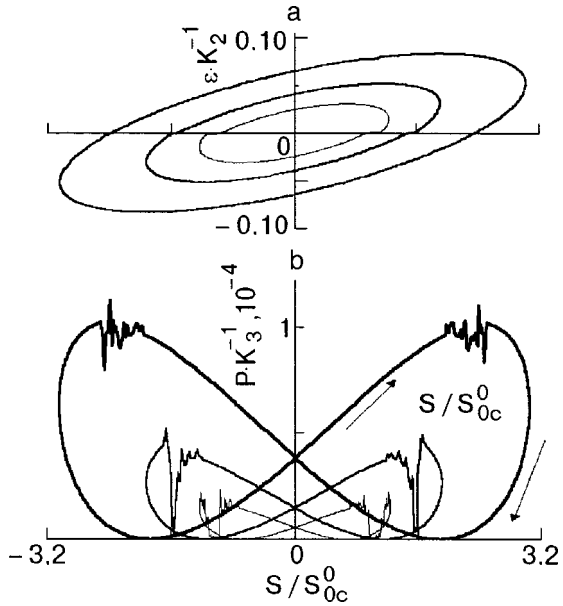


FIG. 5. Dependence of the dislocation-related strain $\varepsilon$ (a) and the power $P$ dissipated by a dislocation loop (b) on the value of the normalized external stress; the curves were calculated for $\gamma\Omega=2.5$ and various values of $S_0/S_{0c}^0$: 1.25 (— — —), 1.8 (——), 3 (——); $K_3=(\Lambda b L_N)$, $K_3=(4C^{3/2})/(L_N A^{1/2})$.

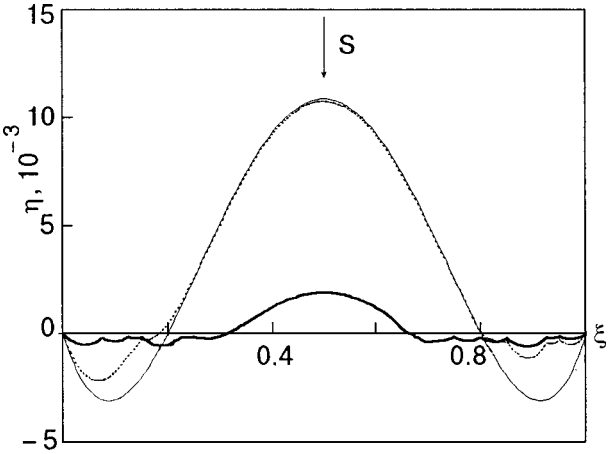


FIG. 6. Shape of the dislocation loop at the times corresponding to its crossing of the line of pinning centers: $\gamma\Omega=1.5$, $S_0/S_{0c}^0=3.5$, at the time $t=1.6T$ (——); $\gamma\Omega=15$, $S_0/S_{0c}^0=3.0$ at the times $t_1=1.72T$ (——) and $t_2=1.73T$ (· · · ·).

tained in the absence of pinning centers on the dislocation (Fig. 3).

This coincidence of the curves, which started in region *II*, was also observed in regions *III* and *IV*. With increasing $S_0$ the value of $\gamma\Omega$ at which these curves begin to coincide decreases, but even at the largest values of $S_0$ the damping level never shifted farther to the left than the middle of region *II*. For $S_0=2S_{0c}^0$ the coincidence begins at $\gamma\Omega=1.25$. As $S_0$ increases further the external stress $S$ at which the loop returns to the pinning centers continues to increase, and when $S$ exceeds $S_{0c}$ a coincidence of the curves $\delta(\gamma\Omega)_{S_{0=\text{const}}}$ is observed. However, even though the $\delta(\gamma\Omega)_{S_{0=\text{const}}}$ curves for different values of $S_0$ coincide in the region of the maximum and to the right of it, the behavior of the loop during its passage through the pinning centers changes as $S_0$ increases. When the amplitude $S_0$ reaches values of $(3-4)S_{0c}^0$, the shape of the dislocation loop deviates substantially from the equilibrium shape as it returns to the pinning centers. The parts of the loop adjacent to its edges lead the central part in phase. Now the depinning from the centers begins independently on the two parts adjacent to the ends of the loop and then propagates to the central part of the loop (Fig. 6). This behavior of the dislocation loop is manifested increasingly as $\gamma\Omega$ increases from the right half of region *II* to regions *III* and *IV*. In these regions, for $S_0=(2.5-3)S_{0c}^0$ a situation arises in which the edge regions of the loop have already become depinned while the central part has not yet reached the line of pinning centers (Fig. 6).

As $\gamma\Omega$ increases from region *I* into regions *II*, *III*, and *IV*, the relations governing the dissipation of energy by the dislocation loop during the oscillation period change substantially (Figs. 4b and 5b). Unlike the case in region *I*, where the energy of the loop is dissipated in the oscillations immediately following its depinning, in regions *III* and *IV* the dissipation of energy by the dislocation occurs for practically the entire oscillation period. It is absent only at the times of the greatest deviation of the dislocation loop from the equilibrium position and also on the part of the hysteresis loop near $S/S_{0c}\approx 1$ if the $\epsilon(S)$ curve has a rectilinear region, corresponding to the pinned state of the dislocation loop. When such a region is present the depinning of the loop for $\gamma\Omega$ values in regions *II–IV* is always accompanied by a jumplike increase in the power dissipation $P$, as is characteristic for region *I* as well.

## DISCUSSION OF THE RESULTS

For $\gamma\Omega<(\gamma\Omega)_c$ the form of the amplitude dependences of the internal friction and the character of their change agree with the theoretical ideas developed in Ref. 13 and generalized to the case of large amplitudes in Ref. 14. The maximum on the $\delta(S_0)$ curve at $S_0=S_{0c}$ is due to the catastrophic character of the depinning of the loop. The independence of $\delta_h$ from $\gamma\Omega$ and its decline with increasing $S_0$ for $S_0>S_{0c}$ are evidence of the absence of amplitude-dependent dynamic losses in this region of $\gamma\Omega$ values. This is also indicated by the function $\delta(\gamma\Omega)$ calculated in the absence of pinning centers on the dislocation loop, which is in good agreement with the Granato–Lücke frequency profile (see Fig. 3). Our numerical values of the decrement for $S_0\approx S_{0c}$ and the character of our function $\delta(S_0)$ for $S_0>S_{0c}$ do not agree with the results of Ref. 14. The reason is that in the calculation of $\delta$ we considered the contribution of only one dislocation loop. Since in the given situation the depinning has a catastrophic character and occurs over a time much shorter than the period of the forced oscillations, while the presence of oscillations on the $\varepsilon(S)$ curve does not have an important effect on the area of the hysteresis loop, the dislocation-related strain $\varepsilon$ can be estimated to good accuracy in the quasistatic approximation. For the case of larger $L_N/L_c$, when the dislocation-related strain prior to depinning can be neglected, $\epsilon$ is described by the relation

$$\varepsilon = \Lambda b^2 \sigma_{0c}/(2L_N - C)\int_0^{L_N}(xL_N x^2)dx$$

$$= \Lambda b^2 \sigma_{0cc} L_N^2/(12C). \quad (9)$$

Here the expression for the decrement becomes

$$\delta_h = \Lambda b^2 \sigma_{0c}^2 L_N^2 G/(12C\sigma_0^2). \quad (10)$$

The values of the numerically calculated decrement for $S_0 = S_{0c}$ and the character of its dependence on $S_0$ for $S_0 > S_{0c}$ are in good agreement with Eq. (10). For analysis of the influence of the degree of damping on the critical amplitude of the depinning stress, we compared the shapes of the dislocation segment prior to depinning under conditions of oscillatory motion and under conditions of static loading. In the latter case the shape of the dislocation segment prior to depinning for the case of pinning centers located at the points $x=0$ and $x=L_c$ was found in analytical form as the solution of the equation

$$C(\partial^2 u/\partial x^2) + b\sigma = 0$$

and had the form

$$u = \frac{b\sigma x L_c - b\sigma x^2}{2C}.$$

A comparison of the shapes of the segment prior to depinning under conditions of oscillatory motion and static loading shows that they are practically the same in the region of small $\gamma\Omega$ (region *I* in Fig. 3). This fact accounts for the absence of an influence of the value of $\gamma\Omega$ on the critical amplitude of the depinning stress in region *I*. Because the time interval required for a dislocation loop to achieve its maximum flexure after depinning is much shorter than the period of the forced oscillations and therefore the oscillations of the dislocation loop around the equilibrium configuration do not have an appreciable effect on the area of the hysteresis loop $\varepsilon(S)$, the value of $\delta_h$ also remains unchanged under the condition $\gamma\Omega < (\gamma\Omega)_c$.

The absence of an influence of $\gamma\Omega$ on the form of the hysteresis loop $\varepsilon(S)$ and on $\delta(S_0)$ and $P(S)$ suggest that for $\gamma\Omega < (\gamma\Omega)_c$ the dislocation-related hysteresis has a pronounced static character throughout the entire range of $S_0$ values investigated, and there are practically no dynamic amplitude-dependent losses.

Unlike the case of region *I*, in regions *II–IV* the dislocation-related hysteresis loops undergo qualitative changes as $\gamma\Omega$ increases (Fig. 4a), and the basic hallmark of static hysteresis—the frequency and velocity independent of the $\varepsilon(S)$ loop—is lost. In regions *II–IV* the inelastic phenomena are not described by the static hysteresis model.[13] The generalization of that theory[13] in Ref. 14 cannot be used for such a description either, since in that paper[14] the dislocation-amplitude-dependent losses were treated for the case when the dislocation-related hysteresis takes place in the low-frequency asymptotic region of the Granato–Lücke frequency profile.[13] In our case the overcoming of the pinning centers by the dislocation loop in regions *III* and *IV* cause hysteresis at the frequencies of the high-frequency maximum of the damped resonance, where, in particular, there is no linear dependence of the dynamic losses on $\gamma\Omega$ (Fig. 3). The results of Ref. 14 can only be compared with the data pertaining to the left half of region *II*, where the $\delta(\gamma\Omega)_{S_0=\text{const}}$ curve is close to linear. The resultant losses (Fig. 3) can be represented in the form of a sum of the hysteresis losses calculated at values of $\gamma\Omega$ corresponding to region *I* plus the dynamic losses calculated in the absence of pinning centers on the dislocation loop.

At amplitudes in the region $S_0 > 1.5S_{0c}^0$ a comparison of the $\delta(\gamma\Omega)_{S_0=\text{const}}$ and $\Delta G/G(\gamma\Omega)_{S_0=\text{const}}$ curves with the Granato–Lücke frequency profile for $\delta$ and $\Delta G/G$, respectively, and also the presence of a plateau on the amplitude dependences of $\delta$ and $\Delta G/G$ indicate that the hysteresis is of a dynamic character. Here the hysteresis loops of the static type are almost completely absent, since at a high damping level $\gamma\Omega$ and such large values of $S_0$ the dislocation loop approaches the pinning centers at stresses higher than $S_{0c}$, and the additional phase shift between $\varepsilon$ and $S$ due to the interaction of the dislocation with the pinning centers does not arise. The decrease in the area of the dynamic hysteresis loop as $\gamma\Omega$ increases for $S_0 > 1.5S_{0c}^0$ agrees with the character of the dependence on the damping level for losses of this type in Ref. 13.

At values of $S_0$ not much greater than $S_{0c}$, the influence of the pinning centers on the behavior of the dislocation loop is always substantial (Figs. 1a, 1b, and 5), and the hysteresis losses are nonzero. A calculation of the energy losses over a period using expressions (3) and (4) does not in general permit one to separate the contributions of the hysteresis losses of the static type from the viscous losses. However, at values of $S_0$ just slightly higher than $S_{0c}$ the relative sizes of the dynamic and hysteresis contributions to the resultant loss can be assessed by proceeding from the following arguments. The hysteresis contribution to the energy dissipated by a dislocation at an arbitrary point in time after depinning is always present if the additional phase shift $\Delta\varphi$ between $\varepsilon$ and $S$ due to the previous interaction of the dislocation with the pinning centers is nonzero. For this reason the hysteresis losses occur in the time interval between the start of the depinning and the time when the loop reaches its maximum flexure. On the other hand, there is absolutely no energy dissipation by the dislocation immediately prior to the depinning and at the time of maximum flexure of the loop, as follows from the $P(S)$ plot (Fig. 5b). The energy dissipated over this time interval, containing both hysteresis and dynamic contributions, is small compared to the energy dissipated over the whole period, and it falls off with increasing $\gamma\Omega$. This is evidence that the contribution of the hysteresis losses to the resultant losses is insignificant and that this contribution decreases as the level of damping increases.

The absence of a substantial contribution of the hysteresis losses to the resultant losses for $S_0 \gg S_{0c}$ is convincingly demonstrated by a comparison of the $\varepsilon(S)$ and $P(S)$ curves with the analogous curves obtained in the case when there are no pinning centers on the dislocation loop (Figs. 4a and 4b). We see that the curves coincide except at the time when the dislocation loop is crossing the line of pinning centers. In this case the presence of the pinning centers has only a small effect on the energy losses over an oscillation period.

Thus on going into regions *II–IV* there is a change in the character of the dislocation hysteresis, from static to dynamic. Further evidence of this change in character of the

dislocation hysteresis as the degree of damping increases can be seen in the behavior of the ratio $r=\delta_h/(\Delta G/G)$ for different $\gamma\Omega$ (Fig. 1c). In Ref. 19 the analysis was limited to the case of static hysteresis and showed that the maximum value of $r$ is not greater than 2 and falls off as the amplitude of the external stress increases. The curves $r(S_0)$ obtained in the present study for $\gamma\Omega$ corresponding to region *I* likewise do not depend on $\gamma\Omega$, the maximum value of $r$ equals 1.8–1.9, and $r$ dependences on $S_0$, decreasing as $S_0$ increases. However, as $\gamma\Omega$ increases into regions *II–IV*, where the dislocation hysteresis begins to take on dynamic traits, the maximum value of $r$ increases sharply, reaching values of 14–16 and higher, while the position of the maximum on the $r(S_0)$ curve is shifted to larger values of $S_0$ as $\gamma\Omega$ increases.

In an experiment the maximum $r$ value $r_{\max}$ and the form of the $r(S_0)$ curve can provide evidence of whether the situation realized is one of static, mixed, or dynamic dislocation hysteresis and can indicate when one type of hysteresis gives way to another. For example, in experiments on the amplitude dependence of the internal friction and elastic-modulus defect under conditions of a sharp change in $B$ (e.g., a change of the electronic drag on dislocations at a superconducting transition) there is indeed a change in character of the dislocation hysteresis. Proof of this could be a change in $r_{\max}$ with a simultaneous shift of the $r(S_0)$ curve along the $S_0$ axis.

The observed influence of the viscosity on the internal friction over the entire interval of stress amplitudes $S_0$ (Fig. 1) is in good agreement with the experimentally established change in the internal friction of metals at a superconducting transition.[20–22] For example, as the viscosity increases, the internal friction increases in the region of large stress amplitudes, while at stresses slightly greater than $\sigma_{0c}$ it decreases. The dependence of the critical amplitude of the depinning stress on $\gamma\Omega$ (see Fig. 2) shows that an increase of $B$ by 3–3.5 orders of magnitude at initial values $B=10^{-7}-10^{-6}\,\mathrm{N\cdot s/m^2}$ in the kilohertz and megahertz frequency ranges leads to only a 10–25% increase in $\sigma_{0c}$; this is also in agreement with the experimental data on the internal friction in this frequency range.[20–22]

The results of this study point to yet another feature of the influence of an *NS* transition on the dislocation-amplitude-dependent internal friction of superconductors. If $\gamma\Omega<(\gamma\Omega)_c$ in the *N* state, then the *NS* transition should have no such influence; for $B=10^{-4}\,\mathrm{N\cdot s/m^2}$ this condition holds for $\omega<10^{-5}(L_N)^{-2}$ Hz.

Let us close by emphasizing that our findings concerning the behavioral regularities of the inelastic properties pertain to the case when the pinning centers are distributed along the initial rectilinear position of the dislocation. The results for the case of a distribution of pinning centers over the entire glide plane of the dislocation are qualitatively different in many ways and will be published in the future.

We thank V. D. Natsik for his interest in this study and for valuable comments.

[1] W. P. Mason, in *Physical Acoustics*, Vol. IV-A, edited by W. P. Mason [Academic Press, New York (1966); Mir, Moscow (1969), p. 345].
[2] A. V. Granato, Phys. Rev. Lett. **27**, 660 (1971).
[3] A. V. Granato, Phys. Rev. B **4**, 2196 (1971).
[4] M. I. Kaganov, V. Ya. Kravchenko, and V. D. Natsik, Usp. Fiz. Nauk **111**, 655 (1973) [Sov. Phys. Usp. **16**, 878 (1974)].
[5] V. L. Indenbom and Yu. Z. Estrin, JETP Lett. **17**, 468 (1973).
[6] Yu. Z. Estrin, Fiz. Nizk. Temp. **1**, 91 (1975) [Sov. J. Low Temp. Phys. **1**, 45 (1975)].
[7] V. L. Indenbom and V. M. Chernov, Fiz. Tverd. Tela (Leningrad) **21**, 1311 (1979) [Sov. Phys. Solid State **21**, 759 (1979)].
[8] A. I. Landau, Phys. Status Solidi **61**, 555 (1980).
[9] S. Asano, J. Phys. Soc. Jpn. **29**, 952 (1970).
[10] A. I. Landau, Phys. Status Solidi **65**, 119 (1981).
[11] A. I. Landau, Phys. Status Solidi **65**, 415 (1981).
[12] A. M. Roshchupkin and V. Ya. Platkov, Fiz. Nizk. Temp. **7**, 11201 (1981) [Sov. J. Low Temp. Phys. **7**, 583 (1981)].
[13] A. V. Granato and K. Lücke, J. Appl. Phys. **27**, 583 (1956).
[14] D. H. Rogers, J. Appl. Phys. **33**, 781 (1962).
[15] V. I. Belan and A. I. Landau, Fiz. Met. Metalloved. **65**, 259 (1988).
[16] R. B. Schwarz, Acta Metall. **29**, 311 (1981).
[17] I. S. Berezin and N. P. Zhidkov, *Computational Methods*, Vol. 2 [in Russian], Fizmatgiz, Moscow (1962).
[18] G. I. Marchuk, *Methods of Computational Mathematics* [in Russian], Nauka, Moscow (1989).
[19] A. B. Lebedev, Philos. Mag. A **74**, 137 (1996).
[20] V. Ya. Platkov, L. N. Polunina, and V. I. Startsev, Fiz. Tverd. Tela (Leningrad) **13**, 1881 (1971) [Sov. Phys. Solid State **13**, 1577 (1972)].
[21] V. Ya. Platkov, L. N. Polunina, and V. I. Startsev, Fiz. Tverd. Tela (Leningrad) **14**, 2772 (1972) [Sov. Phys. Solid State **14**, 2400 (1973)].
[22] V. Ya. Beloshapka and V. Ya. Platkov, Fiz. Nizk. Temp. **8**, 1247 (1982) [Sov. J. Low Temp. Phys. **8**, 631 (1982)].

Translated by Steve Torstveit

# Dislocation drag in the low-temperature phase of $C_{60}$ fullerite due to orientational relaxation of the molecules

V. D. Natsik* and A. V. Podol'skiĭ

*B. Verkin Institute for Low Temperature Physics and Engineering, National Academy of Sciences of Ukraine, pr. Lenina 47, 61164 Kharkov, Ukraine*

(Submitted July 28, 1999; revised September 21, 1999)
Fiz. Nizk. Temp. **26**, 304–313 (March 2000)

The interaction of edge dislocations with pentagonal ($p$) and hexagonal ($h$) orientation states of the molecules in the low-temperature simple cubic phase of $C_{60}$ fullerite is discussed. The temperature interval considered is $T_g<T<T_c$, where $T_c=260$ K is the phase transition temperature and $T_g=90$ K is the orientational glass point. The nonuniform distribution of the $h$ configurations around a sessile dislocation line is described, and the starting force $F_s(T)$ needed to break the dislocation away from the cloud of $h$ configurations formed by it is determined. The dynamic drag force $F_D(T,V)$ arising as a result of thermally activated transitions between the $p$ and $h$ configurations under the influence of the elastic field of a dislocation moving at a constant velocity $V$ is calculated and analyzed. © *2000 American Institute of Physics.* [S1063-777X(00)00703-9]

## INTRODUCTION

The study of plastic deformation of single crystals of $C_{60}$ fullerite by the microindentation method have shown[1–5] that over a wide range of moderately low temperatures 300-80 K the carriers of plasticity in them are dislocations belonging to the slip system $(111)\langle 110\rangle$. In Refs. 1 and 3 the discrete dislocation structure of the slip lines in the vicinity of the impression made by the indenter was revealed by thermal and chemical etching. Therefore, in constructing a consistent microscopic theory of the plasticity and strength of crystalline $C_{60}$, one of the first problems is to analyze the mobility of dislocations in this material.[6]

The motion of a dislocation in a crystal is always accompanied by energy dissipation, which leads to a drag on the dislocation. A portion of the energy loss of the dislocation is due to the discreteness of the crystal structure, and the description of this part requires a microscopic approach—e.g., the drag due to the Peierls potential relief or immovable local impurity barriers.[7–9] Other loss mechanisms have a macroscopic origin and can be analyzed in the framework of the continuum theory.[8–10] These include various relaxation processes occurring in the elastic field of a moving dislocation, e.g, the diffusion of impurity atmospheres, relaxation in a gas of quasiparticles, etc.

In the low-temperature simple cubic (sc) phase of $C_{60}$ fullerite, which exists below $T_c=260$ K, the most efficient mechanism of dissipation of mechanical energy is the lattice-orientation interaction and the orientational relaxation of molecules—thermally activated transitions of molecules between two energetically inequivalent orientations, which have come to be called the pentagonal ($p$) and hexagonal ($h$) configurations. The influence of the orientational relaxation on the thermal and rheological properties of fullerite crystals has been analyzed in detail in our previous paper.[11] There one can also find a list of references reflecting the history of this problem and containing detailed characteristic of the lattice-orientation structure of $C_{60}$ fullerite.[11] Below we describe as briefly as possible only those individual details of this structure which are needed in order to make a clear statement of the problem addressed.

In the sc phase the threefold symmetry axes of the $C_{60}$ molecules are orientationally ordered, and the molecules can only execute small librations and hindered rotations around these axes. In these rotations, two types of minima of the angular dependence of the intermolecular pair interaction are realized: a deeper global minimum (the $p$ configuration) and a local minimum ($h$ configuration); the difference in the energies of these configurations per intermolecular bond is $\Delta \simeq 0.01$ eV. The pentagonal and hexagonal configurations are separated by an energy barrier of the order of 0.3 eV: if the symbol $U_p$ denotes the barrier for the $p\rightarrow h$ transition, then the barrier for the inverse $h\rightarrow p$ transition will have the value $U_h=U_p-\Delta$. In the classical limit (ignoring quantum effects) the ideal thermodynamic equilibrium structure of the fullerite corresponds to the $p$ configuration of all the pair intermolecular bonds, and the $h$ configuration should be regarded as local structural defects that can be excited, for example, by the thermal motion of the molecules. In a state of thermodynamic equilibrium the volume concentrations $N_h$ and $N_p$ of the hexagonal and pentagonal configurations, respectively, is determined by the Boltzmann distribution and the balance relation:

$$\overline{n_h}=\frac{\overline{N_h}}{N_0}=\left(1+\exp\frac{\Delta}{kT}\right)^{-1}; \quad \overline{n_p}=\frac{\overline{N_p}}{N_0}=1-\overline{n_h}; \tag{1}$$

here a bar over a symbol denotes the equilibrium state, and $N_0=N_p+N_h$ is the volume concentration of double-well orientational states.

The mean times $\tau_p$ and $\tau_h$ for the thermally activated destruction of the $p$ and $h$ configurations, respectively, are determined by an activational formula of the form

 

$$\tau_{p,h}=\tau_0\exp\frac{U_{p,h}}{kT}, \tag{2}$$

where $\tau_0$ is the characteristic librational period, which is assumed to be the same for both configurations (empirical estimates lead to values $\tau_0\simeq 10^{-13}-10^{-14}$ s). Accordingly, the time dependence $n_h(t)$ of the nonequilibrium occupation of the defect $h$ configurations (orientational relaxation) is described by the simple kinetic equation

$$\tau\frac{\partial}{\partial t}n_h+n_h=\frac{\tau}{\tau_p},\quad \tau=\frac{\tau_p\tau_h}{\tau_p+\tau_h}. \tag{3}$$

In the temperature interval $T_c>T>T_g\simeq 90$ K the equilibrium concentration of the different $h$ configurations varies over the range $0.4>\overline{n_h}>0.2$, and the characteristic time for the establishment of orientational equilibrium is $\tau<10^3$ s. At such temperatures the thermally activated transitions between the $p$ and $h$ configurations occur rather rapidly on laboratory time scales, and the state of the crystal can be regarded as a kind of orientational liquid (OL). On the other hand, when the fullerite is cooled below $T_g$, thermodynamic equilibrium between the $p$ and $h$ configurations is not established over standard laboratory time scales. Therefore, for $T<T_g$ the crystal is in an orientational glass state, with a concentration of frozen defect configurations $n_{hg}\simeq 0.2$, and the temperature boundary $T_g$ has the meaning of an orientational glass point.

To describe the relation of the rotational degrees of freedom of the molecules with the deformations of the fullerite crystal lattice, in Ref. 11 it was proposed to introduce deformation corrections to the aforementioned intermolecular interaction parameters $U_p$, $U_h$, and $\Delta$. Taking into account the cubic symmetry of fullerite and working in a linear approximation in the components of the strain tensor $\epsilon_{ik}$, we get

$$U_{p,h}^{(\varepsilon)}=U_{p,h}-v_{p,h}\varepsilon_{ll},\quad \Delta^{(\varepsilon)}=\Delta-v_\Delta\varepsilon_{ll}. \tag{4}$$

Here $\varepsilon_{ll}$ is the sum of the diagonal components of the strain tensor, and $v_p$, $v_h$, and $\Delta=v_p-v_h$ are the constants of the deformation potential, for which the following empirical estimates were obtained in Ref. 11: $v_p\simeq v_h\simeq 2.0$ eV, $v_\Delta\simeq 2\Delta\simeq 2.4\times 10^{-2}$ eV.

The model of double-well orientational states of the molecules, supplemented with relations (4) and the kinetic equation (3), fulfills all the prerequisites for analysis of the interaction of a dislocation with the rotational degrees of freedom of the molecules in the low-temperature phase of $C_{60}$ fullerite, including a description of the dynamic drag exerted on the dislocations on account of this interaction. A qualitative picture of this drag was given previously in Ref. 6, in which the dislocation-orientation interaction was described using the linear response approximation which does not take into account the dependence of the orientational relaxation time $\tau$ on the local values of the dislocation strains $\varepsilon_{ik}$. This approximation simplifies the analysis of the problem considerably, but its applicability breaks down in the neighborhood of the dislocation core (this circumstance was noted in Ref. 6). Below we analyze the qualitative and quantitative changes in the dynamic drag on dislocations in $C_{60}$ fullerite when a more rigorous approach is taken to the description of the lattice-orientation interaction proposed in Ref. 11.

### 1. A GENERAL CHARACTERISTIC OF THE DISLOCATION-ORIENTATION INTERACTION

The presence of a dislocation in a $C_{60}$ fullerite crystal disrupts the uniform distribution (1) of pentagonal and hexagonal configurations of the molecules. At a fixed constant temperature a nonuniform equilibrium ''atmosphere'' of defect $h$ configurations, similar to the atmosphere of interstitial impurities surrounding a dislocation line in a bcc metal (the Snoek atmosphere),[8] forms in the elastic field $\varepsilon_{ik}(\mathbf{r})$ of a sessile dislocation. Let us consider the starting force $F_s(T)$ that is capable of rather rapidly (at the formal level, instantaneously) setting in motion a previously sessile dislocation, i.e., of tearing it away from the cloud of $h$ configurations. The value of this force is determined by the change in the elastic energy of the crystal upon the displacement of a dislocation line relative to the center of the cloud, which remains immobile.

The strain field $\varepsilon_{ik}(\mathbf{r}-\mathbf{V}t)$ of a dislocation moving at a constant velocity $\mathbf{V}$ ($V\ll s$, where $s$ is the characteristic sound velocity) disrupts the local thermodynamic equilibrium between the $p$ and $h$ configurations and excites a relaxation process that restores this equilibrium. On account of the energy dissipation accompanying this relaxation process the dislocation experiences an equivalent dynamic drag force $\mathbf{F}_D(\mathbf{V},T)$, which depends on its velocity and the temperature of the crystal.

A consistent description of the dislocation plasticity of $C_{60}$ fullerite requires a calculation of both of the indicated forces, although their relative role is different in different temperature intervals. On general arguments one expects that for $T<T_g$ the relaxation drag is practically absent, and the main role will be played by the starting force $\mathbf{F}_s(T)$, whereas for $T>T_g$ the primary force acting on the dislocation is $\mathbf{F}_D(\mathbf{V},T)$.

For dislocations in anisotropic crystal structures the explicit form of the strain field $\varepsilon_{ik}(\mathbf{r})$ is unknown, and therefore for solving problems like that considered in this paper one must appeal to the model of an equivalent elastically isotropic medium. Two elastic moduli of such a medium are calculated by special methods of averaging of the elastic constants of the crystal. According to the recommendation stated in Ref. 8, in a calculation of the local characteristics of the elastic field of a dislocation it is advisable to use the Voigt averaging method. In the case of a cubic crystal with elastic constants $C_{11}$, $C_{12}$, and $C_{14}$ the Voigt method leads to an equivalent elastically isotropic medium with a bulk modulus $B$ and a shear modulus $G$, which is determined by the relations[8]

$$3B=C_{11}+2C_{12},\quad 5G=3C_{44}+C_{11}-C_{12}. \tag{5}$$

The use of the values of the elastic moduli measured on a fullerite single crystal at room temperature by acoustical methods[12] lead to the estimates $B\simeq 1.1\times 10^{10}$ Pa and $G\sim 0.5\times 10^{10}$ Pa.

In what follows we will be considering a rectilinear edge dislocation, with Burgers vector $\mathbf{b}$, either at rest or moving in its glide plane with a constant velocity $\mathbf{V}$. In a rectilinear

coordinate system with the $x_3$ axis along the dislocation line and the $x_1$ axis along the direction of the vectors **b** and **V**, the dilatation field $\varepsilon_{ll}(\mathbf{r}-\mathbf{V}t)$ of the dislocation in the isotropic approximation has the form[7,8]

$$\varepsilon_{ll}(\mathbf{r}-\mathbf{V}t)\equiv\varepsilon_{ll}(x_1-Vt,x_2)=\varepsilon_0 r_0\psi(x_1-Vt,x_2), \qquad (6)$$

$$\varepsilon_0=\frac{3Gb}{\pi(3B+4G)r_0}, \quad \psi(x_1,x_2)=-\frac{x_2}{x_1^2+x_2^2}.$$

In this formula we have introduced the parameter $r_0$, the radius of the dislocation core, so that later we can remove a nonphysical divergence of (6) on the dislocation line ($x_1=Vt$, $x_2=0$). If we use the standard estimate $r_0\simeq b$ and the above estimates for the elastic moduli $B$ and $G$, we get an estimate of $\varepsilon_0\simeq 0.1$ for the value of the deformation in the core of the dislocation.[1]

Let us first consider the structure of the atmosphere of $h$ configurations formed on a sessile dislocation ($V=0$) at temperatures $T_g<T<T_c$. The excess equilibrium concentration $\overline{\nu}_h^{(\varepsilon)}=\overline{n}_h^{(\varepsilon)}-\overline{n}_h$ of the hexagonal configurations resulting from the dilatation (6) is easily obtained using formulas (1) and (4). Since the inequality $q=v_\Delta\varepsilon_0/kT\ll 1$ holds in the temperature region under consideration ($T>T_g$), an expression for $\overline{\nu}_h^{(\varepsilon)}$ can be written in the approximation linear in $q$, assuming that $|r_0\psi(x_1,x_2)|\leqslant 1$ after the divergence has been removed:

$$\overline{\nu}_h^{(\varepsilon)}(\mathbf{r})=qr_0\overline{n}_p\overline{n}_h\psi(x_1,x_2). \qquad (7)$$

The instantaneous displacement (7) of the dislocation along the $x_1$ axis by a distance $z$ relative to the center of the cloud of $h$ configurations formed by it leads to the following change in the lattice-orientation part of the free energy density of the fullerite at a fixed temperature:[11]

$$\delta W^{(hd)}(x_1,x_2;z)=-\gamma\overline{\nu}_h^{(\varepsilon)}(x_1,x_2) \times[\varepsilon_{ll}(x_1,-z,x_2)-\varepsilon_{ll}(x_1,x_2)], \qquad (8)$$

where $\gamma$ is the phenomenological parameter of the orientation-lattice interaction. Using Eq. (8), we can evaluate $F_s$, the starting force per unit length of the dislocation, which is the force that must be applied to the dislocation in the glide plane in order to tear it away from the cloud of $h$ configurations:

$$F=\gamma\overline{n}_p\overline{n}_h q\varepsilon_0 r_0^2\max|I(z)|, \qquad (9)$$

$$I(z)=\frac{\partial}{\partial z}\int\int_{-\infty}^{\infty}dx_1dx_2\psi(x_1,x_2)\psi(x_1-z,x_2).$$

Of course, the evaluation of this integral presupposes that the correct procedure for removing the divergence of the integrand at the points ($x_1=0$, $x_2=0$) and ($x_1=z$, $x_2=0$) has been specified.

The glide of a dislocation with a constant velocity $V$ through the bulk of a crystal with a uniform equilibrium distribution of hexagonal configurations will disturb the local equilibrium: $n_h(\mathbf{r},t)=\overline{n}_h+\nu_h(\mathbf{r},t)$, where $\nu_h$ is the nonequilibrium increment induced by the elastic field (6) of the dislocation. According to Eqs. (2)–(4), the equation for the nonequilibrium increment $\nu_h(r,t)$ has the form

$$\tau^{(\varepsilon)}\frac{\partial}{\partial t}\nu_h+\nu_h=\frac{\tau^{(\varepsilon)}}{\tau_p^{(\varepsilon)}}-\overline{n}_h. \qquad (10)$$

Here $\tau^{(\varepsilon)}$ and $\tau_{p,h}^{(\varepsilon)}$ are, respectively, the local values of the orientational relaxation time and of the times for the activated destruction of the pentagonal and hexagonal configurations in the elastic field of the moving dislocation:

$$\tau^{(\varepsilon)}=\frac{\tau_p^{(\varepsilon)}\tau_h^{(\varepsilon)}}{\tau_p^{(\varepsilon)}+\tau_h^{(\varepsilon)}},$$

$$\tau_{p,h}^{(\varepsilon)}=\tau_0\exp\left[\frac{U_{p,h}-v_{p,h}\varepsilon_{ll}(x_1-Vt,x_2)}{kT}\right]. \qquad (11)$$

It is easy to show that in the temperature interval under consideration, $T_g<T<T_c$, and outside the core of the dislocation, the right-hand side of Eq. (10) admits a linearization in the dilatation $\varepsilon_{ll}(x_1-Vt,x_2)$ (formally, in the small parameter $q=v_\Delta\varepsilon_0/kT\ll 1$). The relaxation time $\tau^{(\varepsilon)}$, however, does not admit such a linearization: it contains the large parameter $Q=v_p\varepsilon_0/kT$ and remains an essentially nonlinear (exponential) function of the dilatation $\varepsilon_{ll}(x_1-Vt,x_2)$.

Equation (10) is a linear differential equation with variable coefficients, and its solution that satisfies the natural initial condition $\nu_h(\mathbf{r},-\infty)\equiv 0$ can be written in quadratures.[13] In the approximation linear in the parameter $q$ we have

$$\nu_h(x_1,x_2,t)=\frac{qr_0\overline{n}_p}{\tau_p}\int_0^\infty dt'\psi[x_1-V(t-t'),x_2] \times\exp\left\{Qr_0\psi[x_1-V(t-t'),x_2]-\frac{1}{\overline{n}_h\tau_p} \times\int_0^{t'}dt''\exp[Qr_0\psi(x_1-V(t-t'),x_2)]\right\}, \qquad (12)$$

$$q=\frac{v_\Delta\varepsilon_0}{kT}, \quad Q=\frac{v_p\varepsilon_0}{kT}.$$

The relaxation process (12) induced in the system of orientation states by the elastic field of the moving dislocation is accompanied by dissipation of the mechanical energy of the crystal with an equivalent drag force $F_D(V,t)$. The time derivative of the local energy density of the dislocation-orientation interaction is given by the equation

$$\frac{\partial}{\partial t}W^{(hd)}(x_1,x_2,t)=-\gamma\nu_h(x_1,x_2,t)\frac{\partial}{\partial t}\varepsilon_{ll}(x_1-Vt,x_2). \qquad (13)$$

The integration of (13) over the coordinates $x_1$ and $x_2$ gives the value of the dissipative function of the process per unit length of the dislocation. Equating this to the product $F_DV$, we obtain the following expression for the drag force per unit length:

$$F_D=\frac{qr_0^2\varepsilon_0\overline{n}_p\gamma}{\tau_p}\int\int_{-\infty}^{\infty}dx_1dx_2\frac{\partial}{\partial x_1}\psi[x_1-Vt,x_2]$$
$$\times\int_0^{\infty}dt'\psi[x_1-V(t-t'),x_2]$$
$$\times\exp[Qr_0\psi(x_1-V(t-t'),x_2)]\exp\left\{-\frac{1}{\overline{n}_h\tau_p}\int_0^{t'}dt''\right.$$
$$\left.\times\exp[Qr_0\psi(x_1-V(t-t''),x_2)]\right\}. \quad (14)$$

This formula, like Eq. (9), has physical meaning only after the divergence due to the singularity of the function $\psi(x_1,x_2)$ has been removed.

The integrals (9) and (14) give the solution in quadratures for the drag force exerted on a dislocation as a result of the interaction of its elastic field with the orientational configurations of the molecules. The next step of the analysis is to obtain an explicit expression for the dependence of this force on the temperature of the crystal and the velocity of the dislocation and to estimate the characteristic value of the drag force in different temperature-velocity intervals.

## 2. TEMPERATURE DEPENDENCE OF THE STARTING FORCE $F_s(T)$

The simplest way of removing the singularity in the evaluation of the integral $I(z)$ in Eq. (9) is to remove a strip $|x_2|<r_0$ from the integration region, where $r_0$ is the radius of the dislocation core. Then, after making the change of integration variables $\xi x_2=x_1$ and $\eta x_2=z$, we obtain

$$I(z)=-2\int_{-\infty}^{\infty}dx_1\int_{r_0}^{\infty}dx_2\psi(x_1,x_2)\frac{\partial}{\partial x_1}\psi(x_1-z,x_2)$$
$$=-\frac{2}{z}\int_{-\infty}^{\infty}d\xi\int_0^{z/r_0}d\eta\psi(\xi,1)\frac{\partial}{\partial\xi}\psi(\xi-\eta,1)$$
$$=\frac{2}{z}\int_{-\infty}^{\infty}d\xi\psi(\xi,1)\int_0^{z/r_0}d\eta\frac{\partial}{\partial\eta}\psi(\xi-\eta,1)$$
$$=2\int_{-\infty}^{\infty}\frac{d\xi}{(1+\xi^2)^2}\left[\frac{2\xi r_0-z}{r_0^2+(\xi r_0-z)^2}\right].$$

The remaining integral is easily calculated using the residue theorem of complex analysis:

$$I(z)=-\frac{\pi z}{4r_0^2+z^2},\quad \max|I(z)|=\frac{\pi}{4r_0}. \quad (15)$$

Substituting (15) into (9), we obtain the estimate

$$F_s\simeq\frac{\pi r_0\varepsilon_0^2v_\Delta\gamma\overline{n}_p\overline{n}_h}{4kT}=\frac{b^2v_\Delta\gamma\overline{n}_p\overline{n}_h}{4\pi r_0kT}\left[\frac{3G}{3B+4G}\right]^2. \quad (16)$$

In the framework of the phenomenological thermodynamic theory of orientation states[11] the coefficient $\gamma$ is undetermined, remaining a phenomenological parameter of the theory. In this connection it is useful to express this coefficient in terms of fullerite properties that admit experimental determination, e.g., the specific heat. Using the results of Ref. 11, we arrive at the relation

$$\gamma=\frac{v_\Delta kT^2C_v^{(or)}(T)}{\Delta^2\overline{n}_p\overline{n}_h}, \quad (17)$$

where $C_v^{(or)}$ is the orientation component of the heat capacity per unit volume. In addition, the coefficient $\gamma$ can be given a microscopic meaning. Recalling that the excitation of an isolated $h$ configuration is accompanied by an increase in the energy of the crystal by an amount $\Delta$, we obtain

$$C_v^{(or)}=N_0\Delta\left(\frac{d\overline{n}_h}{dT}\right)_V=\frac{N_0\Delta^2\overline{n}_p\overline{n}_h}{kT^2}. \quad (18)$$

A comparison of (17) and (18) gives the following expression for the coefficient $\gamma$:

$$\gamma=N_0v_\Delta. \quad (19)$$

Substituting (1) and (19) into (16), we obtain an explicit expression for the temperature dependence of the starting force:

$$F_s(T)=\left(\frac{3G}{3B+4G}\right)^2\frac{b^2v_\Delta^2N_0}{4\pi r_0kT}\frac{\exp(\Delta/kT)}{[1+\exp(\Delta/kT)]^2}. \quad (20)$$

We note that the parameters $B$ and $G$ appearing in the formulas for $F_s$ are the isothermal elastic moduli, although, strictly speaking, at the level of accuracy with which these formulas have been obtained it does not make sense to distinguish between the isothermal and adiabatic values of the moduli or to take their temperature dependence into account.

## 3. DYNAMIC DRAG FORCE

The divergence in the integral (14) that determines the dynamic drag force on a uniformly moving dislocation is removed in the same way as in the evaluation of the starting force, by excluding a strip $|x_2|<r_0$ from the integration region. In addition, it is easy to see that the integral can be simplified somewhat by the substitution $x_1-Vt\to x_1$ and integration by parts over the variable $t'$:

$$F_D=q\gamma\varepsilon_0r_0^2\overline{n}_p\overline{n}_h\int_{r_0}^{\infty}dx_2\int_{-\infty}^{\infty}dx_1\left[\frac{\partial}{\partial x_1}\psi(x_1,x_2)\right]$$
$$\times\int_0^{\infty}dt\left[\frac{\partial}{\partial t}\psi(x_1+Vt,x_2)\right]$$
$$\times\left\{\exp\left[-\frac{1}{\overline{n}_h\tau_p}\int_0^t dt'\exp[Qr_0\psi(x_1+Vt',x_2)]\right]\right.$$
$$\left.\times\exp\left[-\frac{1}{\overline{n}_h\tau_p}\int_0^t dt'\exp[-Qr_0\psi(x_1+Vt',x_2)]\right]\right\}.$$

It will be convenient to change to dimensionless integration variables $\eta$, $\xi$, $\nu$ through the substitutions $x_1=Qr_0\xi$, $x_2=Qr_0\eta$, $Vt=Qr_0\nu$:

$$F_D=q\gamma\varepsilon_0r_0\overline{n}_p\overline{n}_hI\left(Q,\frac{V_T}{V}\right); \quad (21)$$

$$I\left(Q,\frac{V_T}{V}\right)=\frac{1}{Q}\int_{1/Q}^{\infty}d\eta\int_{-\infty}^{\infty}d\xi\left[\frac{\partial}{\partial\xi}\psi(\xi,\eta)\right]\times\int_0^{\infty}d\nu\left[\frac{\partial}{\partial\xi}\psi(\xi+\nu,\eta)\right]\times\left\{\exp\left[-\frac{V_T}{V}\int_0^{v}d\nu'\exp[\psi(\xi+\nu',\eta)]\right]+\exp\left[-\frac{V_T}{V}\int_0^{v}d\nu'\exp[-\psi(\xi+\nu',\eta)]\right]\right\},\tag{22}$$

$V_T=\dfrac{r_0Q}{\tau_p\overline{n_h}}$.

Asymptotic expressions for the integral (22) can be obtained by considering the limiting cases of low and high dislocation velocities: $V\ll V_T$ and $V\gg V_T$.

### 3.1. Region of low velocities

Turning to an evaluation of the asymptotic behavior of the integral $I(Q,V_T/V)$, we note first of all that for the integrals in the arguments of the exponential functions the following simple asymptotic estimate can be made:

$$I_1^{(\pm)}=\int_0^{v}d\nu'e^{\pm\psi(\xi+\nu',\eta)}\simeq\begin{cases}\nu e^{\pm\psi(\xi,\eta)}, & \nu\to 0;\\ \nu\pm\pi & \nu\to\infty.\end{cases}\tag{23}$$

In the limiting case of very low dislocation velocities $V\to 0$ the main contribution to the integral over the variable $\nu$ is given by the region of small values $\nu\to 0$, which allows us to set $(\partial/\partial\xi)\psi(\xi+\nu,\eta)\simeq(\partial/\partial\xi)\psi(\xi,\eta)$ in the integrand and, with exponential accuracy, to neglect the first term in the curly brackets in (22):

$$I\left(Q,\frac{V_T}{V}\right)=\frac{2V}{QV_T}\int_{1/Q}^{\infty}d\eta\int_0^{\infty}d\xi\left[\frac{\partial\psi(\xi,\eta)}{\partial\xi}\right]^2e^{\psi(\xi,\eta)},$$

$V\to 0$.

Integrating by parts over the variable $\xi$ and making one more change of variables, we bring this integral to the form

$$I\left(Q,\frac{V_T}{V}\right)\simeq-\frac{2V}{V_T}\int_1^{\infty}d\eta\int_0^{\infty}d\xi\left[\frac{\partial^2\psi(\xi,\eta)}{\partial^2\xi}\right]e^{Q\psi(\xi,\eta)}.\tag{24}$$

The main contribution to the integral (24) for $Q\gg 1$ is from a small region around the point $\xi=0$, $\eta=1$. Making the following substitution in the integrand:

$$\frac{\partial^2\psi(\xi,\eta)}{\partial^2\xi}\simeq\left(\frac{\partial^2\psi(\xi,\eta)}{\partial^2\xi}\right)_{\xi=0,\eta=1}=-2,$$

$\psi(\xi,\eta)\simeq 2-\eta-\xi^2$

and doing the integration, we obtain a final asymptotic expression for the integral (22) at low velocities:

$$I\left(Q,\frac{V_T}{V}\right)=\frac{2\sqrt{\pi}e^QV}{Q^{3/2}},\quad V\to 0.\tag{25}$$

A more exact analysis shows that the integral (22) in the low-velocity region conforms rather poorly to the asymptotic expression (25): in the region $V<V_T$ there is a large interval of velocities in which the difference between (22) and (25) is extremely significant. This circumstance is due to the existence of extended regions in the space of variables ($\xi$, $\eta$, $\nu$) in which the upper asymptotic expression in (23) cannot be used. For this reason the integral (22) was evaluated by numerical methods on a computer for sets of values of the parameters $V$ and $Q$ from the intervals $0.1V_T\leqslant V\leqslant V_T$ and $10\leqslant Q\leqslant 25$. The results of these computations allowed us to obtain a simple analytical approximation for the integral (22) having a relative accuracy of the order of 0.1 in the indicated regions of parameter values:

$$I\left(Q,\frac{V_T}{V}\right)\simeq\frac{Q^{3/5}}{8}\left(\frac{V}{V_T}\right)^{2/25},\quad 0,V_T\leqslant V\leqslant V_T.\tag{26}$$

Thus the linear dependence of the integral $I(Q,V_T/V)$ on the dislocation velocity in (25) gives way to the very weak dependence (26) even in the intermediate velocity region $V\leqslant V_T$. Comparing (25) and (26), we easily obtain an estimate for the characteristic value of the velocity $V_{T0}$ that separates the two regions:

$$V_{T0}\simeq\frac{V_TQ^2}{30}e^{-Q}.\tag{27}$$

### 3.2. Region of high velocities

Let us first analyze one of the inner integrals in (22):

$$I_2(\xi,\eta)=\int_0^{\infty}d\nu\left[\frac{\partial}{\partial\xi}\psi(\xi+\nu,\eta)\right]\times\left\{\exp\left[-\frac{V_T}{V}I^{(+)}(\xi,\eta,\nu)\right]+\exp\left[-\frac{V_T}{V}I^{(-)}(\xi,\eta,\nu)\right]\right\}\equiv\int_0^{\infty}d\nu\left[\frac{\partial}{\partial\xi}\psi(\xi+\nu,\eta)\right]\left\{\exp\left[-\frac{V_T}{V}(I_1^{(+)}-\nu)\right]+\exp\left[-\frac{V_T}{V}(I_1^{(-)}-\nu)\right]\right\}\exp\left(-\frac{V_T}{V}\nu\right).$$

Since the derivative

$$\frac{\partial}{\partial\nu}(I_1^{(\pm)}-\nu)=e^{\pm\psi(\xi+\nu,\eta)}-1$$

does not vanish at finite values of $\nu$, and the asymptotic expression (23) is valid, the inequality $|I_1^{\pm}-\nu|\leqslant\pi$ holds. Consequently, for $V\gg\pi V_T$ we have

$$I_2(\xi,\eta)=\int_0^{\infty}d\nu\left[\frac{\partial}{\partial\xi}\psi(\xi+\nu,\eta)\right]\exp\left(-\frac{V_T}{V}\nu\right).\tag{28}$$

Substituting (28) into the integral (22) and doing some straightforward manipulations, we bring this integral to the form

$$I\left(Q,\frac{V_T}{V}\right)=\frac{2}{Q}\int_{1/Q}^{\infty}d\eta\int_{-\infty}^{\infty}d\xi\left[\frac{\partial}{\partial\xi}\psi(\xi,\eta)\right]\times\int_0^{\infty}d\nu\left[\frac{\partial}{\partial\xi}\psi(\xi+\nu,\eta)\right]\exp\left(-\frac{V_T}{V}\nu\right)$$
$$=-\frac{2V_T}{QV}\int_0^{\infty}d\nu\exp\left(-\frac{V_T\nu}{QV}\right)\times\int_t^{\infty}d\eta\int_{-\infty}^{\infty}d\xi\psi(\xi,\eta)\frac{\partial}{\partial\xi}\psi(\xi+\nu,\eta).$$

The integral over the variables $(\eta, \xi)$ is the same as the previously evaluated integral (15) if we set $r_0=1$, $z=-\nu$. Consequently, in the limiting case under consideration we have

$$I\left(Q,\frac{V_T}{V}\right)\simeq\frac{\pi V_T}{QV}\int_0^{\infty}d\nu\frac{\nu\exp\left(-\frac{V_T\nu}{QV}\right)}{\nu^2+4}$$
$$=-\frac{\pi V_T}{QV}\left[\mathrm{ci}\left(\frac{2V_T}{QV}\right)\cos\left(\frac{2V_T}{QV}\right)+\mathrm{si}\left(\frac{2V_T}{QV}\right)\sin\left(\frac{2V_T}{QV}\right)\right],\qquad(29)$$

where $\mathrm{si}(x)$ and $\mathrm{ci}(x)$ are the sine integral and cosine integral, respectively. In the case under consideration, $V\gg\pi V_T$ and $Q\gg1$, the arguments of the functions in formula (29) are small, and we can therefore write the following asymptotic expression for the integral $I(Q,V_T/V)$:

$$I\left(Q,\frac{V_T}{V}\right)\simeq\frac{\pi V_T}{QV}\ln\left(\frac{QV}{2V_T}\right),\quad V\gg\pi V_T.\qquad(30)$$

Expression (30) is a slowly decaying function of velocity which continues the function (26). Formulas (25), (26), and (30) show that in the velocity region $V\sim V_T$ the function $I(Q,V_T/V)$ has a broad peak with an almost flat top (26). The height of this peak depends weakly on temperature:

$$\max_{(V)}I\left(Q,\frac{V_T}{V}\right)\simeq\frac{Q^{3/5}}{8}=\frac{1}{8}\left(\frac{v_p\varepsilon_0}{kT}\right)^{3/5}\qquad(31)$$

For the values of practical interest, $Q\sim10-20$, the value of $\max I\sim1-0.5$. In addition, the position of the peak on the axis of velocities $V_T$ and its characteristic width $V_T-V_{T0}$ are exponentially sensitive to changes in temperature.

### 3.3. Temperature-velocity dependence of the dynamic drag force

The foregoing analysis shows that the dynamic drag force on a dislocation due to the orientation-dislocation interaction and processes of orientational relaxation has an extremely complex dependence on the dislocation velocity $V$ and the crystal temperature $T$. This dependence has been obtained in certain temperature-velocity regions in the form of asymptotic expressions. Before turning to a discussion of these asymptotic expressions, it is useful to compare the dynamic drag force $F_D$ with the starting force $F_s$ calculated in Sec. 2. Using formulas (9), (15), and (21), we obtain

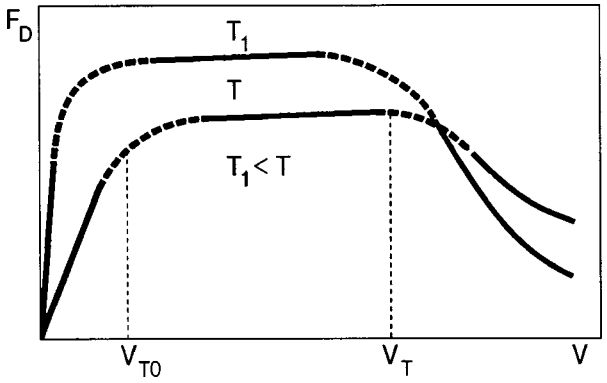


FIG. 1. Schematic illustration of the dependence of the dynamic component of the drag force $F_D(T,V)$ on the velocity $V$ of the dislocation at different temperatures $T$. The temperature dependence of the characteristic values of the velocity $V_T$ and $V_{T0}$ is described by formulas (33). The solid portions of the curves show those regions of the function $F_D(T,V)$ for which the analytical approximations (25), (26), and (30) were obtained.

$$F_D(T,V)=\frac{4}{\pi}F_s(T)I\left[Q(T),\frac{V_T}{V}\right].\qquad(32)$$

We have shown above that $\max I\simeq1$, and therefore the characteristic scale of the force of orientational drag on dislocations is set by the starting force $F_s(T)$. According to Eq. (20), this force increases slowly with decreasing temperature in the interval $(T_g,T_c)$, reaching a maximum value in the region of the orientational glass point.

Figure 1 shows schematically the dependence of the dynamic component of the drag force on the dislocation velocity $V$. This dependence is nonmonotonic: there is a short linear region at low velocities $V\ll V_{T0}$, which gives way to a broad maximum in the velocity region $V\sim V_T$, followed by a slow decline in the region of high velocities $V\gg V_T$. The character of the velocity dependence of the force $F_D(T,V)$ does not change qualitatively as the temperature is changed, but there are significant quantitative changes, since the characteristic velocities $V_T$ and $V_{T0}$ and the slope of the linear part at low velocities depend exponentially on temperature:

$$V_T=\frac{r_0}{\tau_0\bar{n}_h}\left(\frac{v_p\varepsilon_0}{kT}\right)\exp\left(-\frac{U_p}{kT}\right),$$
$$V_{T0}=\frac{r_0}{3\tau_0\bar{n}_h}\left(\frac{v_p\varepsilon_0}{kT}\right)^3\exp\left(-\frac{U_p+v_p\varepsilon_0}{kT}\right).\qquad(33)$$

We note that the conclusion that the force $F_D(T,V)$ depends nonmonotonically on the velocity $V$ was obtained earlier in an analysis of the dynamic interaction of a dislocation with the orientation states of the molecules in the linear-response approximation.[6] This approximation give a qualitatively correct estimate of the velocity $V_T$ and of the character of the velocity dependence of the drag force at $V\gg V_T$. Taking nonlinear effects into account in the neighborhood of the dislocation core leads to a strong broadening of the peak on the velocity dependence of $F_D(T,V)$ on the side of lower velocities and to a stronger temperature sensitivity of the slope of the linear part in the region of low velocities.

## CONCLUSION

We have analyzed the quasistatic and dynamic interactions of an edge dislocation with pentagonal and hexagonal configurations of the molecules in the low-temperature phase of $C_{60}$ fullerite.

We have described the nonuniform distribution of hexagonal configurations (which have an excess energy) arising around a sessile dislocation line for $T_g < T < T_c$, where $T_c = 260\,\mathrm{K}$ is the temperature of the phase transition between the *sc* and *fcc* structures, and $T_g \simeq 90\,\mathrm{K}$ is the orientational glass point. We have calculated the starting force $F_s(T)$ necessary to tear a dislocation away from the atmosphere of *h* configurations formed by it.

We have described the relaxational process of transitions between *p* and *h* configurations of the molecules in the elastic field of a dislocation moving with a constant velocity $V$. We have calculated the dynamic component of the drag forced $F_D(T,V)$ exerted on a dislocation as a result of the orientational relaxation.

We have made a detailed analysis of the temperature dependence of the starting force $F_s(T)$ and the temperature-velocity dependence of the dynamic drag force $F_D(T,V)$. A characteristic feature of the dynamic component of the drag force is that its dependence on the velocity $V$ has a broad peak with an almost flat top, and the position of this peak on the velocity axis depends exponentially on the temperature.

*E-mail: natsik@ilt.kharkov.ua

[1)]The small quantity $\epsilon_0 \ll 1$ to a certain extent justifies the use of the approximation linear in $\epsilon_{ll}$ in the expansions (4).

[1] V. I. Orlov, V. I. Nikitenko, R. K. Nikolaev, I. N. Kremenskaya, and Yu. A. Osip'yan, JETP Lett. **59**, 704 (1994).
[2] M. Tachibana, M. Michiyama, K. Kikuchi, Y. Achiba, and K. Kojima, Phys. Rev. B **49**, 14945 (1994).
[3] M. Tachibana, H. Sakuma, M. Michiyama, and K. Kojima, Appl. Phys. Lett. **67**, 2618 (1995).
[4] L. S. Fomenko, V. D. Natsik, S. V. Lubenets, V. G. Lirtsman, N. A. Aksenova, A. P. Isakina, A. I. Prokhvatilov, M. A. Strzhemechny, and R. C. Ruoff, Fiz. Nizk. Temp. **21**, 465 (1995) [Low Temp. Phys. **21**, 364 (1995)].
[5] S. V. Lubenets, V. D. Natsik, L. S. Fomenko, A. P. Isakina, A. I. Prokhvatilov, M. A. Strzhemechnyĭ, N. A. Aksenova, and R. C. Ruoff, Fiz. Nizk. Temp. **23**, 338 (1997) [Low Temp. Phys. **23**, 338 (1997)].
[6] V. D. Natsik, S. V. Lubenets, and L. S. Fomenko, Fiz. Nizk. Temp. **22**, 337 (1996) [Low Temp. Phys. **22**, 264 (1996)]; Phys. Status Solidi A **157**, 303 (1996).
[7] J. Friedel, *Dislocations* [Pergamon Press, Oxford (1964); Mir, Moscow (1967)].
[8] J. P. Hirth and J. Lothe, *Theory of Dislocations* [Pergamon Press, Oxford (1964); Atomizdat, Moscow (1972)].
[9] A. M. Kosevich and V. D. Natsik, ''Continuum and dynamic theory of dislocations,'' Ch. 14 in *Physical Materials Science in the USSR: History, Current Status, and Prospects for Development*, Naukova Dumka, Kiev (1986).
[10] A. M. Kosevich and V. D. Natsik, Fiz. Tverd. Tela (Leningrad) **8**, 1250 (1996) [Sov. Phys. Solid State **8**, 993 (1996)].
[11] V. D. Natsik and A. V. Podol'skiy, Fiz. Nizk. Temp. **24**, 689 (1998) [Low Temp. Phys. **24**, 523 (1998)].
[12] N. P. Kobelev, R. K. Nikolaev, Ya. M. Soĭfer, and S. S. Khasanov, Fiz. Tverd. Tela (St. Petersburg) **40**, 173 (1998) [Phys. Solid State **40**, 154 (1998)].
[13] V. I. Smirnov, *Course of Higher Mathematics*, Vol. 2 [in Russian] GITTL, Moscow (1950).

Translated by Steve Torstveit

## NEWS ITEMS

# The Second Chernogolovka Workshop on Low Temperature Physics in Microgravity Environment (CWS-99), July 28–August 2, 1999

L. P. Mezhov-Deglin

*Institute of Solid State Physics, Russian Academy of Sciences, 142432 Chernogolovka, Moscow District, Russia*

(Submitted October 13, 1999)
Fiz. Nizk. Temp. **26**, 314–317 (March 2000)

The International Seminar CWS-99, devoted to a discussion of the current status and prospects for development of fundamental research in the field of low-temperature physics in a microgravity environment, was held in at the Research Center of the Russian Academy of Sciences (RCC RAN) in Chernogolovka, Moscow District on July 28–August 2, 1999. This seminar was organized by the Institute of Solid State Physics and the Space Materials Science section of the Space Council of the Russian Academy of Sciences with the financial support of the Russian Fund for Fundamental Research, the Ministry of Science and Technology of the Russian Federation, The Russian Aviation & Space Agency, and the Council on Low Temperature Physics of the Russian Academy of Sciences. The CWS-99 Seminar preceded the International Conference on Low Temperature Physics LT-22, and, as one of the satellite activities of LT-22 conducted in the framework of international scientific cooperation, it received substantial support from the Organizing Committee of LT-22 and from the OLMSA Division of the National Aeronoutics and Space Administration (NASA), USA.  [S1063-777X(00)00803-3]

The range of topics for physical research to be conducted onboard spacecraft in the next few years has broadened considerably. This has come about, on the one hand, as a result of the experience gained in the work of cosmonauts and the development of the technological expertise necessary for performing fundamental scientific experiments under weightless conditions and, on the other hand, in response to the progress that has been made in modern physics and the advent of new scientific fields, for which it may be of fundamental importance to move the experiments from a terrestrial to a microgravity environment. An example is the laser cooling of metal vapors, which has substantially broadened the range of low-temperature research and has enabled making measurements near absolute zero (at $10^{-9}-10^{-10}$ K). Placing such an experiment onboard a spacecraft will increase the existence time of the cold cloud many-fold; this is especially important for fundamental research on phase transitions and Bose–Einstein condensation phenomena in a dilute vapor, for doing wave experiments in atomic physics, etc., and also for the practical implementation of an important engineering project—to create a working model of an atomic clock with a resolution at the level of $10^{-15}-10^{-16}$ s, which is 3–4 order of magnitude higher than that of the existing clocks. This would open up fundamentally new opportunities for basic research in the fields of relativity, cosmology, and astronomy.

The scientific literature of the last two decades has demonstrated the intimate connection between condensed-matter physics and phenomena taking place on cosmic scales (e.g., between the intersection of vortices in superfluid helium and the intersection and recombination of cosmic strings). Therefore, it is important that the research begun earlier on critical phenomena in condensed matter, particularly on thermodynamic and transport phenomena in superfluid and normal helium near the critical point, be continued onboard the future International Space Station (ISS), and that new experiments be designed to investigate critical phenomena occurring in the bulk and on the surface of quantum fluids and crystals (phase transitions in three-dimensional and two-dimensional systems, the equilibrium faceting of crystals, and the features of liquid helium droplets in a microgravity environment).

One of the main goals of the CWS-99 Seminar was to create a forum for the presentation and discussion of recent research results in low-temperature physics and of plans and ideas for new terrestrial experiments to serve as a basis for choosing the most worthwhile and well-thought-out experiments onboard the ISS. In accordance with the proposals from members of the Consulting Committee, the main topics chosen for discussion at this seminar were equilibrium and critical phenomena in liquid helium, levitating droplets, impurity molecules and clusters in superfluid He II, laser cooling and Bose–Einstein condensation phenomena at ultralow temperatures, and the engineering possibilities and equipment for carrying out low-temperature measurements onboard the ISS.

About 150 persons from the various research centers of Russia, Ukraine, Kazakhstan, USA, Japan, England, and Germany took part in this seminar, including 25 undergraduate and postgraduate students doing practicum at the insti-

 

tutes of the RCC RAN. A total of 49 reports from 50 organizations were given at the oral and poster sessions (see below for a listing). A digest of nearly all these reports was published in the Book of Abstracts of CWS-99 prior to the opening of the Seminar. The authors' final versions of most of these reports will be published in a special issue of the Journal of Low Temperature Physics in June of 2000.

## LISTING OF REPORTS PRESENTED AT CWS-99

### 1. Common topics, low-temperature facilities

1. Long-term research program for the Russian segment of International Space Station (RSISS) M. Tsymbaljuk (TSNIMASH).

2. Microgravity fundamental physics program for the new millennium. M. C. Lee (National Aeronautics and Space Administration, Washington, USA).

3. Ukrainian cryogenic facility for ISS and project of HERUBIM experiment. S. Bondarenko (B. Verkin Institute for Low Temperature Physics and Engineering, NASU, Kharkov, Ukraine).

4. Fundamental low temperature researches under space flight conditions: achievements and perspectives of Ukrainian science. S. Bondarenko (B. Verkin Institute for Low Temperature Physics and Engineering, NASU, Kharkov, Ukraine).

5. NASA roadmap for fundamental physics research in space. U. Israelsson (Jet Propulsion Laboratory, California Institute of Technology, Pasadena, CA, USA).

6. Optical characterization of $C_{60}$ single crystals grown in microgravity conditions. E. Steinman *et al.* (Institute of Solid State Physics, RAS, Chernogolovka, Russia; RCC ''Energy;'' Cosmonaut treating center).

7. Research opportunities on low temperature microgravity physics facility. F.-C. Liu (Jet Propulsion Laboratory, California Institute of Technology, Pasadena, CA, USA).

8. Desirable conditions and narrow restrictions: the concept of liquid helium boiling experiment in microgravity. N. Scherbakova (B. Verkin Institute for Low Temperature Physics and Engineering, NASU, Kharkov, Ukraine).

### 2. Heat and mass transfer in helium

9. Some models of heat transfer at film boiling of superfluid helium near critical point. A. Kryukov (Moscow Power Engineering Institute, Department of Low Temperatures, Moscow, Russia).

10. The vapor film evolution at superfluid helium boiling in microgravity. A. Kryukov (Moscow Power Engineering Institute, Department of Low Temperatures, Moscow, Russia).

11. Precision experiment to study cryosorption of He isotopes in the terrestrial conditions and at low gravity. S. Nesterov (Moscow Power Engineering Institute, Department of Low Temperatures, Moscow, Russia).

12. The superfluid $^3$He collective mode study: current situation in experiment and theory. P. Brusov (Physical Research Institute, Rostov-on-Don, Russia).

13. On a theory of multi-gap superfluidity based on the fermi-liquid approach. A. Isaev (Kharkov Institute of Physics and Technology, Kharkov, Ukraine).

### 3. Material science and Universe

14. Universe as condensed matter. G. Volovik (Helsinki University of Technology, Helsinki, Finland; Landau Institute for Theoretical Physics, RAS, Moscow, Russia).

15. Does the Kibble mechanism operate in He II? P. McClintock (Lancaster University, Lancaster, United Kingdom).

### 4. Phenomena in superfluid He II

16. Onset of superfluidity far from equilibrium: dynamical effects on the correlation volume. R. Duncan (University of New Mexico, Albuquerque, USA).

17. Finite-size scailing for the specific heat of confined liquid $^4$He. R. Ferrell (University of Maryland, Maryland, USA).

18. Dissipation and phase slip in confined superfluid He II. S. Mukhin (Moscow Institute for Steel and Alloys, Moscow, Russia).

19. Generation of the second and first sound waves by a pulse heater in fluid helium. V. Efimov (Institute of Solid State Physics, RAS, Chernogolovka, Russia).

20. Interaction of intense heat pulses and vortices in He II. L. Kondaurova (Institute of Thermophysics, Novosibirsk, Russia).

21. Stochastic dynamics of vortex filament induced by a random force with a power like correlator. S. Nemirovskii (Institute of Thermophysics, Novosibirsk, Russia).

22. Numerical simulation of vortex dynamics in superfluid helium. M. Tsubota (Osaka City University, Osaka, Japan).

23. Dimensional crossover and non-linear phenomena in dc superflow; experiment on thin He films formed in $3D$ connected porous glass. M. Kubota (Institute of Solid State Physics, University, Tokyo, Japan).

### 5. Charged droplets and surfaces

24. Levitation of He II drops charged with positive ions. J. Niemela (University of Oregon, Eugene, USA).

25. Static and dynamic phenomena at the charged liquid hydrogen surface. G. Kolmakov (Institute of Solid State Physics, RAS, Chernogolovka, Russia).

### 6. Foreign particles and clusters in liquid helium

26. Ultrasonic investigations of impurity-helium porous solids. V. Khmelenko (Laboratory of Atomic and Solid State Physics, Cornell University, Ithaca, USA).

27. Cryogenic applications of impurity-helium solid phase. E. Popov (Institute of Energy Problems of Chemical Physics, RAS, Chernogolovka, Russia).

28. Gravitational effects in the guest atoms behavior in liquid $^3$He–$^4$He mixtures. A. Shestakov (Institute of Energy Problems of Chemical Physics, RAS, Chernogolovka, Russia).

29. Condensed water in superfluid He II: irreversible gel formation? L. Mezhov-Deglin (Institute of Solid State Physics, RAS, Chernogolovka, Russia).

30. Phonon bands associated with the inner shell electronic absorption lines of Eu atoms in bulk liquid helium. M. Takami (ILS, University of Electrocommunication, Tokyo, Japan).

31. Laser spectroscopy of molecules in ultracold helium droplets. N. Poertner (Max-Plank Institut für Strömungsforschung, Göttingen, Germany).

32. Cryocrystal thin layers influence on optical properties of reflecting surfaces. A. Drobyshev (Research Institute of Experimental and Theoretical Physics, Alma-Ata, Kazakhstan).

#### 7. Laser cooling, atomic physics and Bose–Einstein condensation

33. Laser cooling, atomic physics and BEC in space. N. Bigelow (University of Rochester, Rochester, USA).

34. Gravity and light in trapped bose-condensate. V. Yarunin (Joint Institute for Nuclear Research, Dubna, Russia).

35. Bose–Einstein condensation in quasi-2$D$ trapped gases. G. Shlyapnikov (Kurchatov Institute, Moscow, Russia).

36. Studying the properties of supercooled strongly-coupled plasma created by artificial injection into space. Yu. Dumin (Institute of Earth Magnetism and Ion-Sphere, RAS, Troitsk, Russia).

37. A possibility of life origin at small bodies soon after our supernova explosion. A. Byalko (Landau Institute for Theoretical Physics, RAS, Moscow, Russia).

#### 8. Poster session reports

38. Anti-gravitational instability of neutral helium films. V. Shikin (Institute of Solid State Physics, RAS, Chernogolovka, Russia).

39. Deformation phenomena at the charged helium film in presence of cyclotron pumping. V. Shikin (Institute of Solid State Physics, RAS, Chernogolovka, Russia).

40. Nucleation and new phase growth during phase separation of liquid $^3$He–$^4$He solutions. V. Chagovets (B. Verkin Institute for Low Temperature Physics and Engineering, NASU, Kharkov, Ukraine).

41. Phonon spectra, atomic dynamics and oscillatory thermodynamic characteristics of ''superhomogeneous'' solid solutions. E. Syrkin (B. Verkin Institute for Low Temperature Physics and Engineering, NASU, Kharkov, Ukraine).

42. Oscillations, waves localized near the surface of layered crystal, and their application for creation of highly sensitive sensors. S. Feodosiyev (B. Verkin Institute for Low Temperature Physics and Engineering, NASU, Kharkov, Ukraine).

43. Thermal expansion in strongly anisotropic systems at low temperatures. E. Salamatov (Physicotechnical Institute, Ural Branch, RAS, Izhevsk, Russia).

44. Thin-film Al microstructure as a hot-electron microwave radiation detector. I. Borisenko (Institute of Microelectronics Technology and High-Purity Materials, RAS, Chernogolovka, Russia).

45. Geometry of microgravity excited in the structure of amorphous metal. A. Gurin (B. Verkin Institute for Low Temperature Physics and Engineering, NASU, Kharkov, Ukraine).

46. Formation of periodic structures under crystallization in conditions of microgravity. A. Gus'kov (Institute of Solid State Physics, RAS, Chernogolovka, Russia).

47. Heat transfer of solid parahydrogen with orthodeuterium impurity. B. Gorodilov (B. Verkin Institute for Low Temperature Physics and Engineering, NASU, Kharkov, Ukraine).

48. A $^3$He gas heat switch for the 0.5 K to 0.2 K temperature range. E. Smith (Laboratory of Atomic and Solid State Physics, Cornell University, Ithaca, USA).

Translated by Steve Torstveit